ISBN:978-84-691-9748-6 /DL:T-1249

UNIVERSITAT ROVIRA I VIRGILI
DEPARTAMENT D'ENGINYERIA ELECTRÒNICA, ELÈCTRICA I AUTOMÀTICA

STUDY OF STRUCTURAL AND SENSING PROPERTIES OF TUNGSTEN TRIOXIDE THIN FILMS DEPOSITED BY RF SPUTTERING

Doctoral thesis presented for the qualification of PhD

by

Stella Vallejos Vargas

Supervisor:

Dr. Viacheslav Khatko

February 29, 2008

UNIVERSITAT ROVIRA I VIRGILI
STUDY OF STRUCTURAL AND SENSING PROPERTIES OF TUNGSTEN TRIOXIDE THIN FILMS
DEPOSITED BY RF SPUTTERING
Stella Vallejos Vargas
ISBN:978-84-691-9748-6 /DL:T-1249

Abstract

The ability to produce metal oxides with nanometer grain size is of crucial importance not only from a fundamental approach, but also from an industrial point of view due to numerous applications of nanostructured metal oxides in many devices. For instance, in the field of gas sensors the high surface to volume ratio of nano-grain metal oxide has opened the possibility to enhance the sensing properties of these devices. Hence, a significant fraction of the overall research and development efforts in metal oxide based gas sensors is directed towards obtaining sensing films with smaller grain size. At present the investigation of new strategies to deposit sensing films with nano-grain size compatible with the micro-system fabrication has became imperative.

This dissertation presents a summary of the author's work prepared in the last four years in developing two special regimes of metal oxide thin film deposition by rf sputtering for gas sensing applications. The first regime named as *interruption (or interrupted) regime* implies deposition of the film with one or several interruptions of the deposition process. The second regime named as *floating regime* consists of introducing “extra” interfaces into the body of the film by means of the interruptions and using two power densities of rf sputtering: the first one to deposit the initial interrupted layers within the bulk of the film and the second one to deposit the superficial layer. The work carried out for this dissertation was experimental in nature and it was complemented by means of different characterization techniques used in order to study physical and sensing properties of the films deposited.

The results showed that the introduction of “extra” interfaces in the bulk of the tungsten trioxides (WO_3) films influences on the morphological and structural properties of the deposited films. It was noticed that phase transformation of WO_3 film structure from amorphous to crystalline has different activity in the films deposited with and without interruptions. Slower crystallization process was observed in the films deposited with interruptions. A reduction in grain size in WO_3 thin films deposited using interrupted or floating regime was observed as well. It was determined that gas micro-sensors fabricated with the interrupted and floating regimes have promising sensing characteristics, since they showed better sensitivity and selectivity to low concentrations of oxidizing gases such as NO_2 and O_3, in comparison with the gas micro-sensors fabricated using standard sputtering regime. The advantages of the new gas micro-sensors allow suggesting them as good candidates to monitor air pollutant gases.

Keywords: Tungsten trioxide, RF sputtering, Nano-grain, Gas sensors

Stella Vallejos Vargas, Departament d’Enginyeria Electrònica Elèctrica i Automática, Universitat Rovira i Virgili, Tarragona, Spain.

Resumen

Hoy en día la habilidad de producir capas de óxidos metálicos compuestos por nanogranos es muy importante, no sólo como conocimiento fundamental, sino también desde un punto de vista industrial debido a las numerosas aplicaciones de los óxidos metálicos nanoesctructurados en varios dispositivos electrónicos. Por ejemplo, en el campo de los sensores de gas, la relación superficie-volumen de las capas basadas en nanogranos de óxidos metálicos, ofrece la posibilidad de mejorar las propiedades de detección de estos dispositivos. Por esta razón, una gran fracción del total de la investigación y desarrollo en el campo de los sensores de gas basados en óxidos metálicos está dirigida a obtener capas activas compuestas por nanogranos. En la actualidad el estudio de nuevas técnicas para el depósito de capas activas compuestas por nanogranos y además compatibles con la fabricación de microsistemas se ha convertido en una necesidad imperiosa.

La presente tesis resume el trabajo del autor llevado a cabo en los últimos cuatro años y está relacionado con el desarrollo de dos regimenes especiales para depositar capas finas de óxido metálico por el método de pulverización catódica asistida por radio frecuencia para aplicaciones de sensores de gas. El primer régimen, nombrado *régimen de interrupciones* consiste en depositar la capa óxido metálico con una o varias interrupciones durante el proceso. El segundo régimen, nombrado *régimen flotante* consiste en introducir "extra" interfases dentro del volumen de la capa del óxido metálico por medio de interrupciones y empleando dos densidades de potencia durante el depósito (la primera para depositar el volumen de la capa y la segunda para depositar la capa superficial). El trabajo realizado en esta tesis fue de carácter experimental; además fue complementado por varios tipos de técnicas de caracterización que permitieron estudiar las propiedades físicas y las de detección de las capas depositadas.

Los resultados mostraron que la introducción de "extra" interfases en el volumen de las capas de trióxido de tungsteno (WO_3) influye en las propiedades morfológicas y estructurales de la capa obtenida. Se determinó que la transformación de fase del WO_3, de amorfo a cristalino, tiene diferente tipo de actividad en las capas depositadas con interrupciones en comparación con las depositadas sin interrupciones. Así se observó que el proceso de cristalización es más lento cuando se depositan las capas de óxido metálico mediante el régimen de interrupciones. Por otro lado, se observó una reducción del tamaño de grano en las capas de WO_3 depositadas tanto a través del régimen de interrupciones como del régimen flotante. También se determinó que los microsensores de gas fabricados empleando los dos regimenes estudiados tienen prometedoras características de detección, puesto que estos dispositivos mostraron mejor sensibilidad y selectividad a bajas concentraciones de gases oxidantes, tales como NO_2 y O_3, en comparación con los sensores de gas fabricados a través del régimen convencional de depósito por pulverización catódica. En conclusión, los sensores desarrollados en esta tesis podrían ser usados para monitorizar los principales contaminantes del aire.

Palabras clave: Trióxido de tungsteno, RF sputtering, Nanogranos, Sensor de Gas

Stella Vallejos Vargas, Department d'Enginyeria Electrònica Elèctrica i Automática, Universidad Rovira i Virgili, Tarragona, España.

ISBN:978-84-691-9748-6 /DL:T-1249

Papers included in the dissertation

I. *Micro-machined gas sensors selective to oxidizing gases*
S. Vallejos, V. Khatko, J. Calderer, I. Gràcia, C. Cané, E. Llobet, X. Correig
Sensors and Actuators B: Chemical, in press (2008)

II. *Ozone monitoring by micro-machined sensors with WO_3 sensing films*
S. Vallejos, V. Khatko, K. Aguir, K.A. Ngo, J. Calderer, I. Gràcia, C. Cané, E. Llobet, X. Correig
Sensors and Actuators B: Chemical, 126 (2007) 573 – 578

III. *Technology of metal oxide thin film deposition with interruptions*
V. Khatko, J. Calderer, S. Vallejos, E. Llobet, X. Correig
Surface and Coating Technology, 202 (2007) 453 – 459

IV. *Gas sensing properties of WO_3 thin films deposited by rf sputtering*
V. Khatko, S. Vallejos, J. Calderer, E. Llobet, X. Vilanova, X. Correig
Sensor and Actuators B: Chemical, 126 (2007) 400 – 405

ISBN:978-84-691-9748-6 /DL:T-1249

Conference contributions related with the dissertation

i. *WO_3 Sensors selective to oxidizing gases*
S. Vallejos, V. Khatko, J. Calderer, E. Llobet, X. Correig
Conference on Electronic Devices CDE, Poster presentation, Madrid, Spain (2006)

ii. *Ozone monitoring by micro-machined sensors with WO_3 sensing films*
V. Khatko, S. Vallejos, K. Aguir, K. Ngo, J. Calderer, I. Gràcia, C. Cané, E. Llobet, X. Correig
Proc. 20th European Conference on Solid State Transducers, EUROSENSORS XX, Göteborg, Sweden 2 (2006) 116-117

iii. *Micro - machined WO_3 - based sensors selective to oxidizing gases*
S. Vallejos, V. Khatko, J. Calderer, I. Gràcia, C. Cané, E. Llobet, X. Correig
32nd International Conference on Micro- and Nano-Engineering MNE, Poster presentation, Barcelona, Spain (2006)

iv. *Sensing properties of WO_3 films for monitoring ozone*
S. Vallejos, V. Khatko, K. Aguir, M. Stankova, K. Ngo, J. Calderer, E. Llobet, X. Correig
Proc. Electronic Devices and Systems EDS, Brno, Czech Republic (2006) 222 - 225

v. *Sensor micro-systems with tungsten trioxide sensing films*
V. Khatko, S. Vallejos, J. Calderer, I. Gràcia, C. Cané, E. Llobet, X. Correig
Internacional Meeting on Chemical Sensors IMCS, Poster presentation, Bresia, Italy (2006)

vi. *Structural features of WO_3 thin film sensing layers deposited with interruptions*
V. Khatko, S. Vallejos, J. Calderer, E. Llobet, X. Correig
Proc. Electronic Devices and Systems EDS, Brno, Czech Republic (2005) 264 -268

vii. *Gas sensing properties of WO_3 thin films deposited with interruptions*
V. Khatko, S. Vallejos, J. Calderer, E. Llobet, X. Vilanova, X. Correig
19th European Conference on Solid State Transducers, EUROSENSORS XIX, Barcelona, Spain (2005) TP20

viii. *Technology of metal oxide thin film deposition with interruptions*
V. Khatko, J. Calderer, S. Vallejos, E. Llobet, X. Correig
Euromat, Praga, Poster presentation, Czech Republic (2005)

ISBN:978-84-691-9748-6 /DL:T-1249

Stella Vallejos Vargas gratefully acknowledges the pre-doctoral scholarship from the Universitat Rovira i Virgili (URV).

Furthermore, the collaboration of the Universitat Politècnica de Catalunya (UPC), the Centro Nacional de Microelectrónica (CNM) and the Laboratoire Matériaux et Microélectronique de Provence (L2MP) is gratefully acknowledged.

Agradecimientos

La experiencia se ha encargado de demostrar que no hay trabajo en el mundo que se elabore sin la ayuda de otras personas. Tan cierto es esto que hoy en día se dedican las primeras paginas de los libros y/o tesis, como es el caso, a agradecer a las personas y las instituciones que han colaborado en la consecución del objetivo. Conciente de la importancia de esta ayuda quiero agradecer a todas las personas que contribuyeron directamente al desarrollo y culminación de esta tesis.

- De manera muy especial y públicamente a mi director de tesis el Dr. Viacheslav Khatko por sus enseñanzas a lo largo de estos cuatro años, su apoyo y comprensión. Sin él esta tesis no habría sido posible.
- Al Dr. Josep Calderer por su colaboración y enseñanzas en el trabajo de sala blanca.
- A la Dra. Isabel Gràcia y el Dr. Carles Cané por su contribución en la fabricación de los sustratos micro-mecanizados.
- Al Dr. Xavier Vilanova, al Dr. Eduard Llobet y al Dr. Xavier Correig por todo el apoyo brindado a lo largo de estos cuatro años.
- Al Dr. Khalifa Aguir y al Dr. Kieu An Ngo por su ayuda en la caracterización de los sensores durante mi estancia en Marsella.
- A Mariana Stankova por encaminar mis primeros pasos en el campo de los sensores de gas, su permanente ayuda durante el doctorado y su sincera amistad.
- A Julio Tinoco por sus consejos tanto en la preparación experimental como en la redacción de la tesis, su apoyo y su linda amistad.
- A Edwin Espinosa por su permanente colaboración y ayuda en la realización del montaje experimental, por todas las experiencias compartidas, por ser el “amigo mío” en todo lo que encierra el significado de esa palabra.
- A Raúl Calavia, por su ayuda en el tema de caracterización de gases y las tantas conversaciones compartidas.
- A Francesc Guirado, Mercè Moncusí y Arantxa Vilalta por su colaboración en la caracterización de las capas activas.

También quiero agradecer a todas aquellas personas que me brindaron su apoyo incondicional y cariño a lo largo de estos años, todos ellos saben cuánto los quiero.

- A mis papitos, mi hermano y toda mi familia que desde lejos siempre han estado conmigo apoyándome y dándome ánimos para continuar, los quiero mucho.
- A Lukas por su cariño, su compañía, su ayuda y apoyo todos estos años, especialmente durante la redacción de este documento.
- A Mariona por su sincera amistad en todo momento y el optimismo que me brindo durante la redacción de la tesis.
- A Alex, Fer, Edgar, Eliana, Mauricio y Zdenek, a los cuales considero como una familia. Todos ustedes hicieron inolvidable mi estadía en Tarragona.
- A Margarita por todo su apoyo y consejos y por darme ese positivismo que la caracteriza.
- A mis amigos y compañeros de estudio de Bolivia: Xime, Gon, Toño y Juca, que siempre han estado presentes en mis pensamientos y mi corazón.
- A los compañeros de Marsella Sami Gomri, Tomas Fiorido y Ahmed Labidi por su grata compañía durante mi estancia.

ISBN:978-84-691-9748-6 /DL:T-1249

What we know is not much.
What we do not know is immense.

Pierre-Simon Laplace

ISBN:978-84-691-9748-6 /DL:T-1249

Dedicated to
Ma. Elena, Porfirio,
Sergio & Lukas

Contents

Introduction i

Aim of the dissertation iii
Objectives of the work iii
Scientific contribution iii
Dissertation structure iv

Chapter 1. State-of-the-art

1.1 Solid state gas sensors 2
1.1.1. Gas solid interactions: receptor function 3
1.1.2. Grain size effects: transducer function 7
1.1.3. Microstructure effects: utility factor 9
1.1.4. Grain size effects: experimental approach 11
1.2 Metal oxide deposition techniques 13
1.2.1. Powder/slurry techniques 13
1.2.2. CVD techniques 15
1.2.3. PVD techniques 16
1.3. Tungsten trioxide (WO_3) 20
1.3.1. Structural evaluations of WO_3 thin films 20
1.3.2. WO_3-based gas sensors 23
1.3.3. WO_3 gas sensors based on PVD techniques 27
1.4. Summary and outlook 32
Bibliography 33

Chapter 2. Experimental

2.1. Sensor technology
2.1.1. Micro-machined substrate technology 40
2.1.2. WO_3 thin film deposition 42
2.1.2.1. Interruption regime 42
2.1.2.2. Floating regime 45
2.1.2.3. Gas sensing film formation 47
2.2. Characterization techniques
2.2.1. Morphological characterization 49
2.2.2. Film thickness measurements 50
2.2.3. Structural characterization 50
2.2.4. Gas sensing characterization 51
2.3. Summary and outlook 54
Bibliography 55

ISBN:978-84-691-9748-6 /DL:T-1249

Chapter 3. Results: Part I

3.1. Physical characterization
3.1.1. WO_3 thin films deposited by interruptions regime 58
3.1.1.1. Film thickness 58
3.1.1.2. Structural features 60
3.1.1.3. Morphology of the WO_3 films 62
3.1.1.4. Discussion 66
3.1.2. WO_3 thin films deposited by floating regime 66
3.1.2.1. Structural features 66
3.1.2.2. Morphology of the WO_3 films 68
3.1.2.3. Discussion 69
3.2. Summary and outlook 70
Bibliography 71

Chapter 4. Results: Part II

4.1. Gas sensing characterization of WO_3
4.1.1. WO_3 thin films deposited by interruptions regime 74
4.1.1.1. Sensitivity 74
4.1.1.2. Selectivity 82
4.1.1.3. Stability 83
4.1.1.4. Discussion 85
4.1.2. WO_3 thin films deposited by floating regime 88
4.1.2.1. Sensitivity 88
4.1.2.2. Selectivity 91
4.1.2.3. Stability 93
4.1.2.4. Discussion 94
4.2. Summary and outlook 97
Bibliography 98

Conclusions 101

Appendix 103

UNIVERSITAT ROVIRA I VIRGILI
STUDY OF STRUCTURAL AND SENSING PROPERTIES OF TUNGSTEN TRIOXIDE THIN FILMS
DEPOSITED BY RF SPUTTERING
Stella Vallejos Vargas
ISBN:978-84-691-9748-6 /DL:T-1249

Introduction

UNIVERSITAT ROVIRA I VIRGILI
STUDY OF STRUCTURAL AND SENSING PROPERTIES OF TUNGSTEN TRIOXIDE THIN FILMS
DEPOSITED BY RF SPUTTERING
Stella Vallejos Vargas
ISBN:978-84-691-9748-6 /DL:T-1249

Sensor technology shows itself as one of the most important technologies of the future with a huge variety of applications, which go from the industry sector to the private sector. At present, more and more gas sensors are used to detect and monitor an assortment of gases and vapours including toxic or explosive gases, humidity and odours. The most important field of application of gas sensors are related with the automotive, industrial, and aerospace sector (where gas sensors are needed to detect NO_x, O_2, NH_3, SO_2, O_3, hydrocarbons, or CO_2 in exhaust gases for environment protection), the food industries (where gas sensors are used for control of fermentation process), the domestic sector (where CO_2, humidity and combustible gases have to be detected), the medical sector (where gas sensor are applied in diagnostic and patient monitoring) and the security sector (where gas sensor are required to detect traces of explosives). Although, conventional techniques such as mass spectrometry or gas chromatography can be used in some applications mentioned before with high selectivity and sensitivity, it is obvious that their use is limited by cost, instrumentation, complexity and size. Thus, solid state gas sensors, in particular those ones based on metal oxide films, are the most common alternatives due to their low cost, mobile applications as well as their compatibility with the microelectronic technologies. Unfortunately the lack of selectivity and long term stability represents a big challenge for this kind of devices. As a result, the development of high sensitive gas sensors with small cross sensitivity (high selectivity) and long term stability is the subject of intensive research.

So far, several strategies based, for instance, on specific surface additive, catalyst and promoters, temperature controls and the use of filters have been studied in order to solve partially the problematic of metal oxide based gas sensor. Nevertheless the author believes that the initial fundamental step to improve the performance of these devices is connected with a recent strategy that attempts to find new methods to increase the surface area of the sensing active layer, since the sensor performance is mainly related to the surface-volume ratio of the sensing film.

In essence, the research lines carried out to reach sensitive layers with high surface areas could be classified in two groups. The first one was founded on obtaining nano-particles based metal oxides via chemical or physical processes

and the second one was based on using special methods of preparation for the surface patterning of active layers (e.g. highly nano-porous alumina templates). Later option seems to be a good alternative to tackle this aim but, in our opinion, without methods to prepare nano-particles based sensing films this option will not be feasible. Hence, it is important to develop methods that allow obtaining metal oxide composed with nano-particles.

Aim of the dissertation

The aim of the dissertation is to develop sputtering techniques to deposit gas sensing films with nanometer grain size.

Objectives of the work

The overall objective of this work is to evaluate the structural and sensing properties of WO_3 thin films deposited by the interruption and floating regimes. In this context, the specific goals associated with the overall objective are:

- To deposit WO_3 thin films by rf sputtering technique using the interruption and floating regimes. At the same time, to investigate the influence of various parameters of deposition (e.g. deposition time, sputtering power density, interruption time and number of interruptions) on the physical and sensing properties of the film by means of appropriate and available techniques of characterization.

- To fabricated micro-machined gas sensor based on WO_3 thin films prepared by the interruption and floating regimes, as well as, to characterize the micro-sensor response to various toxic gases by dc measurements.

Scientific contribution

This dissertation presents a summary of the author's work in the last four years in developing new technologies of metal oxide thin film deposition for gas sensing applications using rf sputtering technique. The work carried out for this dissertation was experimental in nature and it was complemented by means of

UNIVERSITAT ROVIRA I VIRGILI
STUDY OF STRUCTURAL AND SENSING PROPERTIES OF TUNGSTEN TRIOXIDE THIN FILMS
DEPOSITED BY RF SPUTTERING
Stella Vallejos Vargas
ISBN:978-84-691-9748-6 /DL:T-1249

different characterization techniques used in order to study the physical and sensing properties of the films deposited.

The novelty of the deposition method consists in the creation of metal oxide films with small grain size using two special regimes during sputtering deposition. The first one – *interruption (or interrupted) regime* – implies deposition of the film with one or several interruptions of the deposition process. In this case "extra" interfaces are introduced into the body of the film, where an equilibrium surface is formed due to the free surface bond saturation by the atoms from residual atmosphere and/or the structural relaxation of the interface during the interruption. The second one – *floating regime* – consists of introducing "extra" interfaces into the body of the film by means of the interruptions and the sputtering power density being changed during the film deposition. As a rule a low deposition rate is set during the initial stage of the film deposition and a high deposition rate is used during the final stage of the deposition.

Dissertation structure

The dissertation is organised as follows:

The first chapter presents an overview of the state-of-the-art where three sections are distinguished. The first section gives a general idea to create a solid state gas sensor, the most important characteristics of the gas interaction with the surface of the semiconductor and the working principles of solid state gas sensor. The attention is focussed on the sensing active layer, specifically, on its contribution to the performance of the whole sensor device. The theory and the experimental data reported until now are contrasted in this section. The second section provides a review of the metal oxide thin film deposition methods used for gas sensing applications given an emphasis on sputtering deposition process, since this technique is used in this work presented here. Finally, the third section summarizes the physical and electrical features of the tungsten trioxide (WO_3) films which were chosen as sensing material due to its good sensitivity to nitrogen dioxide (one of the most important air pollutant gases).

ISBN:978-84-691-9748-6 /DL:T-1249

The second chapter deals with the sensing layer deposition technology. The features and basic fundaments of the special deposition regimes used in this work are described there. On the other hand, a description of the equipment to deposit the films and to characterize the physical and sensing properties of the films is presented as well.

The third chapter presents the results obtained by the structural and morphological characterizations of the sensing films. The influence of the deposition with the interruptions on the thin film properties is confirmed by X-Ray diffraction (XRD), Atomic Force Microscopy (AFM), ellipsometry and Auger spectroscopy. Basically, a decrease in WO_3 grain size is connected with the application of the special deposition regimes.

The fourth chapter summarizes the results obtained by the characterization of the WO_3 based gas sensor to various oxidizing and reducing gases. The characterizations are based on the variations of the electrical conductance either in air or in air plus target gas. The analysis of experimental data shows that WO_3 sensing layer responses are enhanced by the use of the special deposition regimes.

Finally, the conclusions of the thesis are presented.

UNIVERSITAT ROVIRA I VIRGILI
STUDY OF STRUCTURAL AND SENSING PROPERTIES OF TUNGSTEN TRIOXIDE THIN FILMS
DEPOSITED BY RF SPUTTERING
Stella Vallejos Vargas
ISBN:978-84-691-9748-6 /DL:T-1249

CHAPTER 1

State-of-the-art

UNIVERSITAT ROVIRA I VIRGILI
STUDY OF STRUCTURAL AND SENSING PROPERTIES OF TUNGSTEN TRIOXIDE THIN FILMS
DEPOSITED BY RF SPUTTERING
Stella Vallejos Vargas
ISBN:978-84-691-9748-6 /DL:T-1249

1.1. Solid state gas sensors

The semiconductor gas sensors are based on metal oxides with wide band gaps. These devices have the property to change the conductivity of the sensing material in the presence of the determinate gas. The working temperature at which these devices are more efficient can vary depending on the gas atmosphere and properties of the sensor material. As these temperatures range from 200ºC to 800ºC [1, 2], it is necessary to install a heating system in the sensor device. Thus, a simple semiconductor gas sensor is composed by the electrodes to measure the conductivity changes, the heater to reach the optimum sensing temperatures and the substrate which provides the mechanical support and electrical contact to the electrodes, heater and sensing material. In recent years, the evolution of micro-machining as a fabrication technology for gas sensor substrates has allowed miniaturization to progress toward a smaller scale with more convenient fabrication methods. The low thermal conductivity and low thermal mass of the membrane material in micro-machined sensors lead to very low power consumptions (30 - 50 mW) [3]. Although each sensor component plays an important role in the whole performance of a semiconductor gas sensor, the core of this device is placed at the active sensing element which, according to Yamazoe et. al. [4], possesses a receptor function and a transducer function (see Figure 1.1). The receptor is considered to be at the surface of the semiconductor where the chemical species undergo adsorption, reaction and desorption. On the other hand, the microstructure of the semiconductor film is seen as the transducer which converts the chemical signal produced by the gas-solid interaction into an output signal. The output is usually an electric signal, however, the measurement of the thermo-voltage or of the changes in the sensor temperature is also possible [3]. The overall response function of the sensor can be described as a superposition of the sensor's transducer and receptor functions [5].

ISBN:978-84-691-9748-6 /DL:T-1249

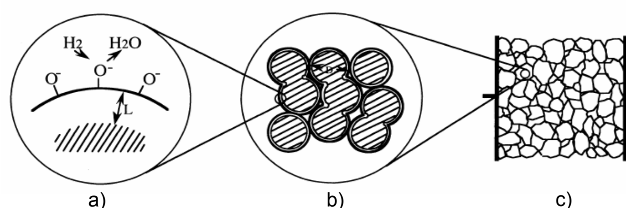

Figure 1.1. Receptor and transducer functions of semiconductor gas sensor. a) surface: receptor function, b) microstructure: transducer function, c) element: output resistance change [4].

1.1.1. Gas-solid interactions: receptor function

As soon as a semiconductor is brought into contact with a gaseous medium its surface begins to be covered by the molecules of the gas, i.e. adsorption has set in. The process ceases when an equilibrium between the surface and gaseous phase is established, i.e. when the number of molecules passing from the gaseous phase to the surface per unit time is equal (on the average) to the number of molecules leaving the surface to the gas over the same interval. The presence of the molecules adsorbed by the semiconductor surface changes the properties of the later. Thus adsorption is the agent by which the ambient acts on the surface and, indirectly, on some of the bulk properties of the semiconductor.

Two types of adsorption are distinguished, namely, physical adsorption (physisorption) and chemical adsorption (chemisorption). The difference between physisorption and chemisorption lies in the difference in the forces that retain the adsorbed molecules on the surface of the solid. Indeed, the forces that arise between a solid and a foreign molecule and produce adsorption can be of different nature. For instance, they may be of electrostatic origin, such as Van der Waals' forces or electrostatic polarization forces. In this case we speak about physical adsorption which is associated with small adsorption energies, up to 0.01−0.1 eV [6]. But if the forces responsible for adsorption are of a chemical nature (forces of the exchange type), we are dealing with chemisorption. Here adsorption constitutes a chemical combination of the molecule with the solid. As in every chemical compound, the forces making up the bond are, in the given case, covalent forces, but ionic interaction may be involved to a certain extent. The adsorption energies, in this case, are about 1 eV [6]. Figure 1.2 depicts an

ISBN:978-84-691-9748-6 /DL:T-1249

adsorption curve that represents the energy E of the system as function of the distance *r* between the adsorbent surface and the particle being adsorbed.

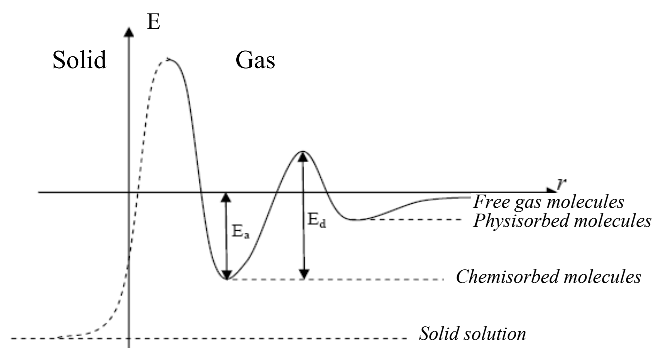

Figure 1.2. Energy of a gas molecule at a solid gas interface. E_a: adsorption energy, E_d: desorption energy [7].

Whereas physisorption is not an activated process, usually chemisorption is activated adsorption. However, the presence of activation energy is not necessarily a criterion of chemisorption, since there are cases where chemisorption proceeds without activation energy. Such is the case of the adsorption of common gases (H_2, CO, O_2 and N_2) by transition metals where there is not activation energy or the difference E_d-E_a (see Figure 1.2) is negligibly small [7].

In fact, when chemisorption occurs the chemical interaction between the semiconductor and the ambient gas molecules leads to charge transfer between the semiconductor and chemisorbed species. Conventional models of gas adsorption on solid surface, such as Langmuir's model [6], explain this interaction assuming that the binding energy between the adsorbate and adsorbent is constant. However, this assumption is inadequate due to in the case of chemisorption on semiconductors where charge transfer is involving the binding energy varies with the degree of coverage of chemisorbed species due to the strong electronic interaction between the adsorbate and adsorbent. The Wolkenstein's model of chemisorption on semiconductors [6] takes into account these electronic interactions and their effect on the adsorptivity of the semiconductor. Thus, this model is widely accepted in the theory of heterogeneous catalysis and semiconductor surface physics and it is generally applicable to different kinds of semiconductor gas sensors [8, 9]

According to Wolkenstein [6], two forms of chemisorption may be distinguished:

1. *Weak* chemisorption, in which the chemisorbed particle (considered together with its adsorption center) remains electrically neutral and the bond between the particle and crystal lattice is established without the participation of a free electron or hole from the crystal lattice.

2. *Strong* chemisorption in which the chemisorbed particle retains in its neighbourhood a free electron or hole from the crystal lattice (and it is, thus, an electrically charged compound) and the free electron or hole plays a direct part in the chemisorption bond. In this context, it can be distinguished two types of strong bonds: *n-bond* (or acceptor bond) is one in which a free electron captured by the adsorbed particle participates, *p-bond* (or donor bond) is one in which a hole captured by adsorbed particle participates.

In agreement with this model the localized electronic states are created by chemisorbed species. These states serve as traps for electrons or holes (acceptor-like or donor-like states, respectively) depending on their nature. Figure 1.3 shows the energy-band diagram for the case of depletive chemisorption of an acceptor-like univalent particle on an (non-degenerate) n-type semiconductor. Considering only one gas species and assuming that chemisorption is the only source for surface charging. Thus, at the beginning of chemisorption (i.e. at zero coverage) the energy bands are assumed to be flat, as shown in Figure 1.3(a). A free particle from the gas phase (designated by A_∞) approaching the surface may become chemisorbed as a neutral adsorbate $A^0_{chem.}$ (weak chemisorption). In this process, the free energy of the system decreases by q^0 (the binding energy of the neutral adsorbate, $E_B\,(A^0_{chem}) = q^0$). If a free electron (designated by ● in Figure 1.3) is available for interaction with a chemisorbed species, the later may capture it and become chemisorbed as negatively charged adion A^-_{chem} (strong chemisorption). In this case the free energy of the system decreases even further by $(E_C^b - E_{SS})$, where E_C^b is the energy level of conduction band electrons in the bulk of the semiconductor and E_{SS} is the energy level of the chemisorption-induced surface state. Thus, the binding energy of the charged adion is $E_B\,(A^-_{chem}) = q^0 + (E_C^b - E_{SS})$. Figure 1.3 shows that $(E_C^b - E_{SS}) = (E_C^S - E_{SS}) + eV_S$, where E_C^S is the conduction

ISBN:978-84-691-9748-6 /DL:T-1249

band edge at the surface and eV_S is the chemisorption-induced surface potential barrier which is associated with a space-charge region (SCR), e is (the absolute value) the electron charge and V_S is the surface potential. The height of eV_S and depth of SCR (W_{SCR}) of the band bending depend on the surface charge which is determined by the amount and type of adsorbed oxygen. At the same time the SCR depends on the Debye length L_D which is a characteristic of the semiconductor material for a particular donor concentration [10].

$$L_D = \sqrt{\frac{\varepsilon_0 \varepsilon k_B T}{e^2 n_d}}$$ **Eq. 1.1.** Debye length

where k_B is Boltzmann's constant, ε the dielectric constant, ε_0 the permittivity of free space, T the operating temperature, e the electron charge, and n_d the carrier concentration which corresponds to the donor concentration assuming full ionization.

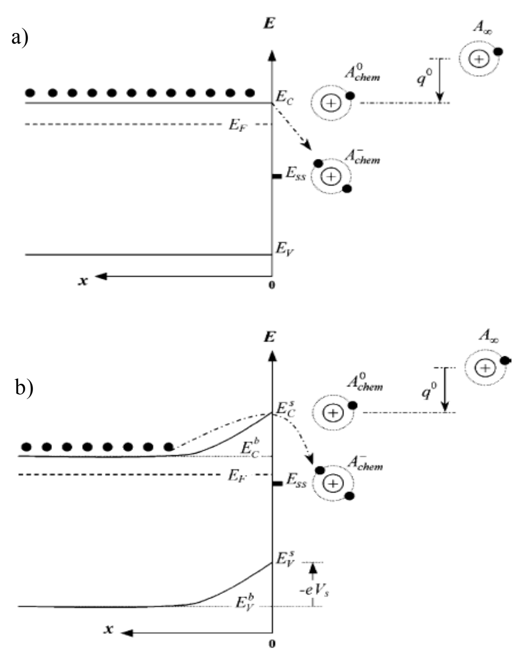

Figure 1.3. Energy-band diagram for depletive chemisorption of an acceptor like adsorbate (e.g. oxygen) on an n-type semiconductor: a) at the beginning of chemisorption (zero coverage), b) at thermal equilibrium. A_∞, A^0_{chem} and A^-_{chem} designate a free particle in the gas phase, a neutral adsorbate, and a negatively charged adion, respectively. E_C, E_V, and E_F are the conduction band, valence band, and Fermi level, respectively. The superscripts ''b'' and ''s'' denote bulk and surface properties, respectively [9].

As mentioned above, when n-type semiconductor undergoes chemisorption, equilibrium SCR near to the surface is formed. The depth of this SCR (W_{SCR}) may be increased by the adsorption of oxidizing gases such as NO_2 or decreased by the adsorption of reducing gases such as CO [3, 11, 12] (see Figure 1.4)

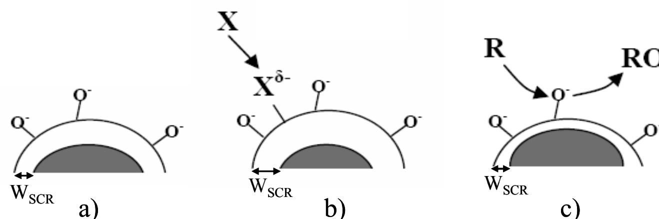

Figure 1.4. Schematic illustration of n-type semiconductor surface when it reacts under exposure to air (a), oxidizing gases (b) and reducing gases (c). W_{SCR} denotes the thickness of the space charge region [3].

1.1.2. Grain size effects: transducer function

So far in the literature, the effects of the microstructure on the sensitivity and specifically on the transducer function of the gas sensor have been formulated in two ways [13, 14]. The first one has been presented in terms of the relative dimension of crystallites or the neck between the crystallites and Debye length in the solid [1, 5, 10, 15-17]. On the other hand, the second one has used percolation theory described as network of barriers where their characteristics depend on the changes in the barrier heights due to gas interactions [13, 18]

First formulation is widely used by the interpretation of grains size effects in metal oxide gas sensor. For this reason, here after, it is presented the basis of this semiquantitative model. According to this model the sensor consists of partially sintered crystallites that are connected to their neighbours by necks. Those interconnected grains form larger aggregates that are connected to the neighbours by grain boundaries (GB).

Three cases can be distinguished according to the relationship between the grain size (D) and the wide of the depletion layer (W_{SCR}), which is produced around the surface of the crystallite due to the chemisorbed adions (see section 1.1.1). Figure 1.5 depicts these three cases.

UNIVERSITAT ROVIRA I VIRGILI
STUDY OF STRUCTURAL AND SENSING PROPERTIES OF TUNGSTEN TRIOXIDE THIN FILMS
DEPOSITED BY RF SPUTTERING
Stella Vallejos Vargas
ISBN:978-84-691-9748-6 /DL:T-1249

1. Case (a) or *GB control*, i.e., when D>>2W_{SCR}, most of the volume of the crystallite is unaffected by the surface interactions with the gas phase. In this case the predominant effect of the ambient gas atmosphere on the sensor conductivity is introduced via GB barriers for intercrystallite charge transport from one grain (agglomerate) to another. Therefore, the conductivity σ depends exponentially on the barrier height eV_B.

   $$\sigma \propto \exp\left(\frac{-eV_B}{k_B T}\right)$$ **Eq. 1.2.** Sensor conductivity

   Here V_B is the GB potential, k_B is Boltzmann's constant, and T is the operating temperature. In this context, for large grains D>>2W_{SCR} the gas sensing mechanism is controlled by the GB barriers. Furthermore, the GB barriers are independent of the grain size and therefore the sensitivity is independent of D.

2. Case (b) or *neck control*, i.e., when D≥2W_{SCR}, as the grain size decreases the depletion region extends deeper into the grains and consequently the core region, which is relatively conductive with respect to the depletion region adjacent to the surface, becomes smaller. When D approaches but still larger than 2W_{SCR}, the depletion region that surrounds each neck forms a constricted conduction channel within each aggregate. Consequently the conductivity depends not only on the GB barriers but also on the cross section area of those channels. This cross section area is proportional to $(X - W_{SCR})^2$, where X is the neck diameter. In agreement with [10, 15], X is roughly proportional to D, being well approximated by X≈0.8D. As a result, the conductivity is a function of the radio X/W_{SCR}. In summary, the current constriction effect adds up to the effect of the GB barriers. Thus, the gas sensitivity is enhanced with respect to case (a). Moreover, the sensitivity to gases becomes grain size dependent from grain size and it increases when D decreases.

3. Case (c) or *grain control*, i.e., when D<2W_{SCR}, in this case the depletion region extends throughout the whole grain and the crystallites are almost fully depleted of mobile charge carries. As a result the conductivity decreases steeply since the conduction channels between the grains are vanished. The energy bands are nearly flat throughout the whole structure of the interconnected grains, and since there are no significant barriers for

intercrystallite charge transport the conductivity is essentially controlled by the intercrystallite (grain controlled).

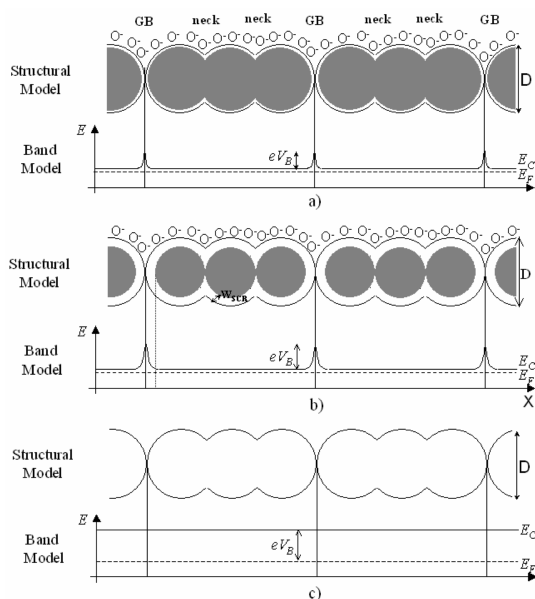

Figure 1.5. Schematic model of the effect of the crystallite size on the sensitivity of metal-oxide gas sensor: a) GB control $D>>2W_{SCR}$, b) neck control $D\geq 2W_{SCR}$ and c) grain control $D<2W_{SCR}$. Adapted from [10].

1.1.3. Microstructure effects: utility factor

Besides the particle size, the of the microstructure of the sensing layer is an important factor to obtain good response time and sensitivity of the gas sensors. Sensing layers are penetrated by oxygen and analyte molecules so that a concentration gradient is formed which depends on the equilibrium between the diffusion rates of the reactants and their surface reaction. This effect produces also a spatial variation of the conductivity through the structure of the sensing film [1, 13]. For this reasons, the microstructure may have effects in both the receptor and transducer function.

Recently, Yamazoe and co-workers investigated the gas-diffusion in thin film semiconductor gas sensor [19-22]. By the studies they found that a lower film thickness together with a higher porosity contributes to a higher sensitivity and faster response time of the sensor. Moreover, they concluded that the sensor

ISBN:978-84-691-9748-6 /DL:T-1249

performance is strongly influenced by what they call *utility factor* which is linked with the microstructure of the sensing layer [23]. This factor concerns the accessibility of inner oxide grains to the target gas. The importance of this factor is obvious when one considers that the target gas reacts with the oxide surface on the way of diffusing into the bulk of device. If the rate of reaction is too large compared with that of diffusion, the gas molecules can not access the grain located at inner sites, leaving them un-utilized for gas sensing and thus resulting in a loss in sensor response. The existence of this factor was suspected a fairly long time ago from familiar volcano-shaped correlations between sensor response and operating temperature, but quantitative understanding of it was made possible only recently for thin film devices derived from SnO_2 sols [20, 21]. When a thin film with pores of a uniform radius is exposed to a target gas at a concentration of C_S, the relative concentration (C/C_S) inside the film can be formulated by solving a simple diffusion-reaction equation under the steady state conditions as:

$$\frac{C}{C_S} = \frac{\cosh\left(1 - x/L\right)m}{\cosh m}$$

Eq. 1.3. Relative concentration of the gas inside a thin sensing film.

Here, C is the concentration of target gas in the film, C_S the concentration of target gas at x=0, x the distance from the surface (see Figure 1.6.a), L the film thickness and m is a non-dimensional quantity defined by $m=L(k/D_k)^{1/2}$, where k is rate constant of a first order surface reaction and D_k the Knudsen diffusion coefficient. According with [20] (see Figure 1.6., b), for $m<1$, significant part of target gas can reach the bottom of the film. On the other hand, for $m>3$, most part of the gas is consumed before arriving at the bottom and at extremely large m only the surface region is accessible to the gas. When the increase of sheet conductance at given x is assumed to be proportional to the target gas concentration at that point as a first approximation, the sensor response of the film can be derived easily by integrating the sheet conductance over the film. On the base of these assumptions, Sakai et al. [20], found the following expression for the sensitivity:

$$S = 1 + C_S \frac{\tanh m}{m}$$

Eq. 1.4. Sensitivity as function of the utility factor

Here, (tanh m)/m is defined as the utility factor. Thus, as m increases the utility factor decreases, therefore m should be kept small or, small L and small k/D_k ratio

ISBN:978-84-691-9748-6 /DL:T-1249

should be combined to keep the utility factor close to unity. Since D_k is directly proportional to pore radius *r*. The pore radius should be *r* as large as possible and *L* as small as possible in order to obtain higher utility factor. The pore radius *r* is known empirically to be roughly comparable to the grain size (D) involved so that, **the utility factor can also be controlled by the grain size.**

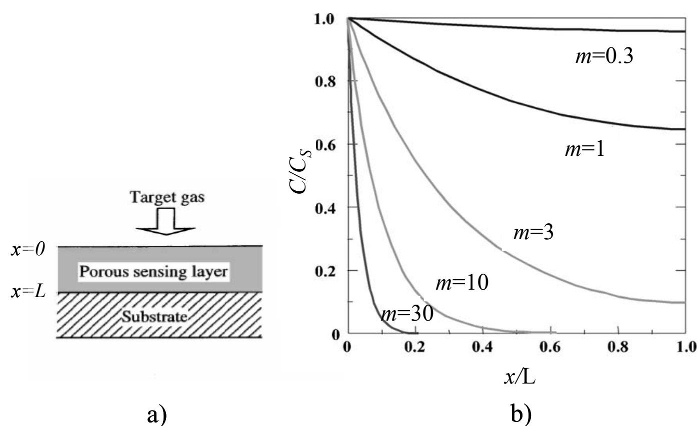

Figure 1.6. Illustration of a gas sensing film (a) and depth profiles of gas concentration inside a porous sensing film at various values *m* (b). Adapted from [20].

1.1.4. Grain size effects: experimental approach

Since from a theoretical point of view the particle size is expected to have a substantial impact on sensor performance, much experimental work has been done to investigate this effect. Table 1.1 shows the correlation between sensor response and grain size effects reported in various studies.

Table 1.1. Correlation between grain size and sensor response reported by various studies.

Deposition technique	Material	Grain size (nm)	Sensor response	Target Gas	Concentration (ppm)	Operating temperature (ºC)	Ref
Sol gel	SnO_2	27 – 5	45 – 170	H_2	800	300	[10]
Sol gel	SnO_2	27 – 5	10 – 60	CO	800	300	[10]
Sol gel	WO_3	33 – 25	25 – 90	NO_2	10	300	[24]
Sol gel	WO_3	33 – 25	40 – 70	NO	200	300	[24]
Sol gel	SnO_2	2 – 300	10 – 110	CO	500	-	[25]
PVD	WO_3	21 – 10.2	14 – 32	NO_2	0.2	150	[26]
PVD	WO_3	10.2 – 9.1	32 – 233	NO_2	0.2	150	[26]
Sol gel	InO_3	50 – 5	1.5 – 40	NO_2	1	250	[27]

ISBN:978-84-691-9748-6 /DL:T-1249

In the early 1990s Yamazoe and co-workers reported the dependence of gas sensor sensitivity on SnO_2 grains size. They found that for H_2 and CO the sensitivity increased steeply as the grain diameter decreased below 10 nm [10]. Some years later the same group investigated the sensitivityof WO_3 nanoparticles ranged from 16 to 57 nm to 10 ppm of NO_2 and 200 ppm of NO. The results showed that WO_3 films composed by grains of D=25 nm present three or four times larger sensitivities than those ones composed by grains of D>33 nm [24]. Recently, Lu et al. described a comparable correlation for SnO_2 nanoparticles in the range of 2-300 nm at 500 ppm CO. They observed that the sensor signal increased drastically if the particle diameter became smaller than 10 nm [25]. Cantalini et al. observed that the sensitivity of WO_3 films to 0.2 ppm of NO_2 was 7 times better when the grain diameter was reduced from 10.2 to 9.1 nm [26]. In addition, Gurlo et al. concluded that nanocrystaline In_2O_3 with the particle size below 50 nm enhanced the sensor sensitivity to NO_2 (1 ppm) [27].

Most recently, Korontcenkov et al. reported that a decreasing grain size increases the sensitivity following the empirical scaling law $S \approx D^{-n}$, where $n \approx 3\text{-}5$. Simultaneously, they observed a decrease of the In_2O_3 response time to O_3 and they proposed the following dependence $\Delta t_{90\%(res)} \approx D^2$ [28]. In contrast to these results, it has also been shown that the grain size is not crucial in In_2O_3 films for the detection of reducing gases [29]. This metal oxide is a highly deficient oxide. Oxygen is chemisorbed as O^{-2} ions on lattice sites oxidizing In^{2+} to In^{3+}. This redox reaction is inverted upon exposure to reducing gases, from which the formation of a surface layer with higher conductance on the grains take place. As a consequence, a size-dependent sensitivity should be expected in In_2O_3 for the detection of oxidizing gases, which should again follow the same mechanism as described above.

Although all these results are not directly comparable to each other, since different materials and different methods for the analysis of the particle size have been applied (X-ray diffraction, transmission electron microscopy, atomic force microscopy). They have demonstrated that, in general, reducing the particle size increases the sensitivity of metal oxide.

1.2. Metal oxide deposition techniques

In section 1.1., it was pointed out the importance of the morphological and microstructural properties of the sensing active layer in metal oxide gas sensors. It was concluded that the performance of the active layer is directly related with its granular structure, which is actually controlled by grain size. At present a significant fraction of the overall research and development efforts in metal-oxide-based gas sensors is directed toward sensor miniaturization which requires sensitive-layer deposition techniques that are compatible to the micro-fabrication processes. Therefore, it is evident the necessity to develop suitable deposition technologies to be able to create metal oxide films with smaller grain sizes and compatible to the micro-fabrication processes. Either traditional thin film deposition methods or modification of these methods have been studied with these purposes. However, the control of an idealized granular structure still represents a big challenge.

In the state-of-the-art three main techniques for metal oxide sensing film deposition are distinguished [30, 31]: powder/slurry, chemical vapor deposition (CVD) and physical vapor deposition (PVD). As it will be noted in the following subsections, each of these techniques involves a different nature of the film formation. Therefore, this section pretends to describe the basic fundamentals of thin film deposition techniques as well as to summarize the progress of these techniques towards the formation of nano-particles metal oxide based-gas sensor

1.2.1. Powder/slurry techniques

Traditionally, powder/slurry techniques such as screen printing [32, 33] or sol-gel based methods [32, 34] have been attributed to thick film technology (several microns of the film thickness). Nevertheless, it is known that some powder/slurry techniques based on sol-gel [34-36] allow to deposit thin metal oxide films as

ISBN:978-84-691-9748-6 /DL:T-1249

well. That's why these techniques are described here. In essence, a sol-gel represents the transition of a system from a liquid sol (colloidal suspension of miniature solid particles in the liquid) to a viscous gel where the suspended particles of metal oxide are organized in a loose [35]. Thus, the sol-gel based techniques take advantages of the specific properties of nano-crystalline particles to form stable dispersions and suspensions that are normally deposited by:

Spray coating, which consists in the deposition of the sol-gel by spraying it onto the substrate, the layers formed by this technique are in most cases inhomogeneous [32], so that this deposition technique is unusual for gas sensing applications.

Drop coating, with this technique a drop of the solution is placed on the substrate surface using a micro-pipette or micro-injector. For a satisfactory reproducibility of the formed layer, an extremely good control of the properties of the solution to be deposited is needed. Several works report the application of this technique for gas sensor fabrication [37-39], furthermore, it is known that this method is used in the industry for the deposition of metal oxide films on micro-machined platforms [32].

Spin coating, with this technique the solution is poured onto the substrate surface and then spin-deposited. It is known that the thickness of the deposited layer can be controlled by varying the revolution rate and the sol viscosity [34]. It was reported that most of the sol-gel deposited sensing films could be used for gas sensing applications [19, 40-43].

Recent developments of sol-gel based methods

Recently, Wang et al. [41] reported a sol-gel technique employed to obtain WO_3 thin films with thickness about 200 nm by spin coating. WO_3 was produce from tungsten (VI) hexacloride dissolved into alcohol. It was shown that WO_3 nano-particles were obtained in the range of 18 nm and 69 nm. Moreover, they noted that particle size of the sol derived thin film seems to be controlled by the calcinations temperature, thus WO_3 films calcined at higher temperature (650ºC) yielded large size particles. On the other hand, Epifani et al. [42] proposed the deposition of spin coated In_2O_3 thin films using the modified process that prevents

precipitation of the indium hydroxide by complexing the indium ions before adding the base. This modification of the process allowed to obtain In_2O_3 nanoparticles ranged between 18 nm and 45 nm [43]. Finally, Choi, et al. [44] investigated a wet-process fabrication of WO_3 thin films which consists of the preparation of $WO_3 \cdot 2H_2O$ sol through a wet process starting from ion-exchange reaction of Na_2WO_4. This sol was then mixed with an organic binder (polyethylene glycol, PEG) in order to deposit uniform WO_3 thin film with 450 nm thickness by spin coating. The morphology analysis showed irregular packing of square plates of WO_3 with 500-1000 nm in width and 200-500 nm in thickness.

1.2.2. CVD techniques

Generally speaking, chemical vapour deposition technique (CVD) is the formation of the thin films via chemical reactions from gaseous precursors. The activation of the chemical reaction is initiated by thermal or electric discharge plasma. Decomposition or reduction of compounds like fluorides, chlorides, bromides, organometallics, hydrocarbons, phosphorous trifluoride and ammonia complexes provides the deposition of the metallic component. After dissociation the elements or compound to be deposited condense (react) on the substrate surface and the volatile component leaves the reaction chamber. Chemical reactions already in the gas phase lead to particle generation (powder formation). The thin film quality depends on the reaction kinetics, temperature, surface preparation, purity of the precursor, gas flow and chamber conditions. To enhance the deposition rate the use of low pressure and high temperature may be required. Plasma assisted CVD also allows to perform the deposition at lower temperature and higher deposition rate [34]. In general, the deposition process is reaction controlled. That means that the dependence of the film growth on the angle distribution of the incoming reactants is very low [45].

Recent developments of CVD

Several methods of chemical vapour deposition techniques have been used to prepare metal oxide sensing thin films. For instance, Liu et al. [46] fabricated nano-structured SnO_2 thin film gas sensors deposited by combustion chemical

UNIVERSITAT ROVIRA I VIRGILI
STUDY OF STRUCTURAL AND SENSING PROPERTIES OF TUNGSTEN TRIOXIDE THIN FILMS
DEPOSITED BY RF SPUTTERING
Stella Vallejos Vargas
ISBN:978-84-691-9748-6 /DL:T-1249

vapour deposition. The morphological characterizations of SnO_2 showed the presence of agglomerates ranged between 1 μm and 3 μm in diameter. These agglomerates were composed by finer crystals less than 30 nm in diameter. Another studied carried out by Lee et al. [47] showed that SnO_2 thin films deposited by inductively coupled plasma chemical vapour deposition (ICP-CVD) can represent an alternative approach for thin films gas sensor preparation. It was shown that SnO_2 films with nano-size grains of 12 nm were obtained by applying this technique. Furthermore, Ashraf et al. [48] reported that the aerosol assisted CVD reactions of $[W(CO)_6]$ in oxygen and containing solvents resulted in the deposition of partially reduced WO_{3-x} composed of small particles. They noticed that the size distribution of the particles varied greatly as function of the solvent. The films prepared using acetonitrile and acetone showed a similar mean particle size (~340 nm), whilst films deposited using 50:50 mixture of toluene and acetone showed a lower mean particle size (~270 nm). On the other hand, Panchapakesan et al. [49] proposed the use of metal nano-particles (e.g. Ni, Co, Fe, Cu, Ag) as seed layers for controlling the microstructure of SnO_2 films deposited by CVD. They observed that significant control of SnO_2 grain sizes between 20 nm and 121 nm was obtained depending on the seed-layer type.

1.2.3. PVD techniques

The physical vapor deposition (PVD) techniques can be divided into two groups: evaporation and sputtering.

Basically, in the *evaporation* process, a material vapor is produced in vacuum by heating the material to be deposited to a sufficiently high temperature. The temperature needed is a function of the vapor pressure of the material. The evaporation process has to be carried out in a high vacuum environment so, the transport from the evaporation point prior to the condensation area should occur without collisions between the vapor atoms and the molecules of the residual gas. The substrate is always located face down above the evaporation point at distances from few to some ten centimeters depending on the deposition area and the required film thickness homogeneity [45]. On contrary, the *sputtering* process itself uses the interaction of accelerated ions with atoms of a so-called target, containing the material to be deposited. The ions can be generated by a cold

plasma or an ion gun. The energy of the ions has to be high enough for multiple scattering in the surface region of the target. The energy and momentum transfer lead to structural changes in the near surface region of the target and to a partial emission of usually neutral atoms and/or clusters of atoms. Due to a considerable kinetic energy, more than 100 eV [50], the sputtered atoms and ions move from the target and condense on a substrate, located opposite to the target at distances between 50 and 500 mm. The target surface erodes in dependence on the ion energy, their density and the angle of incidence [45]. Sputtering is preferred over evaporation in many applications due to a wider choice of materials to work with, better step coverage, and better adhesion to the substrate. A comparison between evaporation and sputtering technique is presented in Table 1.2.

Table 1.2. Comparison between evaporation and sputtering technology [51].

Parameters	Evaporation	Sputtering
Rate	Thousand atomic layers per second	One atomic layer per second
Choice of materials	Limited	Almost unlimited
Purity	Better (no gas inclusions, very high vacuum)	Possibility of incorporating impurities (low-medium vacuum range)
Substrate heating	Very low	Unless magnetron is used substrate heating can be substantial
Surface damage	Very low, with e-beam x-ray damage is possible	Ionic bombardment damage
In situ cleaning	Not an option	Easily done with a sputter etch
Alloy compositions, stochiometry	Little or no control	Alloy composition can be tightly controlled
X-ray damage	Only with e-beam evaporation	Radiation and particle damage is possible
Changes in source material	Easy	Expensive
Decomposition of material	High	Low
Scaling-up	Difficult	Good
Uniformity	Difficult	Easy over large areas
Capital equipment	Low cost	More expensive
Number of depositions	Only one deposition per change	Many depositions can be carried out per target
Thickness control	Not easy to control	Several controls possible
Adhesion	Often poor	Excellent
Shadowing effect	Large	Small
Film properties (e.g., grain size and step coverage)	Difficult to control	Control by bias, pressure, substrate heat

ISBN:978-84-691-9748-6 /DL:T-1249

Recent developments of PVD

Early a lot of studies have been reported about the use of the evaporation [52-56] and sputtering [52, 57-63] techniques for the gas sensor fabrication. One can see that standard deposition regimes of these techniques are used in the most cases. In the last two decades some novel techniques based on evaporation and sputtering were proposed in order to prepare nano-particle based metal oxide sensing films. For instance, in 1990 a new deposition technique named rheotaxial growth and thermal oxidation (RGTO) which can use either sputtering or evaporation was proposed by Sberveglliery et al. [64]. This technique was used to prepare SnO_2 and mixed oxides like $Sn_{l-x}FeO_y$ or SnO_2-Al_2O_3 [65], first growing the metallic alloy and transforming it into an oxide compound by a thermal cycle, that in the case of mixed oxides was set at a temperature higher than the alloy melting point. The experiments carried out by this group demonstrated that this technique is an effective tool for preparing thin films with high surface to volume ratio. Recently, Nicoletti et al. [52] applied this technique to deposit SnO_2 based gas sensor. Their experiments showed that SnO_2 deposited by RTGO has an excellent response to volatile organic compounds (VOC), but the mid-term test revealed that conductivity is affected by a significant drift.

Another technique based on the evaporation was proposed in 1982 by Hara, et al. [65]. This technique is known as multilayer deposition and it allows either the modulation of the material structure or the modification of its catalytic activity. This technique was used to form mixed oxide compounds which are formed at the interface of each layer, thus compounds with low diffusion coefficient were chosen. In fact the gas-semiconductor interface was controlled by the outer layer. It was reported that CdO deposited onto SnO_2 layer forms a multiplayer with stable structure [66]. A similar technique, where RTGO and multilayer deposition were combined, was proposed by Aste et al. in 1995 [53]. This technique consists in the preparation of double-layer granular SnO_2 deposited by RGTO. The first layer is composed by single electrically non-contacted grains and the interconnection between grains is obtained by the deposition of a second layer. Aste et al noted that varying the amount of Sn deposited in the second layer could change the size of the necks between grains and could control the sensing properties of SnO_2.

Most recently Ponzoni et al. [54] presented the method based on the modified thermal evaporation technique to obtain nano-structured WO_3 thin films. This method consists in the sublimation from metallic tungsten wire followed by oxidation in low vacuum conditions and reactive atmosphere with the substrate heated at high temperature (600ºC). Morphological characterizations carried out by atomic force microscopy (AFM) showed that WO_3 agglomerates are composed of particles less than 100 nm in size.

UNIVERSITAT ROVIRA I VIRGILI
STUDY OF STRUCTURAL AND SENSING PROPERTIES OF TUNGSTEN TRIOXIDE THIN FILMS
DEPOSITED BY RF SPUTTERING
Stella Vallejos Vargas
ISBN:978-84-691-9748-6 /DL:T-1249

1.3. Tungsten trioxide (WO_3)

Tungsten trioxide (WO_3) is a wide band gap ($E_g \sim 2.6$ eV [67]), n-type semiconductor that encloses interesting physical and chemical properties, that is why it is useful for a wide spectrum of technologies applications. For instance, tungsten trioxide is an important material for electrochromic [68] and photoelectrochemical devices [69], catalyst [70] and gas sensors [71, 72]. In the present work, WO_3 is used for gas sensing applications. Therefore this section is focused on the sensing properties and structural characteristics of this metal oxide.

As a sensing material, WO_3 has demonstrated to be advantageous due to its quite good mobility (10 $cm^2/V \cdot s$) [4]. In addition, WO_3 has shown good thermal stability and low humidity interferences [73]. The later characteristic is not common for SnO_2-based gas sensors. It is important to mention that nowadays tungsten trioxide occupies up to 7% of the gas sensing applications in comparison with other metal oxides (see Figure 1.7). Although in the last 15 years the attention to WO_3 as gas sensor has increased and many studies about its application have been published, WO_3 sensing properties are not completely known and its potential is not fully exploited.

1.3.1. Structural evaluations of WO_3 thin films

The crystal structure of WO_3 is a distortion of the rhenium oxide (ReO_3) cubic structure in which the tungsten atoms are located on the cube corners and the oxygen atoms are located along the cube edges. Each tungsten atom is surrounded by six oxygen atoms forming an octahedron. The slight rotation of these octahedrons with respect to each other, as well as unequal bond lengths in the octahedral coordination, causes lattice distortion and reduces the symmetry (see Figure 1.8). The displacement of the tungsten atom inside the octahedron is

stabilized by an increase in covalence between the tungsten and oxygen atoms [74].

The distortion of WO_3 from the ideal cubic perovskite results in a number of different phases, which are stable .depending on temperature. The phase transitions and structures are complex because they involve both tilting of WO_3 octahedral and displacement of tungsten atoms away from the centres of the octahedral. Thus, WO_3 has been reported to be triclinic below 17°C, monoclinic from 17ºC to 320°C, orthorhombic from 320ºC to 720°C and tetragonal above 720ºC [75]. The phases of WO_3, lattice parameters and elemental cells angles are presented in Table 1.3.

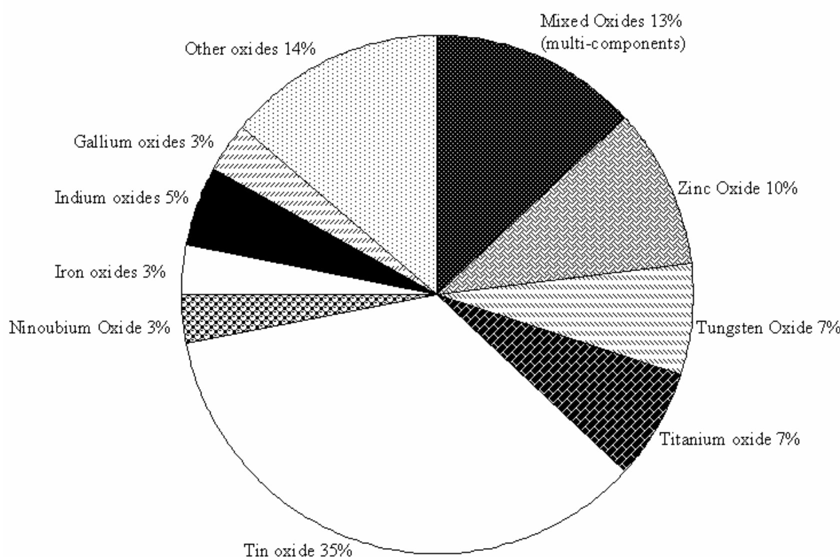

Figure 1.7. Relative comparison of different oxides used for gas- sensing application [71].

On the other hand, tungsten trioxide structure is likely to host several kinds of defects. One of the most elementary defects, as in most metal oxides with a ReO_3-type structure, is the lattice oxygen vacancy, where the oxygen atom is absent from a normal lattice site. Thus the octahedral changes from corner-sharing to edge-sharing lattices and it causes the formation of crystallographic shear planes into the crystal along the (1 m 0) direction. This leads to a family of WO_{3-x} compounds which are presented in [30]. From an electronic point of view, an

ISBN:978-84-691-9748-6 /DL:T-1249

oxygen vacancy causes the increase of the electronic states within the forbidden gap of the WO_3, leading to the formation of donor-like states slightly below the edge of the conduction band of the oxide. It is known that tungsten trioxide films deposited by vacuum techniques showed better control of this defects. Besides, it was observed that these intrinsic defect depends on the annealing procedure, temperature and substrate type [74, 76-78].

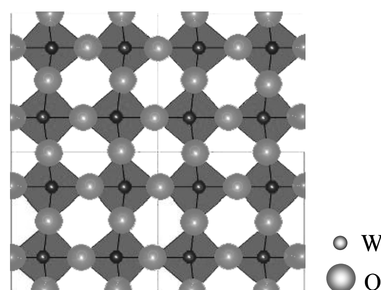

Figure 1.8. Structure of monoclinic WO_3. Blue colour: oxygen atoms, red colour: tungsten atoms

According with Kuzmin et. al. [79], who proposed a structural model of the WO_3 grain surface, two different situations may be present in the surface of an idealized WO_3 film due to the electrical neutrality condition (see Figure 1.9) Considering a surface along the (1 0 0) crystallographic plane. In the first, half of W atoms remain in the valence state 6+ and are connected to the terminal oxygen ions, which give one of their electrons to the nearest W ion, leading to a formation of a W^{5+} state. This situation occurs at the free surface of WO_3 single crystals and was directly observed by STM technique [79-81]. In the second situation, all tungsten atoms at the surface change their valence state to 5+, and the surface is represented by $W^{5+}O_2$ terminal layer. In both cases, the surface W^{5+} sites react with the oxidising atmosphere of air, leading presumably to a formation of the W^{6+}-OH bonds in a humid ambience.

Table 1.3. Bulk equilibrium phases of WO_3 [74].

Structure	Angstroms			Degrees			Stability
	a	b	c	α	β	γ	Range (ºC)
Triclinic	7.31	7.52	7.69	88.8	90.9	90.9	<17
Monoclinic	7.30	7.54	7.69	90	90.9	90	17-320
Orthorombic	7.34	7.57	7.75	-	-	-	320-720
Tetragonal	5.25	5.25	3.92	-	-	-	>720

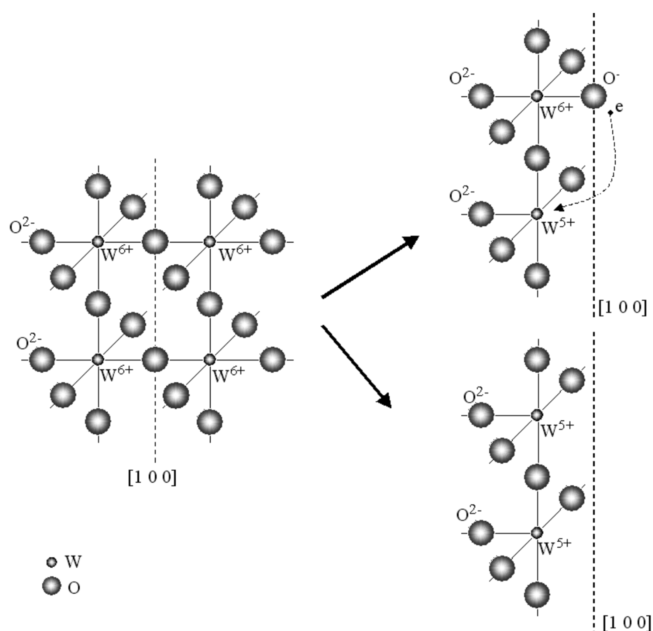

Figure 1.9. Structural model of the WO_3 grain surface. In the left: idealized WO_3 structure with the (1 0 0) fracture plane shown. In the right: two possible states of the grain surface [79].

The formation of tungsten states on the film surface plays a strong role in the gas-solid interactions. So far, it was noted that tungsten states on the surface enhance the oxidation power of NO_x molecules [63], which could explain its good sensitivities not only to this family of gases but also to other gaseous species.

1.3.2. WO_3 – based gas sensors

Certainly, the main asset of WO_3-based gas sensors is connected with its sensitivity to atmosphere pollutants like NO_x [26, 61, 63, 82-85], O_3 [57, 60, 86] H_2S [58, 87, 88], NH_3 [58, 63, 89], SO_2 [88], H_2 [63] and C_2H_6O [89]. As other metal oxide based gas sensors, WO_3 is mostly used in the air at atmospheric pressure. In these conditions, it is believed that most of the gaseous species are detected via their influence on the adsorbed oxygen. In particular, the investigations showed that the key reaction of the gaseous species detection involves oxygen ions adsorbed on the surface of the sensor [1]. Thus, at operating temperatures between 200ºC and 500ºC only O^- species which are the most stable

UNIVERSITAT ROVIRA I VIRGILI
STUDY OF STRUCTURAL AND SENSING PROPERTIES OF TUNGSTEN TRIOXIDE THIN FILMS
DEPOSITED BY RF SPUTTERING
Stella Vallejos Vargas
ISBN:978-84-691-9748-6 /DL:T-1249

reacts with the contaminant gases [90]. Below, it is presented a brief description of the target gases used in this work as well as the reactions produced by the adsorption of these gases on WO_3.

Nitrogen oxides (NO_x: NO_2 and NO) are produced during combustion. These gases are the most common atmospheric pollutants according to the Environment Protection Agency of the USA [91] and the European Environment Agency [92]. Nitrogen oxides are believed to cause lung irritations, decrease the fixation of oxygen molecules on red blood corpuscles, contribute to acid rains and generate the increase of ozone rate in the low atmosphere. The European air quality policies [93] reports that the limit concentration of nitrogen oxides in air should not be higher than 0.1 ppm. Adsorption of the NO_2 on WO_3 results in a decrease of the conductivity which may be explained by the reactions.

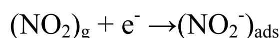
$(NO_2)_g + e^- \rightarrow (NO_2^-)_{ads}$

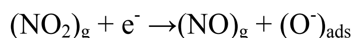
$(NO_2)_g + e^- \rightarrow (NO)_g + (O^-)_{ads}$

Both of these reactions require electrons from the conduction band of WO_3 which leads to a decrease of the conductivity [89, 94]. On the other hand, reactions with NO result in an increase in chemisorbed oxygen in the film decreasing the free carrier concentration, as follow:

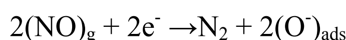
$2(NO)_g + 2e^- \rightarrow N_2 + 2(O^-)_{ads}$

This decrease in the carrier concentration causes the film conductivity to fall [95].

Ozone (O_3) is a strong oxidizing gas. It is naturally presented in our atmosphere due to the interaction of sunlight with certain chemicals emitted to the environment (e.g. automobile emissions and chemical emissions of industrial plants). Severe exposures to this gas may cause problems such as inflammation and congestion of the respiratory tract, besides it contributes to the green house effect and vegetation degradation [96]. The European air pollution policies [93] recommend that the average of O_3 concentration in the air should not exceed values of 0.05 - 0.10 ppm. Basically, the response of a WO_3-based gas sensor to O_3 is interpreted by considering that the oxygen species interact with the surface

UNIVERSITAT ROVIRA I VIRGILI
STUDY OF STRUCTURAL AND SENSING PROPERTIES OF TUNGSTEN TRIOXIDE THIN FILMS
DEPOSITED BY RF SPUTTERING
Stella Vallejos Vargas
ISBN:978-84-691-9748-6 /DL:T-1249

oxygen vacancies. Therefore, when WO_3 is exposed to O_3 the oxygen species given by the dissociative adsorption interact with the surface oxygen vacancies according to:

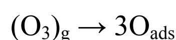

$(O_3)_g \rightarrow 3O_{ads}$

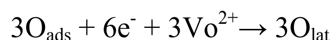

$3O_{ads} + 6e^- + 3Vo^{2+} \rightarrow 3O_{lat}$

As a result, oxygen vacancies and the corresponding free electrons are annihilated and the conductance decreases [81].

Ammonia (NH_3) is one the most abundant alkaline component in the atmosphere. It is known that a considerable amount of this gas comes from the natural breakdown of manure, dead plants and animals. According to the Agency for Toxic Substance and Disease [97], no health effects have been found in humans exposed to typical environmental concentrations of ammonia, however, it is reported that exposure to high levels of ammonia may cause irritation in the skin, eyes, throat and lungs. Ammonia acts as a reducing agent when it interacts with WO_3. Therefore the carrier concentration in the sensing film rises as a result of a decrease in adsorbed surface oxygen, as follow:

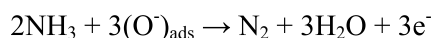

$2NH_3 + 3(O^-)_{ads} \rightarrow N_2 + 3H_2O + 3e^-$

The increment of the free electron concentration within the active film implies an increase in the conductivity [89, 95].

Hydrogen sulphide (H_2S) occurs naturally in crude petroleum, natural gas, volcanic gases, and hot springs. It can also result from bacterial breakdown of organic matter or produced by human and animal wastes. Other sources are industrial activities, such as food processing, coke ovens, craft paper mills, tanneries, and petroleum refineries. High concentrations of H_2S may hurt the eyes, nervous system and respiratory system. At low temperatures, it has been suggested that resistance changes, due to H_2S adsorption, occurs as a consequence of the reaction:

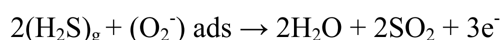

$2(H_2S)_g + (O_2^-)$ ads $\rightarrow 2H_2O + 2SO_2 + 3e^-$

UNIVERSITAT ROVIRA I VIRGILI
STUDY OF STRUCTURAL AND SENSING PROPERTIES OF TUNGSTEN TRIOXIDE THIN FILMS
DEPOSITED BY RF SPUTTERING
Stella Vallejos Vargas
ISBN:978-84-691-9748-6 /DL:T-1249

As H_2S is adsorbed, electrons are released into the conduction band and the conductivity increases. In contrast, for high temperature operation, the reaction is:

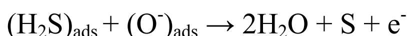

$$(H_2S)_{ads} + (O^-)_{ads} \rightarrow 2H_2O + S + e^-$$

Another mechanism, that can play a role in the gas sensing, is the formation of additional surface oxygen vacancies, created by the interaction of H_2S with lattice oxygen according to:

$$3WO_3 + 7H_2S \rightarrow 3WS_2 + SO_2 + 7H_2O$$

This reaction takes place on the surface and involves a reduction of W^{6+} to W^{4+}. Oxygen leaves the surface thereby releasing electrons into the grains so that the conductivity of the film is increased. However, re-oxidation of the vacancies by O_2 results in a competition with the formation of the oxygen vacancies by H_2S [94].

Carbon monoxide (CO) is formed when carbon in fuel is not burned completely. In cities, 85 to 95 percent of all CO emissions may come from motor vehicle exhaust. Other sources of CO emissions include industrial processes (such as metals processing and chemical manufacturing). Carbon monoxide can cause harmful health effects by reducing oxygen delivery to the body's organs (like the heart and brain) and tissues. The limit concentrations of CO stipulated by the Europe commission [93] are between 9 and 35 ppm. When CO is detected by a metal oxide gas sensor, it reacts with the adsorbed oxygen ions getting oxidized to CO_2 and the released electrons return to the conduction band according to the reaction. Therefore, the conductivity increases [98]:

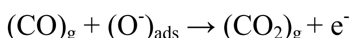

$$(CO)_g + (O^-)_{ads} \rightarrow (CO_2)_g + e^-$$

Ethanol (C_2H_5OH or C_2H_6O) is produced both as a petrochemical, through the hydration of ethylene, and biologically, by the fermentation of sugars. It is best known as the alcohol found in alcoholic beverages. The adsorption of the C_2H_5OH on WO_3 surface can take place by the following route:

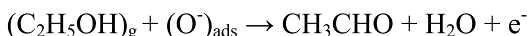

$$(C_2H_5OH)_g + (O^-)_{ads} \rightarrow CH_3CHO + H_2O + e^-$$

The electrons produced by this reaction are injected into the conduction band of WO_3, which induces a increase of the conductance [90, 99].

1.3.3. WO_3 gas sensors based on PVD techniques

Tungsten trioxide films for sensing applications have been deposited by many methods including sol gel, chemical vapour deposition and physical vapour deposition. It was noted that the sensitivity and selectivity of WO_3 based sensors depend on many factors of design (e.g. substrate type, film thickness) and preparation (e.g. annealing temperature, annealing time, substrate temperature during deposition). Therefore, several investigations have been focus on the study of these factors and their influence on the sensing properties of WO_3. Table 1.4 considers the influence of several parameters of WO_3 deposition on the structure and sensing properties of the films.

Influence of film thickness

According to Penza et al. [63], the response of WO_3-based gas sensors to NH_3, H_2, NO_2 and NO showed a film thickness dependence. In this work, several WO_3 films with thickness between 1600 Å and 4800 Å were studied. The results revealed that the sensitivity to NH_3 and H_2 increases with the thickness in the whole range, while the sensitivity to NO_2 and NO increases with the thickness up to 4000 Å showing saturation over this value. Moreover, Boulmani et. al. [86] noticed that the response of WO_3 films to 0.8 ppm of O_3 is higher when the sensing layer has a thickness less or equal to electrode thickness.

Influence of substrate type

Studies carried out by Lee et al. [82] demonstrated that the sensitivity of WO_3 is highly dependent on the roughness of substrate. They noted that the substrate roughness modifies the surface morphology of the sensing film. Their studies included the characterization of various substrate types (unpolished alumina, polished alumina, and silicon). The results showed that WO_3 thin film deposited on unpolished alumina substrates exhibits the highest sensitivity to NO_2 than WO_3 films deposited onto polished alumina and silicon substrates.

ISBN:978-84-691-9748-6 /DL:T-1249

Table 1.4. Review of reports concerning to physical vacuum deposited-WO_3 thin films used as gas sensing material.

Material	Method	Total pressure (mbar)	Power (W)	Substrate type	T_S (ºC)	F-T (Å)	T_a (ºC)	t_a (h)	Application	T_{op} (ºC)	Ref
WO_3	RFS	3-6 x 10^{-2}	100 300	Glass	200-300	1600 4800	400	6	NO, NO_2, NH_3, H_2	250	[63]
WO_3	DCS	1.3 x 10^{-2}		Al_2O_3	200-500	3000	600	4	NO_x	200	[61]
WO_3	VTE	5 x 10^{-6}		Si/Si_3N_4	RT	1500	300 500	24 200	NO_2	150	[26]
WO_3	VTE			Al_2O_3 Si/SiO_2	RT		600	2	NO_x	300	[82]
WO_3	DCS	1Pa		Si/SiO_2	RT 200 300	150	600	4	NO_2	300	[84]
WO_3	VTE	5 x 10^{-6}		Sapphire	RT	1500	500	6 12 24	NO_2	250	[83]
WO_3 WO_3-Pd WO_3-Pt WO_3-Au	RFS	6 x 10^{-2}		Glass	300	3000	400	6	NO, NO_2	250 150 150 200	[85]
WO_3	RFMS	3	60	Si/SiO_2	RT	500	450		O_3	250	[57]
WO_3	VTE RFS	5 x 10^{-6} 2 x 10^{-3}		Al_2O_3	300		250 600	4 30	O_3	400	[60]

ISBN:978-84-691-9748-6 /DL:T-1249

WO_3	RFMS	3×10^{-3}		Si/SiO_2	300	300 400 900 1160	450	1	O_3	250	[86]
WO_3	VTE			Al_2O_3	RT	1200	480	1	H_2S	RT	[87]
WO_3 WO_3-Pt	RFS	5×10^{-3}	200	Si/SiO_2	RT	2500	400	2	H_2S, SO_2	200	[88]
WO_3 WO_3-Pt WO_3-Au WO_3-Ag WO_3-Ti WO_3-SnO_2 WO_3-ZnO WO_3-ITO	RFS	5×10^{-3}	200	Si/SiO_2	RT	2500	400	2	H_2S, NO_2, NH_3	200	[58]
WO_3	RFS	5×10^{-3}	200	Si/SiO_2	RT	2500	350 400 450	24		200	[89]

RFS: RF sputtering, RFMS: RF magnetron sputtering, VTE : vapour thermal evaporation, DCS: DC sputtering, RT: room temperature, F-T: film thickness, Ta: temperature annealing, t_a: annealing time, T_{op}: operating temperature.

.

ISBN:978-84-691-9748-6 /DL:T-1249

Influence of substrate temperature during deposition

It was noted that the sensitivity of WO_3 has a strong dependence on the substrate temperature set up during deposition. Kim et al. [61] reported that the sensitivity to NO and NO_2 shows an increase from 60 to 180 time for the films deposited at 200ºC and 500ºC respectively. They concluded that the quality of the final crystalline phase of WO_3 (post annealing at 600ºC) depends on the initial formation of the phase during deposition. Similar results were published by He et al. [84] which observed that the sensitivity to NO_2 increases from 0.78 to 22 for the films deposited at room temperature and 300ºC respectively. In this case the SEM photographs revealed that the specific surface area is increased (decrease in grain size) when WO_3 is deposited at 300 ºC.

Influence of O_2/Ar ratio during sputtering deposition

Bendahan et al [57, 86] reported that changes of oxygen percentage in the sputtering gas lead to changes in the conductance of WO_3 based sensors. Thus, they noted that the sensitivity to ozone increases with O_2 content in the sputtering gas. The sensors fabricated with 50% of O_2 showed the highest responses. AFM analysis of WO_3 films deposited with 50 % of O_2 revealed a decrease in grain size and an increase in roughness in comparison with films deposited with 18 % and 65% of O_2.

Influence of annealing temperature and annealing time

Cantalini et al. [26, 83] observed that improved sensitivities of WO_3 are achieved when it is annealed near its crystallization temperature (e.g. 300 ºC). These annealing conditions prevent crystal growth and enhance the concentration of possible surface defects. Moreover they noted that improved long term stabilities are achieved when WO_3 is annealed for longer times (e.g. 200 h) due to the stabilization of the surface defects at their equilibrium values. The experimental results presented in these studies showed that after one year of the use, WO_3 films annealed at 300ºC for 24 h had a sharply decrease of sensitivity to NO_2 in comparison with WO_3 films annealed at 300ºC for 200h. In the same way Stankova et al. [89] found that the annealing temperature, rather that the operating

ISBN:978-84-691-9748-6 /DL:T-1249

temperature, is the most important parameter that affect the sensitivity of sputtered WO_3 thin films.

Influence of dopant addition

It was demonstrate that the sensitivity and selectivity of WO_3 films deposited by physical methods can be improved by addition of thin layers of noble metals onto its surface. Penza et al. [85] noted that the addition of Pd, Pt, and Au films enhance the selectivity towards NO_x with respect to some reducing gases (CO, CH_4, H_2, SO_2, NH_3). Moreover, Stankova et al. [58] observed that the addition of Ag and Au becomes WO_3 suitable for the detection of H_2S and NH_3 at moderates temperatures (i.e. 110ºC). Another study showed that sulphur compounds (H_2S and SO_2) can be controlled in CO_2 stream with promising results by combining WO_3 and WO_3/Pt based sensors [88].

UNIVERSITAT ROVIRA I VIRGILI
STUDY OF STRUCTURAL AND SENSING PROPERTIES OF TUNGSTEN TRIOXIDE THIN FILMS
DEPOSITED BY RF SPUTTERING
Stella Vallejos Vargas
ISBN:978-84-691-9748-6 /DL:T-1249

1.4. Summary and outlook

This chapter presented a general overview of the metal oxide based gas sensors. Three main points were discussed focussing in the recent developments of these devices: the working principles of metal oxide based gas sensors, the most common deposition techniques used to form the sensing layer and the metal oxides employed to fabricate this devices. In particular, it was paid attention to tungsten trioxide (WO_3) based gas sensors developed by PVD techniques.

Several theoretical and experimental evidences showed that the performance of the metal oxide gas sensors is significantly related with the granular structure of the sensing layer, which was demonstrated to be controlled by decreasing the metal oxide grain size to nanometric scale. Therefore, at present a significant fraction of the overall research and development efforts in metal-oxide-based gas sensors is directed toward sensor miniaturization. Although, PVD techniques have shown to be advantageous due to their compatibility with the micro-fabrication processes, their feasibility in the industry and their vacuum conditions. The formation of idealized metal oxide structures (with nanometric grain size) for gas sensing applications is not fully achieved by these techniques. Hence, the importance to develop new strategies based on PVD to obtain sensing films with small grain size is very relevant.

Currently, a big amount of metal oxides are studied for gas sensing applications, among them the most popular is tin oxide. However, during the last years other metal oxides, such as WO_3, have called the attention due to their possibility to use in urban air quality monitoring. It becomes WO_3 very attracting to develop new deposition technologies. That is why the preparation of the pure or doped WO_3 thin film sensors with the ability to detect O_3 and/or NO_x compounds with highly selectivity represents a big challenge.

Bibliography

[1] D. E. Williams, "Conduction and gas response of semiconductor gas sensors," in *Solid state gas sensors*, P. T. Moseley and C. Tofield, Eds. Bristol: Adam Hilger, 1987, pp. 71-123.

[2] D. E. Williams, "Semiconducting oxides as gas-sensitive resistors," *Sens. Actuators B*, vol. 57, pp. 1-16, 1999.

[3] S. Isolde, N. Bârsan, M. Bauer, and U. Weimar, "Micromachined metal oxide gas sensors: opportunities to improve sensor performance," *Sens. Actuators B*, vol. 73, pp. 1-26, 2001.

[4] N. Yamazoe, G. Sakai, and K. Shimanoe, "Oxide semiconductor gas sensors," *Catalysis Surveys from Asia*, vol. 7, 2003.

[5] A. Rothschild and Y. Komen, "The effect of grain size on the sensitivity of nanocrystalline metal-oxide gas sensors," *J. Appl. Phys.*, vol. 11, pp. 6374-6380, 2004.

[6] T. Wolkenstein, *Electronic process on semiconductor surface during chemisorption*: Consultants Bureau, 1991.

[7] R. Glang, R. A. Holmwood, and J. A. Kurtz, "High-vacuum technology," in *Handbook of thin film technology*, L. I. Maissel and R. Glang, Eds.: McGraw-Hill, Inc., 1970.

[8] H. Geistlinger, "Electron theory of thin-film gas sensors," *Sens. Actuators B*, vol. 17, pp. 47-60, 1993.

[9] A. Rothschild and Y. Komen, "Numerical computation of chemisorption isotherms for device modeling of semiconductor gas sensors," *Sens. Actuators B*, vol. 93, pp. 362-369, 2003.

[10] N. Yamazoe, "New approaches for improving semiconductor gas sensors," *Sens. Actuators B*, vol. 5, pp. 7-19, 1991.

[11] J. Schalwing, S. Ahlers, P. Kreisl, C. B. Braunmühl, and G. Müller, "A solid-state gas sensor array for monitoring NO_x storage catalytic converters," *Sens. Actuators B*, vol. 101, pp. 63-71, 2004.

[12] M. Franke, T. Koplin, and U. Simon, "Metal and metal oxide nanoparticles in Chemiresistors: does the nanoscale matter?," *Small*, vol. 2, pp. 36-50, 2006.

[13] D. E. Williams and K. F. E. Pratt, "Microstructure effects on the response of gas-sensitive resistors based on semiconducting oxides," *Sens. Actuators B*, vol. 70, pp. 214-221, 2000.

[14] O. Berger, T. Hoffmann, and W. J. Fishcher, "Tungsten-oxide thin films as novel materials with high sensitivity and selectivity to NO_2, O_3 and H_2S. Part II: Application as gas sensors," *J. Mater. Sci. Mater. Electron.*, vol. 15, pp. 483-493, 2004.

[15] C. Xu, J. Tamaki, N. Miura, and N. Yamazoe, "Relationship between gas sensitivity and microstructure of porous SnO_2," *J. Electrochem. Soc. Jpn.*, vol. 58, pp. 1143-1148, 1990.

[16] N. Bârsan and U. Weimar, "Conduction model of metal oxide gas sensors," *J. Electroceramics*, vol. 7, pp. 143-167, 2001.

[17] X. Wang, S. Yee, and P. Carey, "Transition between neck-controlled and grain-boundary-controlled sensitivity of metal-oxide gas sensors," *Sens. Actuators B*, vol. 24-25, pp. 454-457, 1995.

[18] V. Y. Sukhaev, "Percolation model of adsorption-induced response of electrical characteristics of polycristalline semiconductor adsorbents " *J. Chem. Soc. Faraday Trans.*, vol. 89, pp. 559-572, 1993.

[19] D. D. Vuong, G. Sakai, K. Shimanoe, and N. Yamazoe, "Hydrogen sulfide gas sensing properties of thin films derived from SnO_2 sols different in grain size," *Sens. Actuators B*, vol. 105, pp. 437-442, 2005.

[20] G. Sakai, N. Matsunaga, K. Shimanoe, and N. Yamazoe, "Theory of gas-diffusion controlled sensitivity for thin film semiconductor gas sensor," *Sens. Actuators B*, vol. 80, pp. 125-131, 2001.

[21] N. Matsunaga, G. Sakai, K. Shimanoe, and N. Yamazoe, "Formulation of gas diffusion for thin film semiconductor gas sensor based on simple reaction-diffusion equation," *Sens. Actuators B*, vol. 96, pp. 226-233, 2003.

[22] D. D. Vuong, G. Sakai, K. Shimanoe, and N. Yamazoe, "Preparation of grain size-controlled tin oxide sols by hydrothermal treatment for thin film sensor application," *Sens. Actuators B*, vol. 103, pp. 386-391, 2004.

[23] N. Yamazoe, "Towards innovations of gas sensor technology," *Sens. Actuators B*, vol. 108, pp. 2-14, 2005.

[24] J. Tamaki, Z. Zhang, K. Fujimori, M. Akiyama, T. Harada, N. Miura, and N. Yamazoe, "Grain size effects in tungsten oxide-based sensors for nitrogen oxides," *J. Electrochem. Soc.*, vol. 141, pp. 2207-2210, 1994.

[25] F. Lu, Y. Liu, M. Dong, and X. Wang, "Nanosized tin oxide as the novel material with simultaneous detection towards CO, H_2 and CH_4," *Sens. Actuators B*, vol. 66, pp. 225-227, 2000.

[26] C. Cantalini, L. Luca, M. Passacantando, and S. Santucci, "The comparative effect of two different annealing temperatures and times on the sensitivity and long-term stability of WO_3 thin films for detecting NO_2," *IEEE Sensors Journal*, vol. 3, pp. 171-179, 2003.

[27] A. Gurlo, N. Barsan, M. Ivanovskaya, U. Weimar, and W. Göpel, "In_2O_3 and MoO_3 thin film semiconductor sensors: interaction with NO_2 and O_3," *Sens. Actuators B*, vol. 47, pp. 92-99, 1998.

[28] G. Korontcenkov, A. Cerneavchi, V. Brinzari, A. Vasiliev, M. Ivanov, A. Cornet, J. Morante, A. Cabot, and J. Arbiol, "In_2O_3 films deposited by spray pyrolisis as a material for ozone gas sensors," *Sens. Actuators B*, vol. 99, pp. 297-303, 2004.

[29] G. Korontcenkov, V. Brinzari, A. Cerneavchi, M. Ivanova, A. Cornet, J. Morante, A. Cabot, and J. Arbiol, "In_2O_3 films deposited by spray pyrolisis: gas response to reducing (CO, H_2) gases," *Sens. Actuators B*, vol. 98, pp. 122-129, 2004.

[30] I. Jimenez, "Tungsten oxide nanocrystalline powders for gas sensing applications," Universitat de Barcelona, 2003.

[31] N. Bârsan, M. Schweizer-Berberich, and W. Göpel, "Fundamental and practical aspects in the design of nanoscaled SnO_2 gas sensors: a status report," *Fresenius J. Anal. Chem.*, vol. 365, pp. 287-304, 1999.

[32] M. Graf, A. Gurlo, N. Barsan, U. Weimar, and A. Hierlemann, "Microfabricated gas sensor system with sensitive nanocrystalline metal oxide films," *Journal of Nanoparticles Research*, vol. 8, pp. 823-839, 2006.

[33] D. Vincenzi, M. A. Butturi, V. Guidi, M. C. Carotta, G. Martinelli, V. Guarnieri, S. Brida, B. Margesin, F. Giancomozzi, M. Zen, G. U. Pignatel, A. A. Vasiliev, and A. V. Pisliakov, "Development of a low-power thick film gas sensor deposited by screen-printing technique onto a micromachined hotplate," *Sens. Actuators B*, vol. 77, pp. 95-99, 2001.

[34] V. Meille, "Review on methods to deposit catalyst on structured surfaces," *Applied Catalysis A: General*, vol. 315, pp. 1-17, 2006.

[35] L. L. Hench and J. K. West, "The sol-gel process," *Chem. Rev.*, vol. 90, pp. 33-72, 1990.

[36] G. Frenzer and W. F. Maier, "Amorphous porous mixed oxides: sol-gel ways to a highly versatile class of materials and catalysts," *Annu. Rev. Mater. Res.*, vol. 36, pp. 281-331, 2006.

[37] M. Epifani, E. Comini, R. Diaz, J. Arbiol, P. Siciliano, G. Sberveglieri, and J. R. Morante, "Oxide nanopowder from low-temperature processing of metal oxide sols and their application as gas-sensing materials," *Sens. Actuators B*, vol. 118, pp. 105-109, 2006.

[38] G. Neri, A. Bonavita, G. Rizzo, S. Galvagno, N. Pinna, M. Niederberger, S. Capone, and P. Siciliano, "Towards enhanced performances in gas sensing SnO_2 based nanocrystalline oxides applications," *Sens. Actuators B*, vol. 122, pp. 564-571, 2007.

[39] P. Ivanov, J. Laconte, J. P. Raskin, M. Stankova, E. Sotter, E. Llobet, X. Vilanova, D. Flandre, and X. Correig, "SOI-CMOS compatible low-power gas sensor using sputtered and drop-coated metal-oxide active layers," *Microsystem Technologies - Micro-and Nanosystems - Information Storage and Processing Systems*, vol. 12, pp. 160-168, 2005.

[40] X. Wang, G. Sakai, K. Shimanoe, N. Miura, and N. Yamazoe, "Spin-coated thin films of SiO_2-WO_3 composites for detection of sub ppm NO_2," *Sens. Actuators B*, vol. 45, pp. 141-146, 1997.

[41] S. H. Wang, T. C. Chou, and C. C. Liu, "Nano-crystalline tungsten oxide NO_2 sensor," *Sens. Actuators B*, vol. 94, pp. 343-351, 2003.

[42] M. Epifani, S. Capone, R. Rella, P. Siciliano, L. Vasanelli, G. Faglia, P. Nelli, and G. Sberveglieri, "In_2O_3 thin films obtained through a chemical complexation based sol-gel process and their application as gas sensor devices," *J. Sol-Gel Sci. Tech.*, vol. 26, pp. 741-744, 2003.

[43] A. M. Taurino, M. Epifani, T. Toccoli, S. Iannotta, and P. Siciliano, "Innovative aspects in thin film technologies for nanostructured materials in gas sensor devices," *Thin Solid Films*, vol. 136, pp. 52-63, 2003.

[44] Y. G. Choi, G. Sakai, K. Shimanoe, and N. Yamazoe, "Wet process-based fabrication of WO_3 thin film for NO_2 detection," *Sens. Actuators B*, vol. 101, pp. 107-111, 2004.

[45] K. Wetzig and C. M. Schneider, *Metal based thin films for electronics*, 2003.

[46] Y. Liu, E. Koep, and M. Liu, "A highly sensitive and fast-responding SnO_2 sensor fabricated by combustion chemical vapor deposition," *Chem. Mater*, vol. 17, pp. 3997-4000, 2005.

[47] Y. C. Lee, O. K. Tan, H. Huang, and M. S. Tse, "Deposition and gas sensing properties of tin oxide thin films by inductively coupled plasma chemical vapor deposition," *J. Electroceram*, vol. 16, pp. 507-509, 2006.

[48] S. Ashraf, C. S. Blackman, R. G. Palgrave, S. C. Naisbitt, and I. P. Parkin, "Aerosol assisted chemical vapour deposition of WO_3 thin films from tungsten hexacarbonyl and their gas sensing properties," *Journal of Materials Chemistry*, vol. 17, pp. 3708-3713, 2007.

[49] B. Panchapakesan, D. L. DeVoe, M. R. Widmaier, R. Cavicchi, and S. Semancik, "Nanoparticles engineering and control tin oxide microstructures for chemical microsensor applications," *Nanotechnology*, vol. 12, pp. 336-349, 2001.

[50] G. K. Wehner and G. S. Anderson, "The nature of physical sputtering," in *Handbook of thin film technology*, L. I. Maissel and R. Glang, Eds.: McGraw-Hill, 1970.

[51] M. Stankova, "Gas sensing properties of rf sputtering WO_3 thin films," Universitat Politecnica de Catalunya, 2004.

[52] S. Nicoltetti, S. Zampolli, I. Elmi, L. Diori, and M. Severi, "Use of different sensing materials and deposition techniques for thin-film sensors to increase sensitivity and selectivity " *IEEE Sensors Journal*, vol. 3, pp. 454-459, 2003.

[53] T. Aste, R. Botter, and D. Beruto, "Double-layer granular SnO_2 sensors," *Sens. Actuators B*, vol. 24-25, pp. 826-829, 1995.

ISBN:978-84-691-9748-6 /DL:T-1249

[54] A. Ponzoni, E. Comini, M. Ferroni, and G. Sberveglieri, "Nanostructured WO_3 deposited by modified thermal evaporation for gas-sensing applications," *Thin Solid Films*, vol. 490, pp. 81-85, 2005.

[55] G. Williams and G. S. V. Coles, "Gas sensing properties of nanocrystalline metal oxide powders produced by laser evaporation technique," *J. Mater. Chem.*, vol. 8, pp. 1657-1664, 1998.

[56] H. Kawasaki, J. Namba, K. Iwatsuji, Y. Suda, K. Wada, K. Ebihara, and T. Ohshima, "NO_x gas sensing properties of tungsten oxide thin films synthesized by pulsed laser deposition method," *Appl. Surf. Sci.*, vol. 197-198, pp. 547-551, 2002.

[57] M. Bendahan, R. Boulmani, J. L. Seguin, and K. Aguir, "Characterization of ozone sensors based on WO_3 reactively sputtered films: influence of O_2 concetration in the sputtering gas and working temperature," *Sens. Actuators B*, vol. 100, pp. 320-324, 2004.

[58] M. Stankova, X. Vilanova, J. Calderer, E. Llobet, J. Brezmes, I. Gràcia, C. Cané, and X. Correig, "Sensitivity and selectivity improvement of rf sputtered WO_3 microhotplate gas sensors," *Sens. Actuators B*, vol. 113, pp. 241-248, 2006.

[59] M. Gillet, K. Aguir, M. Bendahan, and P. Mennini, "Grain size effects in sputtered tungsten trioxide thin fims on the sensitivity to ozone " *Thin Solid Films*, vol. 2005, pp. 358-363, 2005.

[60] C. Cantalini, W. Wlodarski, Y. Li, M. Passacantando, S. Santucci, E. Comini, G. Flagia, and G. Sberveglieri, "Investigations on the O_3 sensitivity properties of WO_3 thin films prepared by sol-gel, thermal evaporation and r.f. sputtering techniques," *Sens. Actuators B*, vol. 64, pp. 182-188, 2000.

[61] T. S. Kim, Y. B. Kim, K. S. Yoo, G. S. Sung, and H. J. Jung, "Sensing characteristics of dc reactive sputtered WO_3 thin films as an NO_x gas sensor," *Sens. Actuators B*, vol. 62, pp. 102-108, 2000.

[62] C. J. Jin, T. Yamazaki, Y. Shirai, T. Yoshizawa, T. Kikuta, N. Nakatani, and H. Takeda, "Dependence of NO_2 gas sensitivity of WO_3 sputtered films on film density," *Thin Solid Films*, vol. 474, pp. 255-260, 2005.

[63] M. Penza, M. A. Tagliente, L. Mirenghi, C. Gerardi, C. Martucci, and G. Cassano, "Tungsten trioxide (WO_3) sputtered thin films for a NO_x gas sensor," *Sens. Actuators B*, vol. 50, pp. 9-18, 1998.

[64] G. Sberveglieri, G. Faglia, G. A., P. Nelli, and A. Camanzi, "A new technique for growing large surface-area SnO_2 thin film (RGTO technique) " *Semiconductor Science and Technology*, vol. 5 pp. 231-1233 1990.

[65] G. Sberveglieri, "Recent developments in semiconducting thin-film gas sensor," *Sens. Actuators B*, vol. 23, pp. 109-109, 1995.

[66] G. Sberveglieri, S. Gropelli, and P. Nelli, "Highly sensitivite and selective NO_x and NO_2 sensor based on Cd-doped SnO_2 thin films," *Sens. Actuators B*, vol. 4, pp. 457-461, 1991.

[67] L. Ottaviano, L. Lozzi, M. Passacantando, and S. Santucci, "On the spatially resolved electronic structure of polycrystalline WO_3 films investigated with scanning tunneling spectroscopy," *Surface Science*, vol. 475, pp. 73-82, 2001.

[68] C. G. Granqvist, "Electrocrhomic tungsten oxide films: review of progress 1993-1998," *Solar Energy Materials & Solar Cells*, vol. 60, pp. 201-262, 1999.

[69] A. Di Paola, L. Palmisano, A. M. Venezia, and V. Augugliano, "Coupled semiconductor systems for photocatalysis. Preparation and characterization of polycrystalline mixed WO_3/WS_2 powders," *J. Phys. Chem. B*, vol. 103, pp. 8236-8244, 1999.

[70] A. Löfbeg, A. Frennet, G. Leclercq, L. Leclercq, and J. M. Giraudon, "Mechanism of WO_3 reduction and carburization in CH_4/H_2 mixtures leading to bulk tungsten carbide powder catalysts," *Journal of Catalysis*, vol. 189, pp. 170-183, 2000.

[71] G. Eranna, B. C. Joshi, D. P. Runthala, and R. P. Gupta, "Oxide Materials for development of integrated gas sensors - a comprehensive review," *Critical reviews in Solid State and Materials Sciences*, vol. 29, pp. 111-188, 2004.

[72] P. J. Shaver, "Activated tungsten oxide gas detector," *Appl. Phys. Lett.*, vol. 11, pp. 255-256, 1967.

[73] S. R. Aliwell, J. F. Halsall, K. F. E. Pratt, J. O'Sullivan, R. L. Jones, R. A. Cox, S. R. Utembe, G. M. Hansford, and D. E. Williams, "Ozone sensors based on WO_3: a model sensor drift and a measurement correction method," *Meas. Sci. Technol.*, vol. 12, pp. 684-690, 2001.

[74] L. J. LeGore, R. J. Lad, S. C. Moulzolf, J. F. Vetelino, B. G. Frederick, and E. A. Kenik, "Defects and morphology of tungsten trioxide thin films," *Thin solid films*, vol. 406, pp. 79-86, 2002.

[75] P. M. Woodward, A. W. Sleight, and T. Vogts, "Structure refinement of triclinic tungsten trioxide," *J. Phys. Chem. Solids*, vol. 56, pp. 1305-1315, 1994.

[76] A. Al Mohammad and M. Gillet, "Phase transformations in WO_3 thin films during annealing " *Thin Solid Films*, vol. 408, pp. 302-309, 2002.

[77] S. C. Moulzolf, S. Ding, and R. J. Lad, "Stoichiometry and microstructure effects on tungsten oxide chemiresistive films," *Sens. Actuators B*, vol. 77, pp. 375-382, 2001.

[78] S. C. Moulzolf, L. J. LeGore, and R. J. Lad, "Heteroepitaxial growth of tungsten oxide films on sapphire for chemical gas sensors," *Thin Solid Films*, vol. 400, pp. 56-63, 2001.

[79] A. Kuzmin, J. Purans, E. Cazzanelli, C. Vinegoni, and G. Marioto, "X-ray diffraction, extended x-ray absorption fine structure and raman spectroscopy studies of WO_3 powders and $(1\text{-}x)WO_{3\text{-}y} \cdot xReO_2$ mixtures," *J. Appl. Phys.*, vol. 84, pp. 5515-5523, 1998.

[80] M. Li, E. I. Altman, A. Posadas, and C. H. Ahn, "Surface phase transitions upon reduction of epitaxial WO_3 (1 0 0) thin films," *Thin Solid Films*, vol. 446, pp. 238-247, 2004.

[81] M. Bendahan, J. Guérin, R. Boulmani, and K. Aguir, "WO_3 sensor response according to operating temperature: experiments and modelling," *Sens. Actuators B*, vol. 124, pp. 24-29, 2007.

[82] D. S. Lee, K. H. Nam, and D. D. Lee, "Effect of substrate on NO_2 -sensing properties of WO_3 thin film gas sensors," *Thin Solid Films*, vol. 375, pp. 142-146, 2000.

[83] C. Cantalini, M. Pelino, H. T. Sun, M. Faccio, S. Santucci, L. Lozzi, and M. Passacantando, "Cross sensitivity and stability of NO_2 sensors from WO_3 thin film," *Sens. Actuators B*, vol. 35-36, pp. 112-118, 1996.

[84] X. He, J. Li, X. Gao, and L. Wang, "NO_2 sensing characterisitics of WO_3 thin film microgas sensor " *Sens. Actuators B*, vol. 93, pp. 463-467, 2003.

[85] M. Penza, C. Martucci, and G. Cassano, "NO_x gas sensing characteristics of WO_3 thin films activated by noble metals (Pd, Pt, Au) layers," *Sens. Actuators B*, vol. 64, pp. 52-59, 1998.

[86] R. Boulmani, M. Bendahan, C. Lambert-Mauriat, M. Gillet, and K. Aguir, "Correlation between rf-sputtering parameters and WO_3 sensor response towards ozone " *Sens. Actuators B*, vol. 125, pp. 622-627, 2007.

[87] J. L. Solis, S. Saullo, L. Kish, C. G. Granqvist, and V. Lantto, "Semiconductor gas sensor based on nanostructured tungsten oxide," *Thin Solid Films*, vol. 391, pp. 255-260, 2001.

ISBN:978-84-691-9748-6 /DL:T-1249

[88] M. Stankova, X. Vilanova, J. Calderer, E. Llobet, P. Ivanov, I. Gràcia, C. Cané, and X. Correig, "Detection of SO_2 and H_2S in CO_2 stream by means of WO_3-based micro-hotplate sensors," *Sens. Actuators B*, vol. 102, pp. 219-225, 2004.

[89] M. Stankova, X. Vilanova, E. Llobet, J. Calderer, C. Bittencourt, J. J. Pireaux, and X. Correig, "Influence of the annealing and operating temperatures on the gas-sensing properties of rf sputtered WO_3 thin film sensors," *Sens. Actuators B*, vol. 105, pp. 271-277, 2005.

[90] F. Hellegouarc'h, F. Arefi-Konsari, R. Planade, and J. Amouroux, "PECVD prepared SnO_2 thin films for ethanol sensors," *Sens. Actuators B*, vol. 73, pp. 27-34, 2001.

[91] http://www.epa.gov/air/urbanair/6poll.html.

[92] http://reports.eea.europa.eu/.

[93] http://ec.europa.eu/enterprise/environment/reports_studies/reports/study1.pdf.

[94] L. F. Reyes, A. Hoel, S. Saukko, P. Heszler, V. Lantto, and C. G. Granqvist, "Gas sensor response of pure and activated WO_3 nanoparticle films made by advanced reactive gas deposition," *Sens. Actuators B*, vol. 117, pp. 128-134, 2006.

[95] B. T. Marquis and J. Vetelino, "A semiconductor metal oxide sensor array for the detection of NO_x and NH_3," *Sens. Actuators B*, vol. 77, pp. 100-110, 2001.

[96] http://www.greenfacts.org/air-pollution/ozone-o3/index.htm.

[97] http://www.atsdr.cdc.gov/.

[98] L. Mädler, T. Sahm, A. Gurlo, J. D. Grunwaldt, N. Bârsan, U. Weimar, and S. E. Pratsinis, "Sensing low concentration of CO using flame-spray-made Pt/SnO_2 nanoparticles " *Journal of Nanoparticles Research*, vol. 8, pp. 783-796, 2006.

[99] A. Labidi, E. Gillet, R. Delamare, M. Maaref, and K. Aguir, "Ethanol and ozone sensing characteristics of WO_3 based sensors activated by Au and Pd," *Sens. Actuators B*, vol. 120, pp. 338-345, 2006.

UNIVERSITAT ROVIRA I VIRGILI
STUDY OF STRUCTURAL AND SENSING PROPERTIES OF TUNGSTEN TRIOXIDE THIN FILMS
DEPOSITED BY RF SPUTTERING
Stella Vallejos Vargas
ISBN:978-84-691-9748-6 /DL:T-1249

CHAPTER 2

Experimental

UNIVERSITAT ROVIRA I VIRGILI
STUDY OF STRUCTURAL AND SENSING PROPERTIES OF TUNGSTEN TRIOXIDE THIN FILMS
DEPOSITED BY RF SPUTTERING
Stella Vallejos Vargas
ISBN:978-84-691-9748-6 /DL:T-1249

2.1. Sensor technology

The experiments included gas sensor micro-system fabrication and sensing layer characterization. The micro-system fabrication consisted of two steps: (1) preparation of the micro-machined substrate arrays and (2) WO_3 thin film deposition by r.f. sputtering.

2.1.1. Micro-machined substrate technology

The sensor substrate employed to fabricate the WO_3 based-gas sensors consists of four-element micro-hotplates array mounted on a TO-8 package (Figure 2.1, left). This integrated sensor substrate (chip) was developed at the National Center of Microelectronics (CNM, Bellaterra, Barcelona, Spain) using micro-systems technology [1-4]. The design was carried out by finite-element analysis in order to achieve a low power consumption which was demonstrate to be about 30 mW in air for an average temperature over the heater resistor of 350 ºC [1, 2]. The chips were fabricated on double-side polished p-type <100> Si substrates with 300 µm thickness. Each chip had four Si_3N_4 membranes, of 1 mm × 1 mm and 0.3 µm of thickness, grown by LPCVD. Boron was implanted in order to reduce the stress. Onto each membrane was deposited:

- *a heater* which consists of a $POCl_3$-doped polysilicon meander shaped resistor of 16 Ω/sq with a thickness of 0.47 µm and a temperature coefficient of resistance (TCR) of 6.79×10-4/ºC;
- *a SiO_2 layer* in order to insulate the heater from the electrodes and the sensing film. It has a thickness of 0.8 µm;
- *an interdigitated electrode* which consists of Pt deposited by sputtering. The electrode area and the electrode thickness are 400 µm x 400 µm and 0.2 µm, respectively. Two types of interdigitated electrode configurations were

included in the chip, one with 100 µm gap and another with 50 µm gap (Figure 2.1, right).

- *a sensing layer* which consists of WO_3 thin films deposited by rf sputtering.

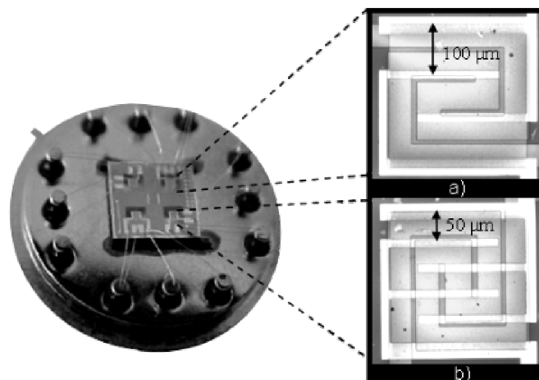

Figure 2.1. On the left: view of the micro-array mounted on standard TO-8. On the right: detailed views of the micro-machined sensor membranes with interdigitated electrodes. 100 µm gap (a) and 50 µm gap (b).

After deposition of the sensing layer, a back side anisotropic etch process using KOH at 75ºC and 40% wt. was performed. Etching was automatically stopped on the interface between the dielectric membrane and the edge of the highly boron doped silicon plug. A schematic picture of the micro-machined sensor after etching is presented in Figure 2.2. The technology of the micro-machined WO_3-based sensor fabrication included next steps as well: photolithography, lift-off operation, annealing of WO_3 sensing layer, cutting of silicon wafer, bonding and capsulation of the chips in the TO-8 package. The deposition technology and annealed process are described in next section.

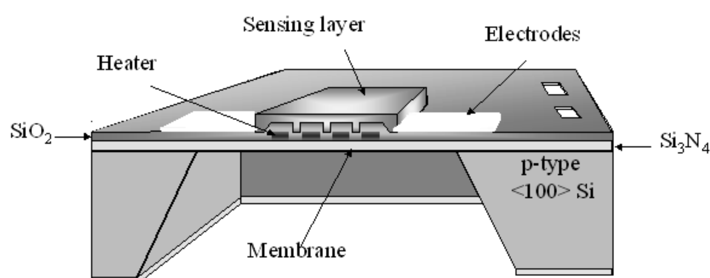

Figure 2.2. Schematic picture of the micro-sensor section.

UNIVERSITAT ROVIRA I VIRGILI
STUDY OF STRUCTURAL AND SENSING PROPERTIES OF TUNGSTEN TRIOXIDE THIN FILMS
DEPOSITED BY RF SPUTTERING
Stella Vallejos Vargas
ISBN:978-84-691-9748-6 /DL:T-1249

2.1.2. WO_3 thin film deposition

Previously it was shown that the sensing properties of metal oxides depend strongly on the methods and conditions used during sensing layer formation. Furthermore, grain size reduction in metal oxide films is one of the key factors to enhance the gas sensing properties of semiconductor layers [5, 6]. In this work the idea to create metal-oxide films with small grain size consists in the use of special regimes of thin film deposition by r.f. sputtering of pure metal target. These regimens were named as interruption (or interrupted) regime and floating regime. Next two subsections will present the physical essence of these sputtering techniques and their effects, from the theoretical point of view, on the properties of the deposited thin films.

2.1.2.1. Interruption regime

Basically, the interruption regime implies the deposition of the thin films with one or several interruptions during the thin film formation [7-9]. The interruptions of the deposition process are carried out by closing the shutter placed between the target and the substrate. This technique was used in some previous investigations about the influence of the interruptions on the thin film formation of pure metals [10-12] and double-layer granular SnO_2 [13]. Figure 2.3 shows a schematic illustration of the metal oxide thin film deposited by applying interruption regime (e.g: with three interruptions).

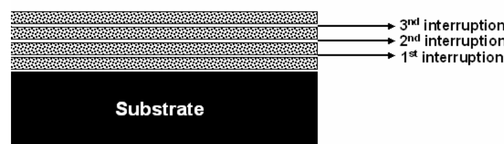

Figure 2.3. Schematic illustration of thin film deposited with three interruptions.

Early, systematic investigations of the growth kinetics of pure metals evaporated on amorphous carbon substrates have revealed that, after interrupting a continuous vapour deposition period by closing the beam shutter, the metal particles continued to grow for up to several minutes with decreasing speed [10-12]. At constant temperature, after re-opening the shutter, particle growth resumed

with a delay being similar to that of particle nucleation. It was shown that there are at least two different mechanisms of adatom diffusion. There exist at least two binding states for the metal atoms with energies of about 1 eV for regular states and in the range from 1.5 to 1.7 eV with abundance of 10^{13} to 10^{14} cm^{-2} [10, 12]. The occurrence of growth transients after closing the beam shutter requires re-emission of adatoms from the sites with higher energy in an activated process of particle growth. Porosities in the substrate surface could be responsible for temporarily trapping of adatoms in states with higher energy. The detailed evolution of stress in thin films that grow by the Volmer–Weber (VW) mechanism during ultra-high vacuum deposition and growth interrupts was explored using real-time wafer curvature measurements [14-16]. It was shown that reversible stress changes during the interruption of thin film growth are phenomenologically similar in the pre-coalescence and post-coalescence growth regimes. It was suggested that the reversible stress changes are associated with changes in the concentration of atomic defects on the substrate and film surface [16]. At the pre-coalescence stages of growth initiation, the dominant defects are isolated adatoms. At the post-coalescence stages, film surface is likely to be atomically rough, with excess adatoms, ledges and other defects. When film growth is interrupted, the defect population decays to the equilibrium value as excess adatoms diffuse to incorporation sites and excess defects are eliminated [16].

During the interruption of the deposition process at the post-coalescence stages of film growth, an equilibrium film surface can be formed due to the free surface bond saturation by the atoms from the residual atmosphere and/or the structural relaxation of the interface [17]. Figure 2.4 illustrates, for the two possible cases, the way in which the equilibrium surface is formed during an interruption process. The saturation of metal films by oxygen atoms from the residual atmosphere has been shown earlier by the investigation of sputtering-deposited molybdenum films [18]. It could be realized by the formation of bonds between metal atoms and O-ions accelerated from the target (Figure 2.4.b). It is known that a deposited thin film tries to minimize its total energy by keeping its surface area as small as possible to obtain an ideally flat surface. Surface diffusion of the adatoms makes possible the occupancy of empty sites in the film lattice and can lead to less surface area by filling in the valleys and leveling the atom peaks to give a lower

ISBN:978-84-691-9748-6 /DL:T-1249
Study of structural and sensing properties of tungsten trioxide thin films deposited by rf sputtering

surface energy [16, 19, 20] (Figure 2.4.c). Thus, the surface diffusion of adatoms during interruption of the deposition could promote both film growth continuation [10-12] and structure relaxation of the film surface [16, 19, 20].

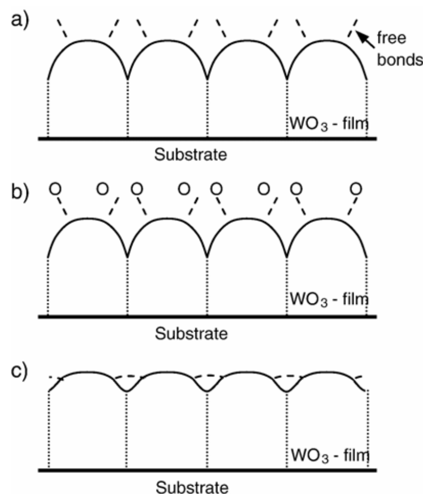

Figure 2.4. Schematic illustrations of the manner of a film growth (a) and an equilibrium surface formation during interruption processes (b, c). Subplots b and c show the saturation of surface free bonds by oxygen atoms (b) and the structural relaxation of the surface (c).

For the subsequent prolongation of the deposition process, film growth begins over again on the new "extra" equilibrium surface (relaxed surface) and the average grain size of the film at the surface could be smaller than in the original film. The equilibrium surface is sufficiently rough and there can be coalescence between both new islands and a new island and an existing film grain [20]. Figure 2.5 shows a qualitative representation of the influence of the deposition interruptions on thin film thickness and grain size growth [17]. The qualitative views of the dependencies of film thickness and grain size on deposition time were built on the base of theoretical and experimental data presented in Ref.[19]. So, Figure 2.5,a sketches out the change in film thickness after each interruption. Lines 0, 1 and 2 present the change in film thickness as a function of deposition time for the film deposited without interruptions (line 0) and with one (line 1) and two (line 2) interruptions, respectively. Lines 1 and 2 show the time delay necessary for the nucleation of new particles [10]. The points 0, 1 and 2 define the film thickness after the end of the deposition process. Figure 2.5,b shows a

reiteration of the nucleation of grains on each new "extra" equilibrium surface formed after the interruption of the deposition process. Lines 0′, 1′ and 2′ present grain growth in the film as a function of deposition time for the film deposited without interruption (line 0′) and with one (line 1′) and two (line 2′) interruptions, respectively. The points 0′, 1′ and 2′ define grain size in the films after the end of the deposition process. The differences in grain size after the first and second interruption are related to the coalescence between both new islands and a new island and an existing grain in the film [10, 20].

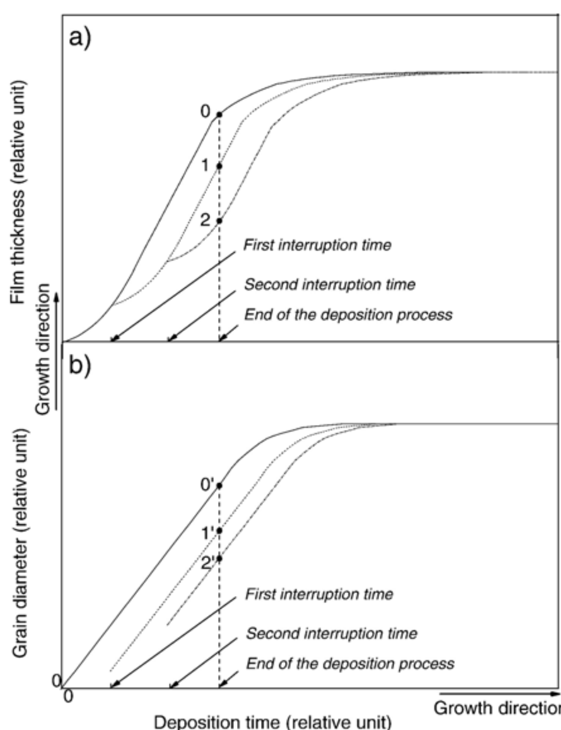

Figure 2.5. Qualitative views of the dependencies of film thickness (a) and grain size (b) on deposition time. Labels 0, 1 and 2 correspond to deposition processes without and with one and two interruptions, respectively.

2.1.2.2. Floating regime

Actually, floating regime implies the deposition of the film with one or several interruptions (as in the interruption regime) with the peculiarity that two power densities are used: the first one to deposit the first interrupted layers within the bulk of the film and the second one to deposit the superficial layer. Figure 2.6

ISBN:978-84-691-9748-6 /DL:T-1249

shows a schematic illustration of the metal oxide thin film deposited using floating regime (e.g: three interruptions).

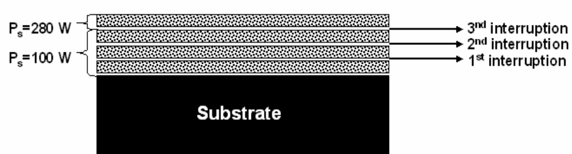

Figure 2.6. Schematic illustrations of thin film deposited using floating regime

The idea consists in the use of low deposition rate during the initial stage of film formation and high deposition rate during the final stage of the deposition. So that the grain size in the surface of the film could become smaller. The decrement of the grain size (due to the increment of deposition rate) is related with the fact that film atoms just impinged on the surface (although they may possess a large surface mobility) rather penetrate into the superficial layers at high deposition rates than diffuse along the surface [19]. This effect takes place only after a minimal deposition rate has been exceeded (see Figure 2.7). Before this value the grain size in the film is limited by the temperature. On the other hand, the increment of deposition rate during the final stage of film formation may also lead to the film surface with higher purity. Several studies demonstrated that at higher deposition rates most impurities should be preferentially removed (during resputtering) relative to the atoms of the main film [21].

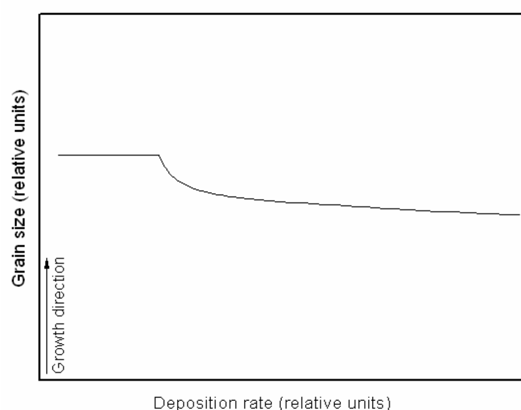

Figure 2.7. Dependence of grain size on deposition rate [19].

ISBN:978-84-691-9748-6 /DL:T-1249

2.1.2.3. Sensing layer formation

Tungsten trioxide thin films were deposited by r.f. magnetron sputtering on boron-doped Si (100) wafers and silicon micro-machined substrates. The WO_3 films deposited on silicon wafers were employed as test structure to carry out the morphological and structural investigations of WO_3 thin films. The deposition of WO_3 films on silicon micro-machined substrates allowed studying their sensing properties. During scientific work two sets of the sensing layer formation on silicon micro-machined substrates were done. Throughout the second set of the sensing layer formation on silicon micro-machined substrates the operations of film deposition, annealing of thin film deposited and lift-off were optimized.

The depositions were performed using an ESM100 Edwards sputtering system. WO_3 thin films were deposited using a tungsten target of 99.95% purity with a diameter of 100 mm and a thickness of 3.175 mm. The target to substrate distance was set to 70 mm. The substrate temperature was kept constant during films deposition at room temperature. The base pressure in the sputtering chamber was 6×10^{-3} mbar. The sputtering atmosphere consisted of Ar-O_2 mixed gas and its flow rate was controlled by separated gas flow-meters to provide Ar:O_2 flow ratio of 1:1. The pressure in the deposition chamber during sputtering was 5×10^{-3} mbar. The sensing films were deposited using two sputtering regimes. First one included three interruptions of the deposition process. The rf sputtering power was 100 W and the interruption time was changed from 0.5 min to 5.0 min. Second one comprised a deposition by using floating regime. The thin film was deposited with three interruptions. In the first two interruptions the sputtering power was 100 W and in last one the sputtering power was set to 280 W. Table 2.1 presents the parameters of the WO_3 film deposition with the interruption and floating regimes and the conditions used for each regime.

The active layer thickness was up to 0.09 µm for silicon wafers, 0.25 - 0.27 µm for the first set of deposition on silicon micro-machined substrates (with interruptions only), 0.2 µm for the second set of deposition on silicon micro-machined substrates (with interruption and floating regimes). After deposition the thin films were annealed at 400 ºC during 2 h.

UNIVERSITAT ROVIRA I VIRGILI
STUDY OF STRUCTURAL AND SENSING PROPERTIES OF TUNGSTEN TRIOXIDE THIN FILMS
DEPOSITED BY RF SPUTTERING
Stella Vallejos Vargas
ISBN:978-84-691-9748-6 /DL:T-1249

Table 2.1. Interruption and floating regime conditions during WO_3 thin film deposition. The total deposition time was 40 min for samples deposited onto Si wafers and 120 min for samples deposited on Si micro-machined substrates.

Substrate	Interruption regime		Floating regime	
	N_i	t_i (min)	N_i	t_i (min)
Test structure	0	-	3	1.5
(Si wafer)	1	0.5		
	2	0.5		
	3	0.5; 1.5; 3; 5		
Si micro-machined	0	-		
(1st set of samples)	3	1.5		
Si micro-machined (2nd set of samples)	3	1.5	3	1.5

N_i and t_i represent the number of interruptions and the time of interruptions, respectively.

ISBN:978-84-691-9748-6 /DL:T-1249

2.2. Characterization techniques

2.2.1 Morphological characterization

The study of the surface morphology of the WO_3 thin film samples deposited using the interruption and floating regimes was performed under ambient conditions on an Atomic Force Microscope (AFM) from Molecular Imagining Corp. (PicoScan controller). AFM is a powerful microscope technique with high spatial resolution that is used to study the morphology of a surface by scanning it with a special tip (needle). The working fundaments of the AFM technique are described in detail in [22].

The instrument used for the experiments was operated in dynamic (ac) mode, also known as tapping mode, in order to reduce surface distortions during imaging [23]. During the first experiments carried out for WO_3 thin films deposited with interruptions the surface was scanned by a silicon tip (from Micromash Inc.) with a nominal radius of curvature up to 10 nm and a frequency up to 300KHz. Later, a new tip (from BudgetSensors) with the same parameters was used in the experiments. The estimation of the mean grain size and image processing were achieved using MetaMorph 6.1 and WSxM 4.0 software respectively. The mean diameter of grains was calculated for a population of one hundred elements in all cases, and the standard error of the mean diameter of grains (*SEM*) was calculated with the following expression:

$$SEM = \frac{SD}{\sqrt{n}}$$

Eq. 2.1. Standard error of the mean.

Where *SD* is the standard deviation and *n* the number of elements.

UNIVERSITAT ROVIRA I VIRGILI
STUDY OF STRUCTURAL AND SENSING PROPERTIES OF TUNGSTEN TRIOXIDE THIN FILMS
DEPOSITED BY RF SPUTTERING
Stella Vallejos Vargas
ISBN:978-84-691-9748-6 /DL:T-1249

2.2.2 Film thickness measurements

The WO_3 film thickness and refractive index were measured by ellipsometry [24]. The measurements were performed at 50º and 60º of incidence angle with a Plasmos 2000 ellipsometer. As-deposited and annealed tungsten oxide films had refractive index of 2.08 - 2.13 that corresponded those obtained in Ref.[25]. In order to check the film thickness the samples were measured by stylus profilomentry [24]. The instrument used for this purpose was a Dektak 3030 with a 2.5 micron diamond stylus.

2.2.3 Structural characterization

The structural features of the WO_3 thin films samples were studied by X-ray diffraction (XRD). This technique is ideally suited for the characterization and identification of polycrystalline phases. Basically, it is based on the interaction of the X-rays with the sample in order to obtain a diffraction pattern, which acts like a fingerprint of the material. The working fundaments of X-ray diffraction are well explained in [26].

X-ray diffraction (XRD) measurements were made using a Siemens D5000 diffractometer (Bragg-Brentano parafocusing geometry and vertical θ-θ goniometer) fitted with a curved graphite diffracted-beam monochromator and Soller slit, 0.2 mm receiving slit and scintillation counter as detector. The angular range was between 19º and 70º for 2θ. Data were collected with an angular step of 0.02º and 6 s per step and sample rotation. $CuK_{\forall}$ radiation was obtained from a Cu X-ray tube operated at 40 kV and 30 mA.

To run XRD measurements at high temperature, an Anton–Paar HTK10 temperature chamber with a platinum ribbon as a heating stage was attached to the diffractometer. The patterns were collected at ΔT=100ºC after 300 s of delay time at heating/cooling rate of 0.17 ºC/s. Temperature range used for the analysis was set to 23-800 ºC. A static air atmosphere was introduced in the chamber throughout the measurement. X-ray diffractograms were analyzed using a Fundamental Parameters Approach convolution algorithm implemented in the TOPAS programme. TOPAS was necessary to configure previously to fit

ISBN:978-84-691-9748-6 /DL:T-1249

diffractograms obtained in grazing incidence geometry. It was used the profile fitting procedure of TOPAS for all diffractograms measured for WO_3 samples at various temperatures.

2.2.4 Gas sensing characterization

The WO_3 micro sensors were characterized towards various oxidizing (nitrogen dioxide NO_2, ozone O_3, nitrogen oxide NO) and reducing (ammonia NH_3, sulfur hydrogen H_2S, carbon monoxide CO, ethanol C_2H_6O) target gases. Most of these gases, at relative low concentrations, are considered very harmful not only to our health but also to the environment in which we live. For these reason monitoring these contaminants represents a very important task. The WO_3-sensor responses were measured to various gas concentrations and various sensor operating temperatures (between 250ºC and 450ºC). All gases were diluted in synthetic air in order to obtain the desire concentration. For most of the experiments the total flow was adjusted at 100 cm^3/min, some experiments were carried out with a total flow of 200 cm^3/min. Table 2.2 presents a list of the measured target gases and their concentrations.

Table 2.2. Target gases and their concentrations.

Target gases	Concentrations, ppm
Nitrogen dioxide, NO_2	0.5, 1, 2
Ozone, O_3	0.2, 0.4, 0.8
Nitrogen monoxide, NO	1, 2, 3
Ammonia, NH_3	1, 2, 3, 20
Sulfur hidrogen H_2S	3, 5
Carbon monoxide, CO	10, 20, 30
Ethanol, C_2H_6O	10, 25, 50, 100

The sensitivity was defined as:

$$S = \frac{R_{air}}{R_{gas}}$$

Eq. 2.2. Sensitivity to oxidizing gases.

$$S = \frac{R_{gas}}{R_{air}}$$

Eq. 2.3. Sensitivity to reducing gases.

ISBN:978-84-691-9748-6 /DL:T-1249

Where, R_{air} is the air sensor resistance at the stationary conditions and R_{gas} represents the resistance after the exposure of the sensor in the toxic gas atmosphere during definite time.

In order to investigate the gas sensing properties of the WO_3 active layers, the response of the sensors to various target gases was measured using a continuous flow system to control the gaseous species tested and a measurement electronic system to acquire the output resistance changes of the sensor. A schematic illustration of the experimental set-up is presented in Figure 2.8.

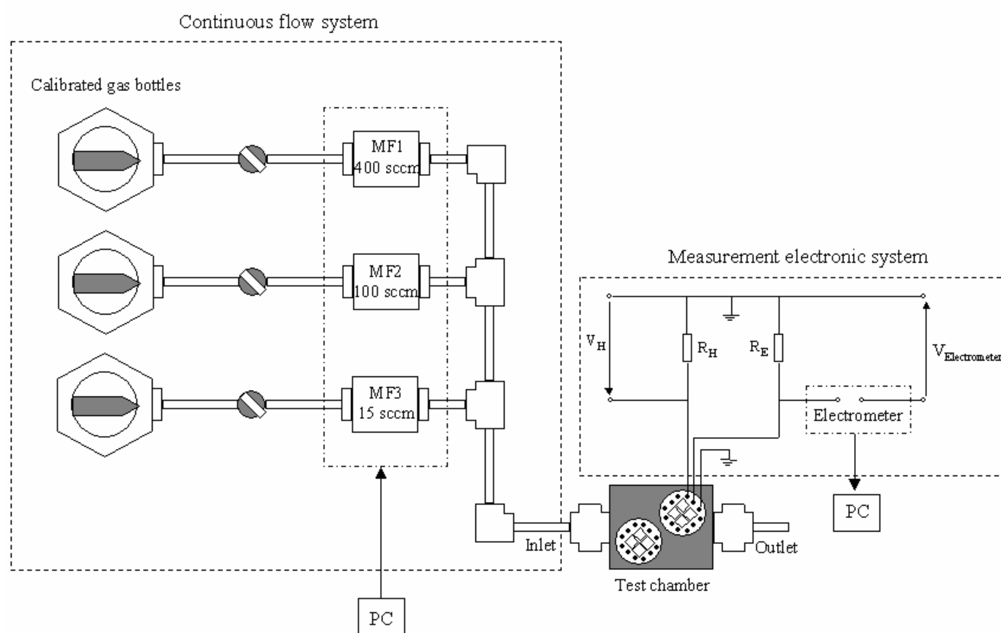

Figure 2.8. Experimental set-up. The measurement electronic system is described for one micro-sensor. MF: mass flow, VH: heater voltage, RH: heater resistance, RE: electrode resistances.

The continuous flow system was consisted of:

- *3 mass flow (MF) devices* which were used to study the sensor response to target gases from commercial available bottles (NO_2, NO, NH_3, CO). The MF devices had different maximum flow levels (MF1: 400 sccm, MF2: 100 sccm, MF3: 15 sccm) that were calibrated with synthetic air (this did not lead to

significant errors since in the experiments the measured analytes measured were highly diluted in air). These devices were controlled by a desktop PC that worked as a mass flow controller (Bronkhorst hi-tech 7.03.241). Furthermore, behind the mass flow system there was a sensor which controlled the temperature and humidity of the gas mixture. Thus, in the experiments the temperature and relative humidity (R.H). of the gases were kept at 30 ºC and 10 % respectively. More details about the mass flow system are described in [27].

- *An ozone generator* which was used to study the sensor response to O_3. The sensor characterization to ozone was carried out at the Laboratory of Materials and Microelectronics of Provence (L2MP) in Marseille, France. The generator was made by UPV, Inc. and it consists of a stable source of 185 nm radiation, a quartz reduction duct and radiation housing. This system produce a stable source of ozone for 100 h of operation, moreover the ozone concentrations can be obtained in the range of 0.1-0.8 ppm by adjusting the system in accordance with the calibration curves of the generator [28]. More details about flow system to measure ozone are described in [29].
- *A test chamber*, where two micro-systems with four micro-sensors each one were placed. The volume of the test chamber was up to 36 cm^3.

The measuring electronic system consisted of:

- *An electrometer* (from Keithley Instruments Inc., model 6517A) that measured the sensor resistance output. This electrometer had a current measurement range of $10^{-16} – 2·10^{-2}$ A, with an error of 1–0.1% in accordance with the range. Besides, it included a scanner card: model 6522 voltage/current made by the same company that provided up to ten channels with 3-lug triax input connectors.
- *A power supply* (FAC 363B 30V/2A) to obtain the required heater voltage (V_H) by the operation.

UNIVERSITAT ROVIRA I VIRGILI
STUDY OF STRUCTURAL AND SENSING PROPERTIES OF TUNGSTEN TRIOXIDE THIN FILMS
DEPOSITED BY RF SPUTTERING
Stella Vallejos Vargas
ISBN:978-84-691-9748-6 /DL:T-1249

2.3. Summary and outlook

In this chapter, it was presented and discussed two ideas to obtain metal-oxide films with small grain size that are based on the use of special regimes of thin film deposition by r.f. sputtering of pure metal target. The first idea included the deposition of thin films with one or several interruptions during the deposition process (interruption regime). The second idea included the deposition of thin film using two rates of sputtering deposition, one to form the bulk of the film and the other to form the superficial layer of the film (floating regime). Although some studies about the influence of these regimes on the film properties are found in the state-of-the-art, their application in gas sensor devices have not been investigated. That is why these regimes are considered as a novel strategy to deposit sensing films. The theoretical background of these regimes suggests that it is possible to obtain metal oxide films with better surface characteristics for gas sensing application. In this context, the study of the surface, structural and sensing features of the films deposited using these regimes is essential.

This chapter includes the description of the micro-machined substrates, the experimental set-up and the equipments employed to study the physical and sensing characteristics of the films deposited using the interruption and floating regimes.

Bibliography

[1] A. Götz, I. Gràcia, C. Cané, E. Lora-Tamayo, M. C. Horillo, J. Getino, C. Garcia, and J. Gutiérrez, "A micromachined solid state integrated gas sensor for the detection of aromatic hydrocarbons," *Sens. Actuators B*, vol. 44, pp. 483-487, 1997.

[2] M. C. Horillo, I. Sayago, L. Arés, J. Rodrigo, J. Gutiérrez, A. Götz, I. Gràcia, L. Fonseca, C. Cané, and E. Lora-Tamayo, "Detection of low NO_2 concetration with low power micromachined tin oxide gas sensor," *Sens. Actuators B*, vol. 58, pp. 325-329, 1999.

[3] D. G. Rickerby, N. Wächter, M. C. Horillo, J. Gutiérrez, I. Gràcia, and C. Cané, "Structural and dimensional control in micromachines integrated solid state sensors," *Sens. Actuators B*, vol. 69, pp. 314-319, 2000.

[4] I. Gràcia, J. Santander, C. Cané, M. C. Horillo, I. Sayago, and J. Gutiérrez, "Results of the reability of silicon micormachined structures for semiconductor gas sensors," *Sens. Actuators B*, vol. 77, pp. 409-415, 2001.

[5] G.-J. Li, Z. X.-H, and S. Kawi, "Relationships between sensitivity, catalytic activity, and surface areas of SnO_2 gas sensors," *Sens. Actuators B*, vol. 60, pp. 64-70, 1999.

[6] G. Zangh and M. Liu, "Effect of particle size and dopant on properties of SnO_2 - based gas sensor," *Sens. Actuators B*, vol. 69, pp. 144-152, 2000.

[7] V. Khatko, J. Calderer, E. Llobet, and X. Correig, "New technology of metal oxide thin film preparation for chemical sensor application," *Sens. Actuators B*, vol. 109, pp. 128-134, 2005.

[8] V. Khatko, S. Vallejos, J. Calderer, E. Llobet, X. Vilanova, and X. Correig, "Gas sensing properties of WO_3 thin films deposited with interruptions," presented at 19th European Conference on Solid State Transducers, EUROSENSORS XIX Barcelona, Spain, 2005.

[9] V. Khatko, S. Vallejos, J. Calderer, E. Llobet, X. Vilanova, and X. Correig, "Gas sensing properties of WO_3 thin films deposited by rf sputtering " *Sens. Actuators B*, vol. 126 . pp. 400-405, 2007.

[10] A. A. Schmidt and R. Anton, "Anomalous growth behaviour of Pd-Au and Ag-Au alloy particles during vapour deposition on carbon substrates at elevated temperatures," *Surf. Sci.*, vol. 322, pp. 307-324, 1995.

[11] A. A. Schmidt, H. Eggers, H. Herwing, and R. Anton, "Comparative investigation of the nuclation and growth of fcc-metal particles (Rh, Ir, Ni, Pd, Pt, Cu, Ag, Au) on amorphous carbon and SiO_2 substrates during vapor deposition at elevated temperatures," *Surf. Sci.*, vol. 349, pp. 301-316, 1996.

[12] R. Anton and A. A. Schmidt, "Anomalous nucleation and growth of metal and alloy particles during vapor deposition on amorphous substrates," *Surf. Sci.*, vol. 357-358, pp. 835-839, 1996.

[13] T. Aste, R. Botter, and D. Beruto, "Double-layer granular SnO_2 sensors," *Sens. Actuators B*, vol. 24-25, pp. 826-829, 1995.

[14] J. A. Floro, S. J. Hearne, J. A. Hunter, P. Kotula, E. Chason, S. C. Seel, and C. V. Thompson, "The dynamic competition between stress generation and relaxation mechanisms during coalescence of Volmer-Weber thin films," *J. Appl. Phys.*, vol. 89, pp. 4886-4897, 2001.

[15] C. Friesen and C. V. Thompson, "Reversible stress relaxation during precoalescence interruptions of Volmer-Weber thin film growth," *Phys. Rev. Lett.*, vol. 89, pp. 6163, 2002.

[16] C. Friesen, S. C. Seel, and C. V. Thompson, "Reversible stress changes at all stages of Volmer-Weber film growth " *J. Appl. Phys.*, vol. 95, pp. 1011-1020, 2004.

UNIVERSITAT ROVIRA I VIRGILI
STUDY OF STRUCTURAL AND SENSING PROPERTIES OF TUNGSTEN TRIOXIDE THIN FILMS
DEPOSITED BY RF SPUTTERING
Stella Vallejos Vargas
ISBN:978-84-691-9748-6 /DL:T-1249

[17] V. Khatko, J. Calderer, S. Vallejos, E. Llobet, and X. Correig, "Technology of metal oxide thin film deposition with interruptions," *Surface and Coatings Technology* vol. 202 pp. 453-459., 2007.

[18] T. T. Bardin, J. C. Pronko, and R. C. Budhan, "The effect of oxygen concentration in sputter-deposited molybdenum films," *Thin Solid Films*, vol. 165 pp. 243-247, 1988.

[19] C. A. Neugebauer, "Condentation, nucleation and growth of thin films," in *Hand book of thin film technology*, L. Maissel and R. Glang, Eds., 1970.

[20] F. Spaepen, "Interfaces and stresses in thin films," *Acta Mater*, vol. 48, pp. 31-42, 2000.

[21] L. Maissel, "Application of sputtering to the deposition of films " in *Hand book of thin film technology*, L. I. Maissel and R. Glang, Eds.: McGraw-Hill, 1970.

[22] V. L. Mironov, *Fundamentals of the scanning probe microscopy*: Nizhniy Novgorod, 2004.

[23] J. Kopniczky, "Nanostructures studied by atomic force microscopy," Uppsala university, 2003.

[24] A. Wagendristel and Y. Wang, *An introduction to physics and technology of thin films*, 1994.

[25] D. J. Taylor, J. P. Cronin, L. F. Allard, and D. P. Birnie, "Microstructure of laser-fired, sol-gel-derived tungsten oxide films," *Chemistry of Materials*, vol. 8, pp. 1396-1401, 1996.

[26] B. D. Cullity, *Elements of x-ray diffraction,* , 2nd ed. ed. Massachusetts, USA: Addison Wesley 1978.

[27] A. Vergara, "Improving the performance of micro-machined metal oxide gas sensors: optimization of the temperature modulation mode via pseudo-random sequences," Universitat Rovira i Virgili, 2006.

[28] http://uvp.com.

[29] A. Labidi, E. Gillet, R. Delamare, M. Maaref, and K. Aguir, "Ethanol and ozone sensing characteristics of WO_3 based sensors activated by Au and Pd," *Sens. Actuators B*, vol. 120, pp. 338-345, 2006.

ISBN:978-84-691-9748-6 /DL:T-1249

CHAPTER 3

Results Part I

ISBN:978-84-691-9748-6 /DL:T-1249

3.1. Physical characterization

In this chapter some physical properties of WO_3 thin films deposited using interruption and floating regimes will be presented. Film thickness, structural features and morphology of WO_3 thin films are investigated as a function of the number of the interruptions (interrupted regime) and the sputtering power (floating regime). The WO_3 films deposited on silicon wafers were employed for the investigation of their film thickness, phase composition and morphology. One part of the silicon wafers used was oxidized in dry oxygen at 1100° C. The thickness of the SiO_2 films was about 150 nm.

3.1.1. WO_3 thin films deposited using interruption regime

Four types of tungsten oxide films were prepared. The first type a non-interrupted sputtered process was used. In the deposition of films type 2, 3 and 4, the sputtering process was interrupted once, two and three times, respectively. A shutter was used to interrupt the deposition process. As a rule, the actual deposition time without interruption was 40 min. Nevertheless, for several tungsten oxide films deposited with interruptions on silicon wafers, the deposition time was up to 2 hours. The interruption time changed from 0.5 min to 5.0 min for the different samples.

3.1.1.1. Film thickness

Figure 3.1 shows the relative change of the metal oxide film thickness (d_{int}/d_o) as a function of the number of interruptions (Figure 3.1,a) and interruption time (Figure 3.1,b) [1]. Here, d_{int} and d_o are the thickness of WO_3 thin films deposited with a definite number of interruptions ($int = 1, \ldots, 3$) and without interruptions ($int = 0$), respectively. For comparison, the experimental data obtained at the r.f.

sputtering power of 200 W taken from previous study [2] is presented in Figure 3.1,a as well.

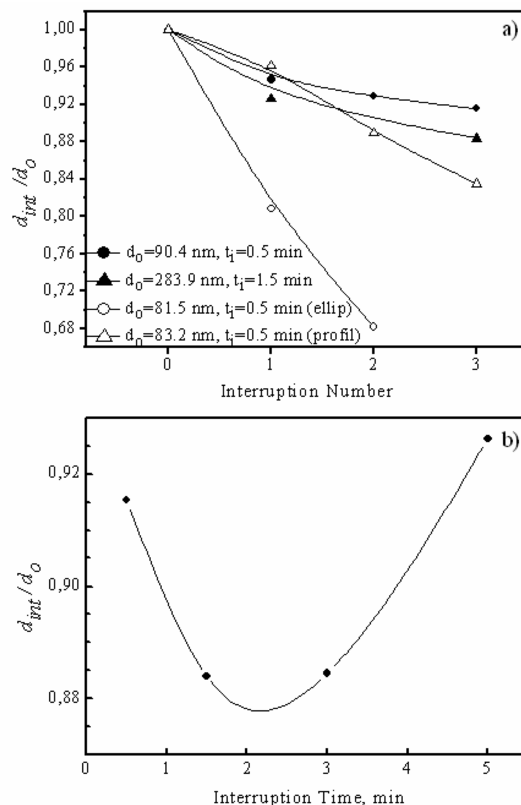

Figure 3.1. Relative change of WO_3 film thickness (d_{int} / d_o) as function of the number of interruptions (a) and interruption time (b). Full (▲) (●) and open (○) (Δ) scatters represents thin films deposited with sputtering power of 100 W and 200 W respectively.

It can be seen that the total thickness (d_{int}) of WO_3 thin films deposited with interruptions decreases when the number of interruptions during the deposition process increases (Figure 3.1,a). This result is verified for the different total thickness of WO_3 thin films and the different r.f. sputtering power of the deposition process. The relative change in the metal oxide film thickness decreases when the total thickness of WO_3 thin films and r.f. sputtering power increases. In the latter case, the use of higher sputtering power (200 W) has an extremely strong influence on the properties and total thickness of the WO_3 thin films [2]. There is a

UNIVERSITAT ROVIRA I VIRGILI
STUDY OF STRUCTURAL AND SENSING PROPERTIES OF TUNGSTEN TRIOXIDE THIN FILMS
DEPOSITED BY RF SPUTTERING
Stella Vallejos Vargas
ISBN:978-84-691-9748-6 /DL:T-1249

difference in the thickness measured by profilometry and ellipsometry for the tungsten oxide thin films deposited with interruptions during the deposition process. For example, the relative changes in the thickness of the films deposited with two interruptions have values of 0.89 and 0.68 measured by profilometry and ellipsometry, respectively (Figure 3.1,a). This result shows that "extra" interfaces are introduced into the body of a thin film during each interruption of the deposition process. At this point we can conclude that the features of the surface relaxation process influence on the formation of "extra" interfaces.

This is confirmed by a stress relaxation study [3-5] and the experimental data presented in Figure 3.1,b. It can be seen that the duration of interruption influences on the total thickness and the relative change of the metal oxide film thickness. For explaining this functional dependence we will use the experimental data obtained in [6] and [7]. It can be assumed that there is some relation between the time in which a film continues to grow after the shutter has been closed and the time delay for the film to resume its growth after re-opening the shutter. Increasing the time in which the film continues to grow could decrease the time delay before resuming its growth. In this case, the relative change of the metal oxide film thickness can have a minimum at a definite value of the interruption time, just as Figure 3.1,b shows. We can conclude that the process of film surface relaxation has a definite time (the time for the connection of all free bonds).

3.1.1.2. Structural features

Figure 3.2 shows the X-ray diffractograms of WO_3 thin films deposited onto a silicon substrate from 2θ = 23.0° to 35°. XRD data showed that the structure of as deposited WO_3 films is amorphous [1, 8]. After annealing at 400 °C one monoclinic phase is present in the thin film that is described with the space groups Pc (ICDD card no. 87-2386, cell parameters: a = 5.277 Å, b = 5.156 Å, c = 7.666 Å, β = 91.742°). XRD patterns contain (110), (200) and (112) reflections from the monoclinic phase (Pc).

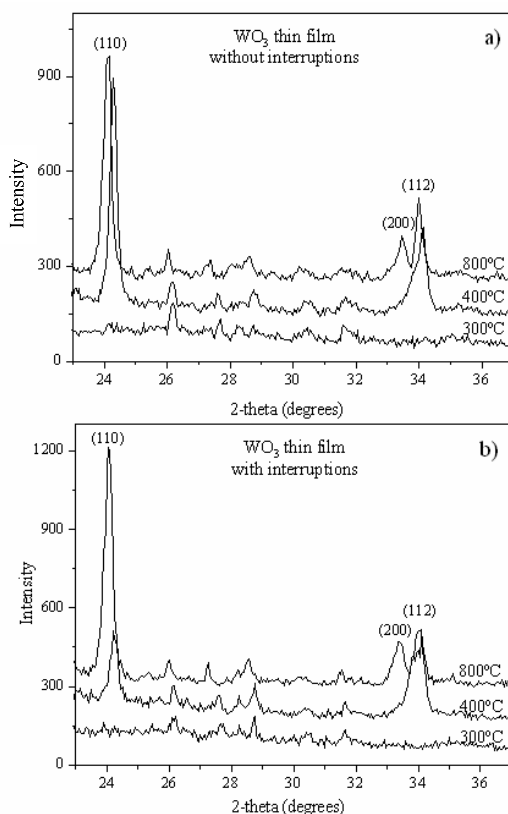

Figure 3.2. X-ray diffractograms of WO_3 thin films deposited without (a) and with three interruptions (b). The corresponding temperatures of the XRD measurements are indicated in the plot.

It can be seen that the process of thin film crystallization has a different activity for both types of WO_3 thin films. The crystallization in the thin film prepared with three interruptions during its deposition (Figure 3.2,b) is slower than in the films prepared without interruptions (Figure 3.2,a). This can be derived by comparing the intensities of (110) peaks and their full widths at half maximum (see Figure 3.3). WO_3 thin films prepared without interruptions have maximum intensity of (110) peak and full width at half maximum of this peak is minimal. It is worth noting that the low-temperature monoclinic phase in WO_3 thin films was stable in a temperature range from 400°C to 800°C. WO_3 thin films were sublimated at 900°C. The same result was obtained for WO_3 thin films deposited onto non oxidized silicon wafers.

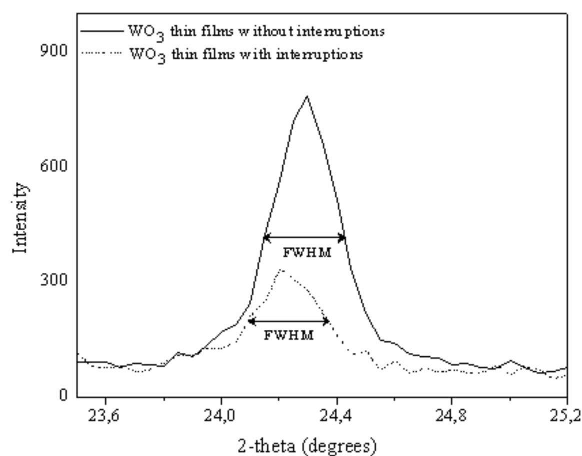

Figure 3.3. Comparison of the intensity and full wide at half medium (FWHM) of the (110) peak for the WO_3 thin films deposited without (——) and with three interruptions (·····).

The fact that the monoclinic phase with Pc symmetry exists in WO_3 thin film deserves some comments. The existence of low-temperature Pc phases has been reported in gas-evaporated WO_3 microcrystals analyzed by Raman spectroscopy [9, 10]. The reason for the existence of Pc phase in these microcrystals could be either high compression stresses or surface effects on the grains or interfaces [11]. In our case the basic reason for the existence of a Pc phase in WO_3 thin films could be compressive stresses into the layers.

3.1.1.3. Morphology of the WO_3 films

Atomic force microscopy (AFM) analysis was performed to find a confirmation that the "extra" interfaces built in the film body at the interruption time influence on the morphology, roughness and mean grain size of the WO_3 surface layer formed during thin film growth. Therefore, Si–SiO_2–WO_3 structures as deposited and annealed at 400 °C and 450 °C were studied by AFM (this structures are used in the micro-machined substrates). The results obtained were compared with the experimental data obtained for Si–WO_3 structures annealed at 400 °C. The films analysed in this section correspond to the films obtained in the first set of the sensing layer formation.

ISBN:978-84-691-9748-6 /DL:T-1249

Figure 3.4 and Figure 3.5 show the surface morphology and roughness profiles of the WO_3 films as deposited and annealed. It can be seen that tungsten oxide grains in the films deposited without interruptions try to reach an ordered distribution after annealing. That is not so clear for all of the films with three interruptions. The occurrence of an ordered distribution is correlated to the results obtained by XRD. The crystalline structure in the films prepared with three interruptions is not fully ordered as in the films prepared without interruptions. On the other hand, the roughness profile analysis along the horizontal lines of the AFM pictures shows that the samples deposited with three interruptions are smoother than those ones deposited without interruptions.

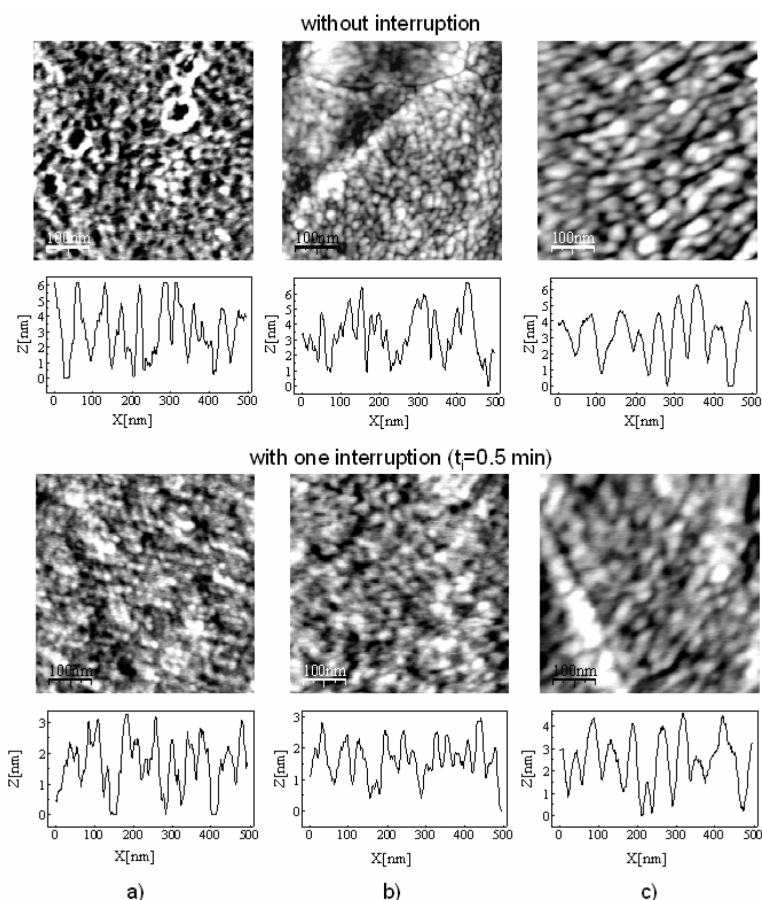

Figure 3.4. AFM surface morphology and roughness profile of WO_3 thin films deposited without interruptions and with one interruption. As deposited (a), annealed at 400ºC (b), annealed at 450ºC (c).

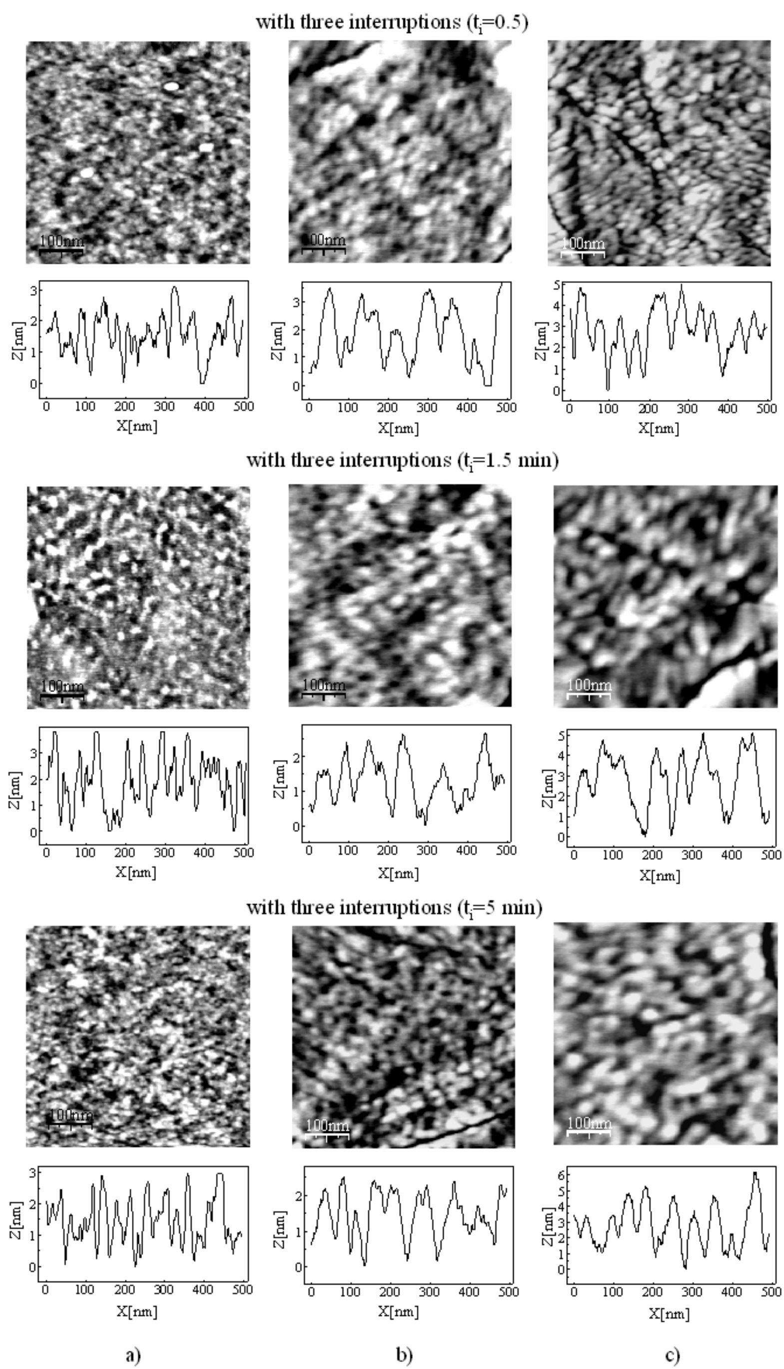

Figure 3.5. AFM surface morphology and roughness profile of WO_3 thin films deposited with three interruptions and interruption time of 0.5 min, 1.5 min and 5 min. As deposited (a), annealed at 400ºC (b), annealed at 450ºC (c).

Figure 3.6 shows the mean diameter of grains in WO_3 films as a function of the number of interruptions and their duration. It can be seen that grain diameter decreases from 20.5 nm down to 17.0 nm in as deposited $Si–SiO_2–WO_3$ structures without and with three interruptions respectively. Increasing the interruption time from 0.5 min up to 5 min results in a further reduction of grain size from 17 nm down to 14 nm. When annealing at 400 °C, the process of WO_3 film crystallization results in a slight increase in the diameter of the grains. There is a tendency showing that the higher the number of interruptions is, the lower the increase in grain size during the annealing process is.

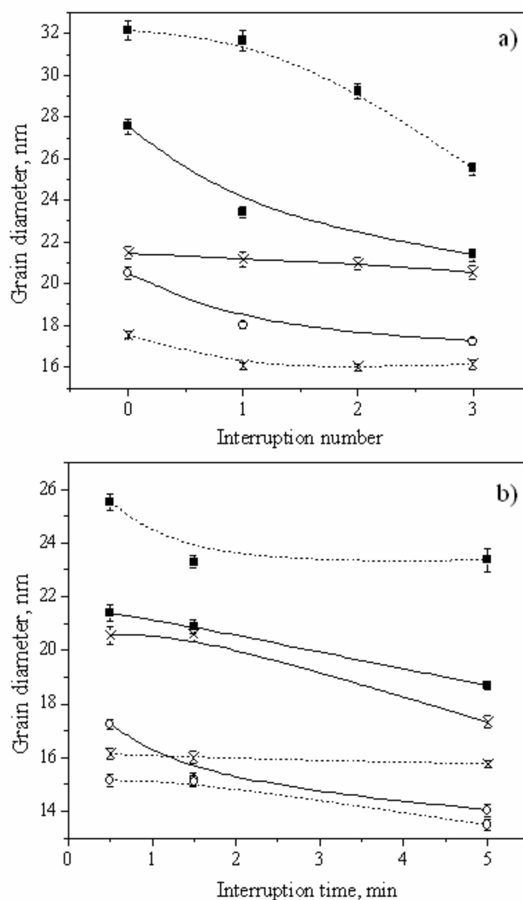

Figure 3.6. Mean diameter of grains in WO_3 films ─ as deposited (○), annealed at 400ºC (x) and annealed at 450ºC (■) ─ as a function of the number of interruptions (a) and interruption time (b). Continuous line (──) and dashed line (---) represent $Si-SiO_2-WO_3$ and $Si-WO_3$ samples respectively. The standard error of the mean is presented in the plot.

ISBN:978-84-691-9748-6 /DL:T-1249

3.1.1.4. Discussion

On the base of the experimental results obtained we can summarize that the introduction of the "extra" interfaces during the deposition interruptions influences the process of WO_3 film crystallization retarding it.

Figure 3.7 shows Auger profiles for two types of as-deposited WO_3 thin films on silicon wafers. It can be seen that the chemical element composition on the surface of tungsten oxide film corresponds to stoichiometric WO_3. The change in the ratio of tungsten to oxygen atoms observed after argon ion etching of the film surface is due to the difference in the scattering coefficient of oxygen and tungsten [12]. The existence of a narrow area (up to 20 nm) close to the film-substrate interface containing a high amount of tungsten atoms could be explained by the formation of WO_{3-x} (Magneli phases) [13]. Nevertheless WO_{3-x} phases were not detected by the XRD method.

The basic conclusion from Figure 3.7 is that there is no heterogeneity at the profiles of tungsten and oxygen atoms. The absence of any segregation of oxygen or tungsten atoms into the thin film body evidences that the process of free bond saturation by the atoms from residual atmosphere on the "extra" interface is not clearly realized or can not be detected by Auger spectroscopy. This result is similar the one presented in Ref. [3] where oxide layers were not observed in Al films deposited with two interruptions. The tendency to obtain smoother surfaces in WO_3 films deposited with several interruptions shows that the process of minimization of film surface energy was repeated several times during interruptions. It could be suggested that the "extra" interface is formed due to the structural relaxation of the additional interface during the interruption time.

3.1.2. WO_3 thin films deposited using floating regime

3.1.2.1. Structural features

Figure 3.8 shows the X-ray diffractograms of WO_3 thin films deposited on silicon substrate using interruption and floating regime. The XRD data of the WO_3 films deposited by floating regime shows that the structure of the as deposited

films is amorphous as well. After annealing at 400 °C a monoclinic phase is present in both samples prepared using interruption and floating regimes. This phase is described with the space groups Pc (ICDD card no. 87-2386, cell parameters: a = 5.277 Å, b = 5.156 Å, c = 7.666 Å, β = 91.742°). XRD patterns contain (110), (200) and (112) reflections from the monoclinic phase (Pc).

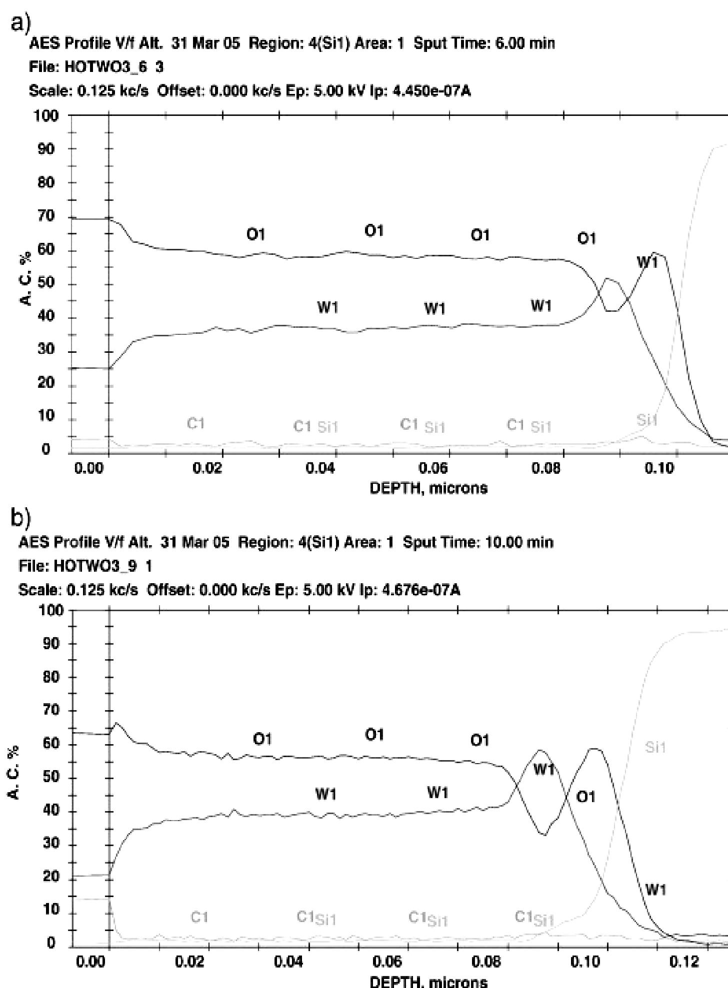

Figure 3.7. Auger profile of chemical elements into WO_3 thin films prepared without (a) and with three interruption (b) during the deposition process. A.C. stands for atomic concentration in %.

ISBN:978-84-691-9748-6 /DL:T-1249

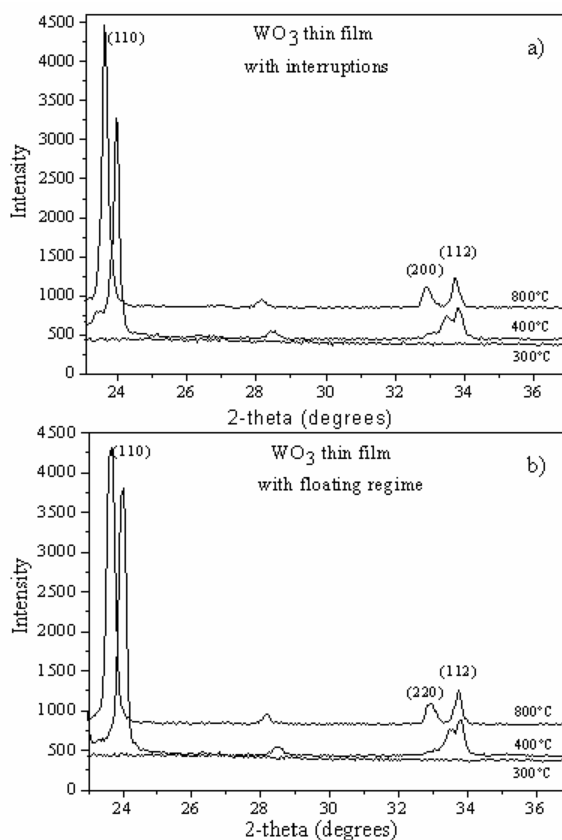

Figure 3.8. X-ray diffractograms of WO_3 thin films deposited with interuptions (a) and with floating regime (b). The corresponding temperatures of the XRD measurements are indicated in the plot.

3.1.2.2. Morphology of the WO_3 films

Figure 3.9 shows the AFM topography images of the WO_3 thin films deposited on silicon wafers using either interruption or floating regime after an annealing at 400ºC (these films correspond to the second set of the sensing layer formation). The AFM analysis did not shown any substantial difference in the grain size and roughness of these samples. It was determined that in both cases the grain size and roughness is approximately 11 nm and 0.30 nm, respectively.

ISBN:978-84-691-9748-6 /DL:T-1249

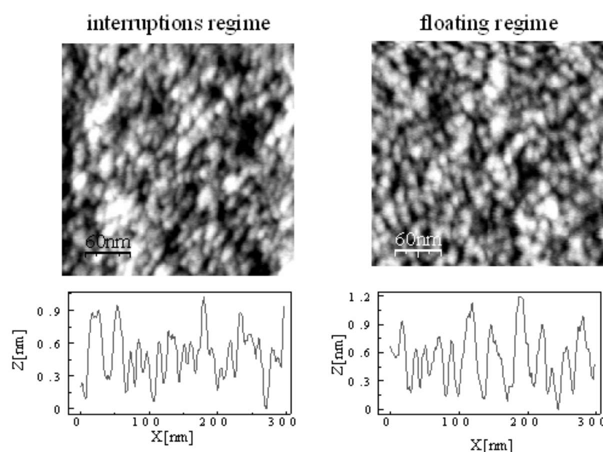

Figure 3.9. AFM surface morphology and roughness profile of WO_3 thin films deposited with interruptions and floating regime. N_i=3 and t_i=1.5 min

3.1.2.3. Discussion

The structural and morphological results obtained by XRD and AFM for two types of WO_3 thin films do not show any differences in the crystallization and grain size growth. This result was not expected since according to Ref. [14], the grain size in the sputtered-deposited films has to decrease when the sputtering power increases (i.e. the films deposited using floating regime have to have smaller grains). It could be possible if the grain size was determined by the diameter of the AFM tip which is around 10 nm, that the grain size decreases in a range less that the diameter of the tip. Therefore it is not possible to determinate the size of the WO_3 grains.

UNIVERSITAT ROVIRA I VIRGILI
STUDY OF STRUCTURAL AND SENSING PROPERTIES OF TUNGSTEN TRIOXIDE THIN FILMS
DEPOSITED BY RF SPUTTERING
Stella Vallejos Vargas
ISBN:978-84-691-9748-6 /DL:T-1249

3.2. Summary and outlook

On the base of the reference analysis and experimental data obtained it could be suggested that "extra" interface is formed into the body of the film due to the surface relaxation during its interrupted growth. At the same time, the experimental data obtained by Auger spectrometry did not show any segregation of oxygen or tungsten atoms into the WO_3 film body.

The introduction of "extra" interfaces in the bulk of the film revealed the possibility to influence on the morphological and structural properties of the deposited films. It was noticed that WO_3 films deposited with interruptions present a retard in the crystallization as well as a decrement in the grain size growth. WO_3 films deposited by floating regime showed similar characteristics. On the base of these results it is possible to conclude that promising WO_3 surface characteristics for the gas sensing applications could be obtained using the interruption and floating regimes during WO_3 sensing layer deposition.

Bibliography

[1] V. Khatko, J. Calderer, S. Vallejos, E. Llobet, and X. Correig, "Technology of metal oxide thin film deposition with interruptions," *Surface and Coatings Technology* vol. 202 pp. 453-459., 2007.

[2] V. Khatko, J. Calderer, E. Llobet, and X. Correig, "New technology of metal oxide thin film preparation for chemical sensor application," *Sens. Actuators B*, vol. 109, pp. 128-134, 2005.

[3] J. A. Floro, S. J. Hearne, J. A. Hunter, P. Kotula, E. Chason, S. C. Seel, and C. V. Thompson, "The dynamic competition between stress generation and relaxation mechanisms during coalescence of Volmer-Weber thin films," *J. Appl. Phys.*, vol. 89, pp. 4886-4897, 2001.

[4] C. Friesen and C. V. Thompson, "Reversible stress relaxation during precoalescence interruptions of Volmer-Weber thin film growth," *Physical Review Letters*, vol. 89, 2002.

[5] C. Friesen, S. C. Seel, and C. V. Thompson, "Reversible stress changes at all stages of Volmer-Weber film growth " *J. Appl. Phys.*, vol. 95, pp. 1011-1020, 2004.

[6] A. A. Schmidt and R. Anton, "Anomalous growth behaviour of Pd-Au and Ag-Au alloy particles during vapour deposition on carbon substrates at elevated temperatures," *Surf. Sci.*, vol. 322, pp. 307-324, 1995.

[7] A. A. Schmidt, H. Eggers, H. Herwing, and R. Anton, "Comparative investigation of the nuclation and growth of fcc-metal particles (Rh, Ir, Ni, Pd, Pt, Cu, Ag, Au) on amorphous carbon and SiO_2 substrates during vapor deposition at elevated temperatures," *Surf. Sci.*, vol. 349, pp. 301-316, 1996.

[8] V. Khatko, S. Vallejos, J. Calderer, E. Llobet, X. Vilanova, and X. Correig, "Gas sensing properties of WO_3 thin films deposited by rf sputtering " *Sens. Actuators B*, vol. 126 . pp. 400-405, 2007.

[9] M. Arai, S. Hayashi, K. Yamamoto, and S. S. Kim, "Raman Studies of Phase-Transitions in Gas-Evaporated WO_3 Microcrystals," *Solid State Communications*, vol. 75, pp. 613-616, 1990.

[10] S. Hayashi, H. Sugano, H. Arai, and K. Yamamoto, "Phase-transitions in gas-evaporated WO_3 microcrystals - a raman-study," *Journal of the Physical Society of Japan*, vol. 61, pp. 916-923, 1992.

[11] A. G. Souza, P. T. C. Freire, O. Pilla, A. P. Ayala, J. Mendes, F. E. A. Melo, V. N. Freire, and V. Lemos, "Pressure effects in the Raman spectrum of WO_3 microcrystals," *Physical Review B*, vol. 62, pp. 3699-3703, 2000.

[12] D. Briggs and M. P. Seah, *Practical surface analysis*, 1990.

[13] A. Al Mohammad and M. Gillet, "Phase transformations in WO_3 thin films during annealing " *Thin Solid Films*, vol. 408, pp. 302-309, 2002.

[14] C. A. Neugebauer, "Condentation, nucleation and growth of thin films," in *Hand book of thin film technology*, L. Maissel and R. Glang, Eds., 1970.

UNIVERSITAT ROVIRA I VIRGILI
STUDY OF STRUCTURAL AND SENSING PROPERTIES OF TUNGSTEN TRIOXIDE THIN FILMS
DEPOSITED BY RF SPUTTERING
Stella Vallejos Vargas
ISBN:978-84-691-9748-6 /DL:T-1249

CHAPTER 4

Results Part II

UNIVERSITAT ROVIRA I VIRGILI
STUDY OF STRUCTURAL AND SENSING PROPERTIES OF TUNGSTEN TRIOXIDE THIN FILMS
DEPOSITED BY RF SPUTTERING
Stella Vallejos Vargas
ISBN:978-84-691-9748-6 /DL:T-1249

4.1. Gas sensing characterization

In this dissertation, gas sensor characterizations were carried out by dc measurements and they were mainly addressed to analyse the three well known S: sensitivity, selectivity and stability. This chapter consists of two basic sections.

The first one presents the experimental data obtained by the investigation of the sensing properties of the test sensing structures and sensing layers deposited on the silicon micro-machined substrates during first set of experiments. The sensing structures were prepared by the deposition of the WO_3 thin films on the top of the silicon wafers oxidised in dry oxygen. The top contacts to the sensing layers were formed using air dry silver paste (Heraeus AD1688-06) and annealed at 400 ºC during 2 h for the contact formation. The diameter of both point contacts was up to 1 mm and the distance between their centrums was up to 3 mm. Using this paste, the test samples were fixed on a ceramic heater prepared according to the method reported in [1]. The WO_3 thin films were deposited using the basic regime (without interruptions) and interrupted regime with different times of the interruptions. During the first set of experiments with CNM wafers the WO_3 sensing layers were deposited on the silicon micro-machined substrates using the basic and interrupted regimes.

The second section of this chapter presents the experimental data obtained by the investigation of the sensing properties of the sensing layers deposited on the silicon micro-machined substrates during second set of experiments. In this case the WO_3 sensing layers were deposited using the interrupted and floating regimes.

4.1.1. WO_3 thin films deposited using interrupted regime

4.1.1.1. Sensitivity

Initially the sensing properties of WO_3 test sensing structures deposited using the basic regime and interrupted regime with different times of the interruption

ISBN:978-84-691-9748-6 /DL:T-1249

(0.5 min. 1.5 min and 5 min) were analysed [2, 3]. The sensor response of the test sensing structure to nitrogen dioxide (NO_2), ethanol (C_2H_6O) and ammonia (NH_3) was investigated. The test structures were placed in moisture controlled test chamber and their operating temperatures were adjusted in the range from 150ºC to 300ºC. Figure 4.1 shows the transient responses (resistance change as function of the time) of the WO_3 thin films to NO_2, NH_3 and C_2H_6O. Figure 4.2 shows the average sensor responses to these gases. It can be seen that WO_3 thin films deposited with three interruptions and interruption duration of more than 1.5 min have the best responses to ammonia, nitrogen dioxide and ethanol. It is important to remark that these results were based on five different deposition batches, which resulted in 80 samples being produced and analysed. Thus, it can be concluded that the deposition method led to reproducible results.

On the base of this preliminary study both interrupted and floating regimes were developed for the sensing layer deposition on the micro-machined substrates Three interruptions and interruption time of 1.5 min were selected for the sensing layer formation.

Table 4.1 shows the mean responses of the WO_3 sensors fabricated using the basic and interruption regimes towards various ozone concentrations [4, 5]. The micro-sensors were operated at different temperatures (250ºC, 350ºC and 450ºC). The responses of four different types of sensors are presented in this table, which correspond to the films prepared with interruptions (S_i) or without them (S_b) and deposited on narrow gap (50 μm) or wide gap (100 μm) electrodes. The sensing response was calculated by using the relationship: R_{gas}/R_{air}. The sensor response measurements for each ozone concentration and operating temperature were carried out eight times. The standard errors (S.E.) of the mean response for the WO_3 sensors deposited with interruptions were below ±0.054 and ±0.771 in the case of the sensors with the electrode gap of 50 μm and 100 μm, respectively. These values were calculated over 8 sensor responses obtained through each pair of two different sensors on the chip.

From Table 4.1, it can be noted that two types of active layers and electrode configurations present the higher responses at the operating temperature of 350 ºC. On the other hand, it is possible to see that the response of the sensors deposited

ISBN:978-84-691-9748-6 /DL:T-1249
Study of structural and sensing properties of tungsten trioxide thin films deposited by rf sputtering

with interruption (S_i) is higher than that of the sensors deposited without interruptions (S_b).

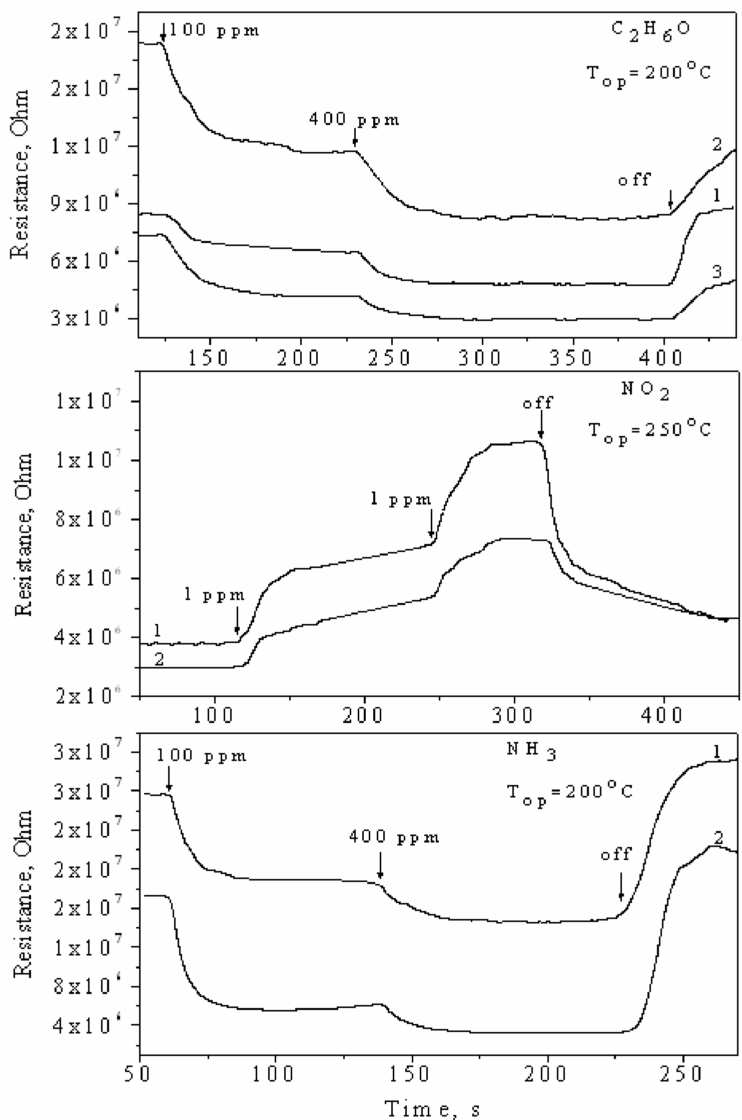

Figure 4.1. Sensor responses of WO_3 thin films to C_2H_6O, NO_2 and NH_3. 1, 2 and 3 are thin films prepared without (1) and with three interruptions (2, 3) of the deposition process and interruption time of 0.5 min (2) and 5 min (3). T_{op} is the operating temperature.

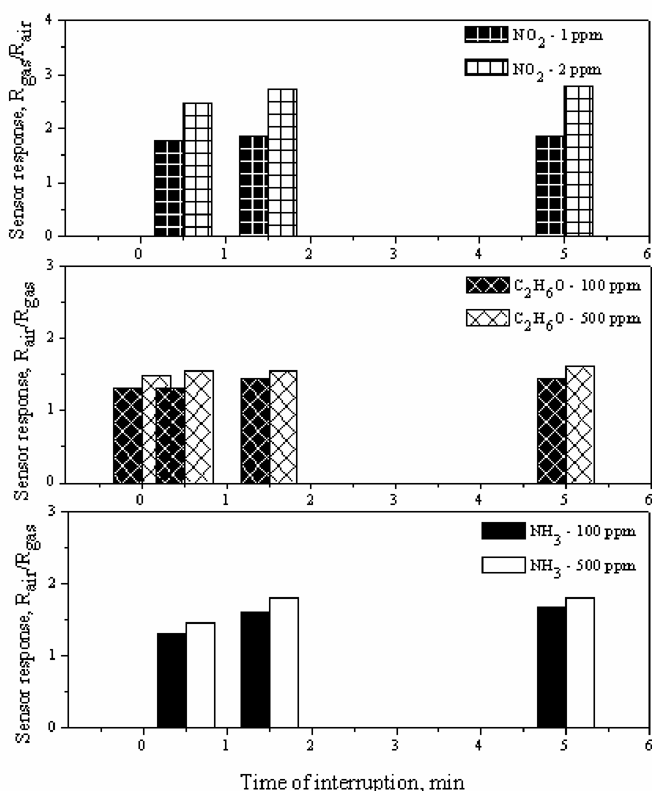

Figure 4.2. Sensor responses in presence of NO_2 (at 250ºC), C_2H_6O (at 200ºC) and NH_3 (at 200ºC) as a function of interruption time.

Table 4.1. Mean responses of the WO_3 micro-sensors to ozone as a function of the operating temperature.

T(ºC)	Interruption regime S_i					Basic regime S_b				
Electrode gap : 100 µm										
	0.1	0.2	0.4	0.6	0.8	0.1	0.2	0.4	0.6	0.8
450	1.22	1.69	2.81	4.10	4.26	1.01	1.03	1.07	1.08	1.18
350	1.34	1.85	3.01	4.21	4.48	1.10	1.24	1.49	1.73	1.84
250	1.03	1.08	1.12	1.17	1.39	1.05	1.09	1.19	1.27	1.35
Electrode gap : 50 µm										
	0.1	0.2	0.4	0.6	0.8	0.1	0.2	0.4	0.6	0.8
450	1.05	1.15	1.33	1.50	1.75	1.03	1.05	1.10	1.14	1.19
350	1.16	1.36	1.76	2.15	2.39	1.08	1.17	1.35	1.48	1.52
250	1.05	1.14	1.21	1.25	1.41	1.04	1.09	1.18	1.28	1.32

0.1, 0.2, 0.4, 0.6, 0.8 denote the ozone concentration (ppm). S_i and S_b represent the sensors deposited with interruption and basic regimes, respectively. T (ºC) is the operating temperature of the sensor.

ISBN:978-84-691-9748-6 /DL:T-1249

Figure 4.3 presents the isothermal responses of the micro-machined sensors to ozone at 350 ºC, where the sensor response is the maximum for all ozone concentrations measured and two types of electrode configurations used. It can be seen that the response of the micro-machined sensors to ozone is completely reversible for the four types of sensors, as it was observed in previous studies for WO_3 sensing films [6].

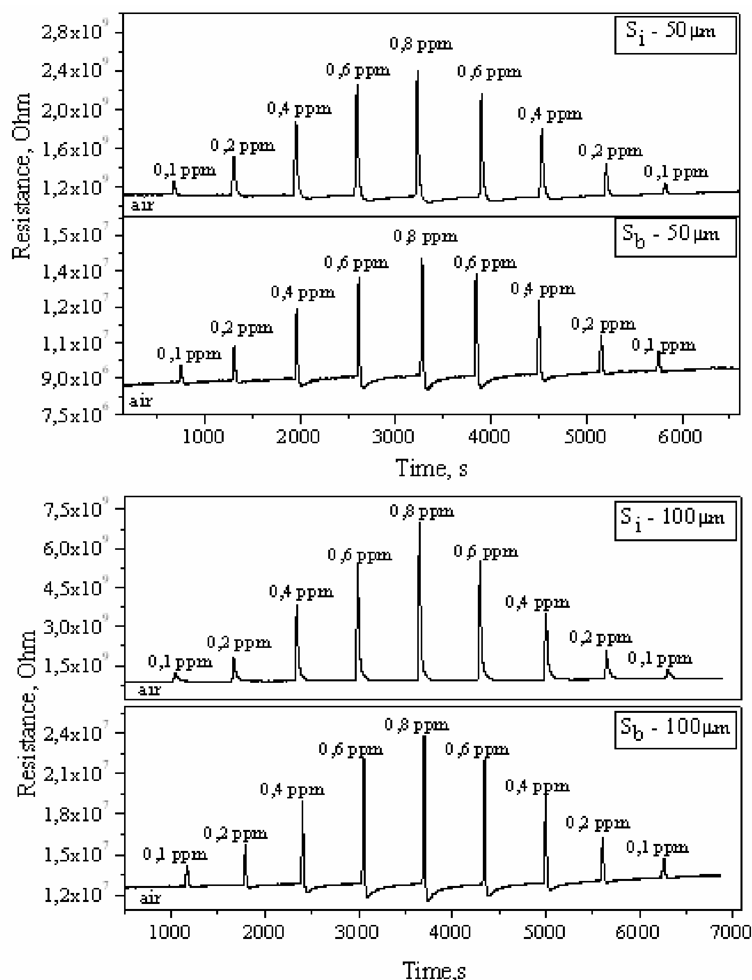

Figure 4.3. Isothermal responses of two types of the sensing layers and electrode configuration to a series of ozone exposures at 350 ºC. S_i – 50 µm and S_i – 100 µm represent the response of the WO_3 sensors deposited with interruptions (a). S_b – 50 µm and S_b – 100 µm represent the response of the WO_3 sensors deposited with basic technology (b). The constant total flow during the measurements was 200 cm^3/min.

A comparison of the sensor response trends obtained for the different types of electrodes and deposition technologies is represented in Figure 4.4. The results show that the response of the films deposited both with and without interruptions is higher in the sensors with a 100 µm electrode gap. The difference in the responses of the micro-sensors with two different electrode configurations is not very high for the sensing films that were deposited using standard technology in comparison with the films deposited with interruptions. The standard error (S.E.) for each type of sensor, the S.E. for each pair of the similar sensors presented on one micro-system chip and the S.E. for the four similar sensors from two different chips was calculated using eight measurements. The measurements performed at the same flow rates and exposure time at the operating temperature of 350 ºC were employed in these calculations. Figure 4.5 presents a comparison of these S.E. It can be noticed that the sensors with a narrow electrode gap (50 µm) have better reproducibility than the sensors with a wide electrode gap (100 µm).

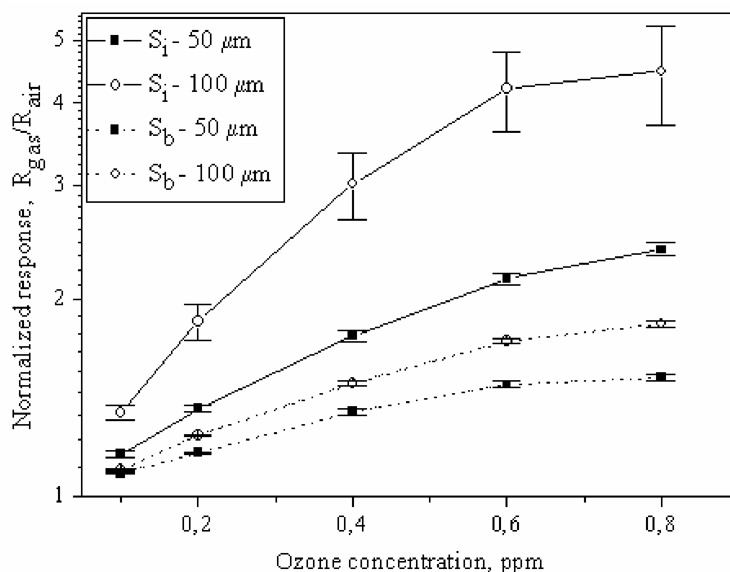

Figure 4.4. Responses of the sensors as a function of ozone concentration. Standard errors of the measurements are presented.

UNIVERSITAT ROVIRA I VIRGILI
STUDY OF STRUCTURAL AND SENSING PROPERTIES OF TUNGSTEN TRIOXIDE THIN FILMS
DEPOSITED BY RF SPUTTERING
Stella Vallejos Vargas
ISBN:978-84-691-9748-6 /DL:T-1249

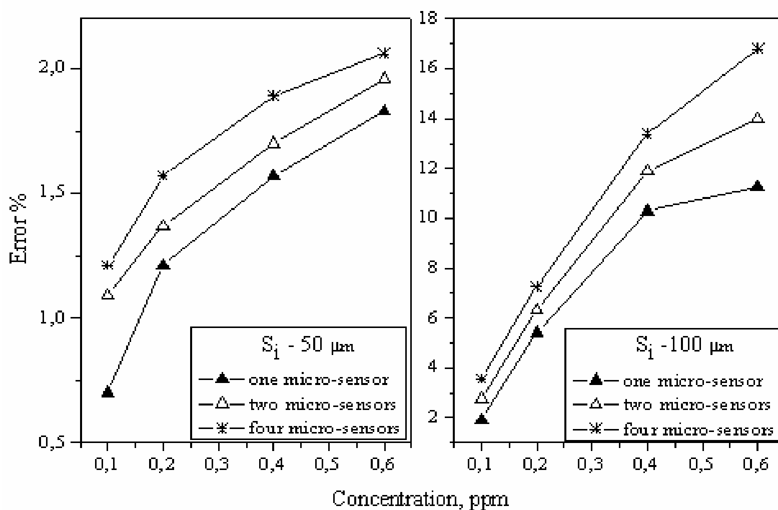

Figure 4.5. Standard errors of the measurements for the WO_3 sensors deposited with interruptions. The constant total flow was 200 cm^3/min. The filled triangles represent the S.E. of one micro-sensor from the sensor array. The empty triangles represent the S.E. estimated for two micro-sensors with the same electrode geometry from the sensor array. The stars represent the S.E. estimated for four micro-sensors with the same electrode geometry from two sensor arrays.

Figure 4.6 shows the baseline normalized responses of WO_3 micro-sensors with two different electrode geometries to various oxidizing (ozone O_3. nitrogen dioxide NO_2, nitrogen oxide NO_x) and reducing (ammonia NH_3, carbon monoxide CO, ethanol C_2H_6O) target gases [7]. The responses of the sensors to reducing gases were not as high as the one observed for oxidizing gases. Table 4.2 shows the maximum sensor responses of the WO_3 sensors to O_3, NO_2, NO_x, NH_3, CO and C_2H_6O at various operating temperatures and gas concentrations. Our results show that the optimal operating temperature changes as a function of the target gas used and its concentration. It can be seen that the higher sensor responses to O_3, NO_x and C_2H_6O were obtained at 250 ºC. In the case of high NO_2 concentrations, WO_3 sensors showed higher responses at 450ºC. The maximal values of the responses to NH_3 and CO were obtained at 350ºC. The results presented in Figure 4.6 and Table 4.2 show that the response of the films deposited both with and without interruptions is higher in the sensors with a 100 µm electrode gap.

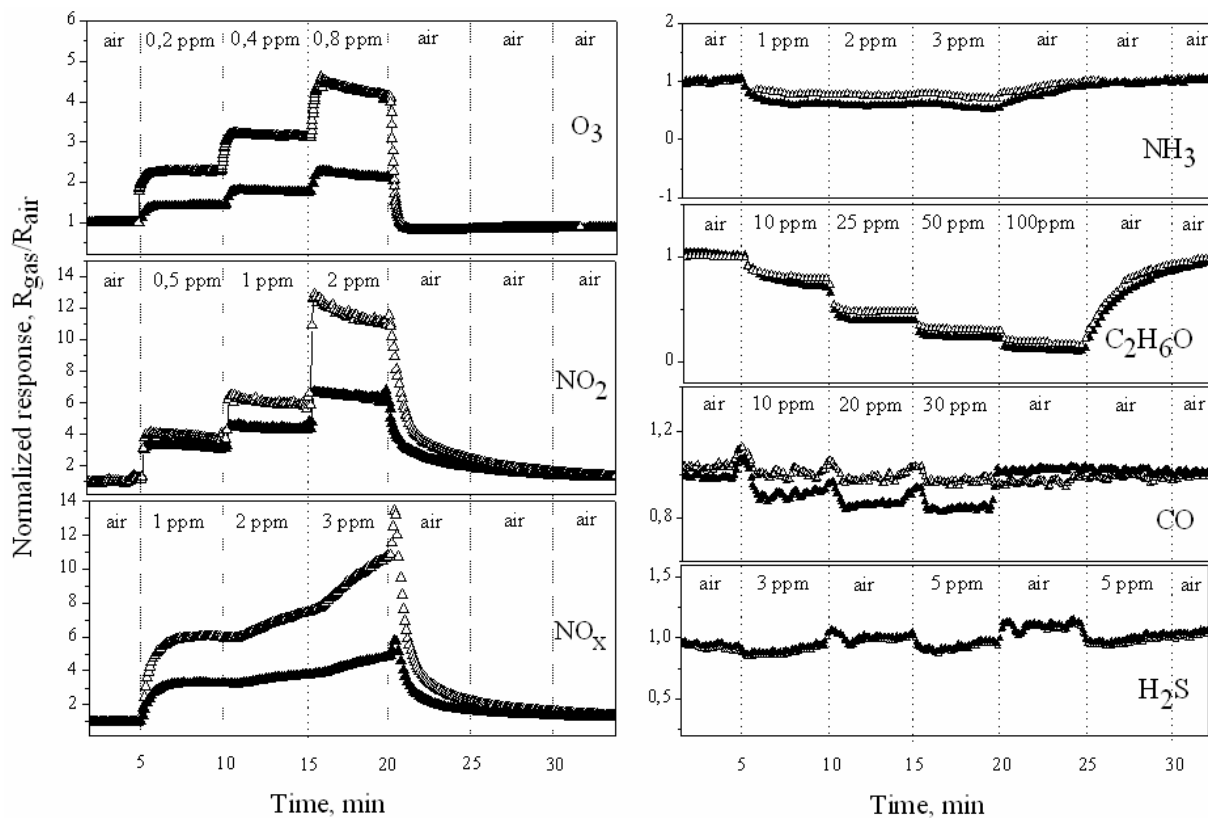

Figure 4.6. Baseline normalized WO_3-sensor responses to various oxidizing (O_3, NO_2, NO_x) and reducing (NH_3, C_2H_6O, CO) gases. The sensors operated at 350 ºC. Responses acquire with electrodes of 100 µm (Δ) and 50 µm (▲) gap. The constant total flow during the measurements was 100 cm^3/min.

ISBN:978-84-691-9748-6 /DL:T-1249

Table 4.2. Maximun responses of the WO_3 micro-sensors to ozone (O_3), nitrogen dioxide (NO_2), nitrogen oxide (NO_x), hydrogen sulphide (H_2S), ammonia (NH_3), carbon monoxide (CO) and ethanol (C_2H_6O).

Gas	C (ppm)	250	350	450	250	350	450
		Electrode gap : 100 µm			Electrode gap : 50 µm		
O_3	0.2	2.8	2.3	1.9	1.7	1.4	1.3
	0.4	4.5	3.1	2.6	2.3	1.8	1.5
	0.8	6.8	4.2	3.5	2.8	2.1	1.8
NO_2	0.5	2.9	3.8	3.5	2.3	3.5	3.3
	1	4.0	5.7	4.8	3.1	4.8	5.6
	2	6.4	10.7	20.6	4.1	6.9	18.4
NO_x	1	6.7	5.9	2.7	3.0	3.2	2.0
	2	9.0	7.7	4.5	4.2	3.8	2.3
	3	11.5	10.7	6.8	5.6	4.9	2.9
NH_3	1	1.0	1.3	1.0	1.0	1.6	1.0
	2	1.0	1.3	1.0	1.0	1.6	1.0
	3	1.0	1.4	1.0	1.0	1.8	1.0
H_2S	3	1.0	1.1	1.0	1.0	1.1	1.0
	5	1.0	1.1	1.0	1.0	1.1	1.0
CO	10	1.0	1.0	1.0	1.0	1.1	1.0
	20	1.0	1.0	1.0	1.0	1.1	1.0
	30	1.0	1.0	1.0	1.0	1.2	1.0
C_2H_6O	10	1.5	1.4	1.2	1.6	1.3	1.2
	25	2.5	2.5	2.0	2.9	2.5	2.0
	50	8.3	4.3	3.4	9.4	4.3	3.4
	100	15.2	9.6	6.2	16.7	9.5	6.1

250, 350, 450 denote the sensor operating temperature (ºC). C(ppm) represents the target gas concentration.

Figure 4.7. shows the response time of micro-sensors for three oxidizing gases (O_3, NO_2 and NO_x). The response time was defined as the time elapsed from 10% to 90% of the response measured from the baseline resistance. It can be seen that the response to O_3, NO_2 and NO_x is faster at the temperature ranged from 350 ºC to 450ºC.

4.1.1.2. Selectivity

Figure 4.8 shows the sensor response spaces obtained combining the response of two micro-sensors with wide and narrow gap electrode configurations. X-axis and y-axis of the sensor response space represent the response for the micro-sensors with wide and narrow electrode configurations, respectively. The sensor response spaces contain the sensor responses to various target gases at different gas concentrations (each measurement was replicated 5 times). The responses

were obtained at operating temperatures 250ºC (Figure 4.8,a). 350ºC (Figure 4.8,b) and 450ºC (Figure 4.8,c). It can be noted that the repeatability of the micro-sensors with a narrow electrode gap is higher (S.E. up to 1.8 %) than the one achieved by the micro-sensors with a wide electrode gap (S.E. up to 14 %). Moreover, in the sensor space it can be seen that measurements show a tendency to cluster together according to the target gas and its concentration. This behaviour is clearer at the operating temperature of 350 ºC where a minimal dispersion of the responses to O_3 (0.2 ppm, 0.4 ppm, 0.8 ppm). NO_2 (0.5 ppm, 1 ppm, 2 ppm) and NO_x (1 ppm, 2 ppm, 3 ppm) is observed. On the contrary, the dispersions of the responses to the gases are worse at the other temperatures. At 450 ºC the dispersions are higher, especially for NO_x and O_3.

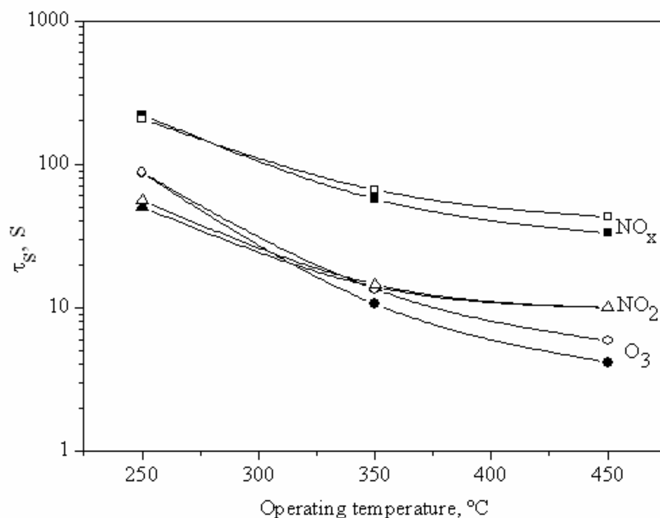

Figure 4.7. Response time of the micro-sensors to various oxidizing gases: O_3 (0.2 ppm), NO_2 (0.5 ppm) and NO_x (1 ppm). Response obtained with wide (empty scatters) and narrow (full scatters) interdigitated gap electrodes.

4.1.1.3. Stability

Figure 4.9 shows the sensing layer resistance in air for the micro-sensors fabricated using interrupted regime over nine months approximately. The resistance was measured for the micro-sensors with wide (100 µm gap) and narrow (50 µm) gap electrode configurations. Basically the resistance measured

ISBN:978-84-691-9748-6 /DL:T-1249

with the first set of micro-sensors was kept at 600 MΩ for the sensors with 100 µm electrode gap and 200 MΩ for the sensors with 50 µm electrode gap.

Figure 4.10 presents a comparison of the normalized sensor responses to NO_2 after eight months of the sensor use. It can be seen that over this period the sensor responses decreased about 37% and 33% for the sensors with electrode configuration of 100 µm and 50 µm gap, respectively.

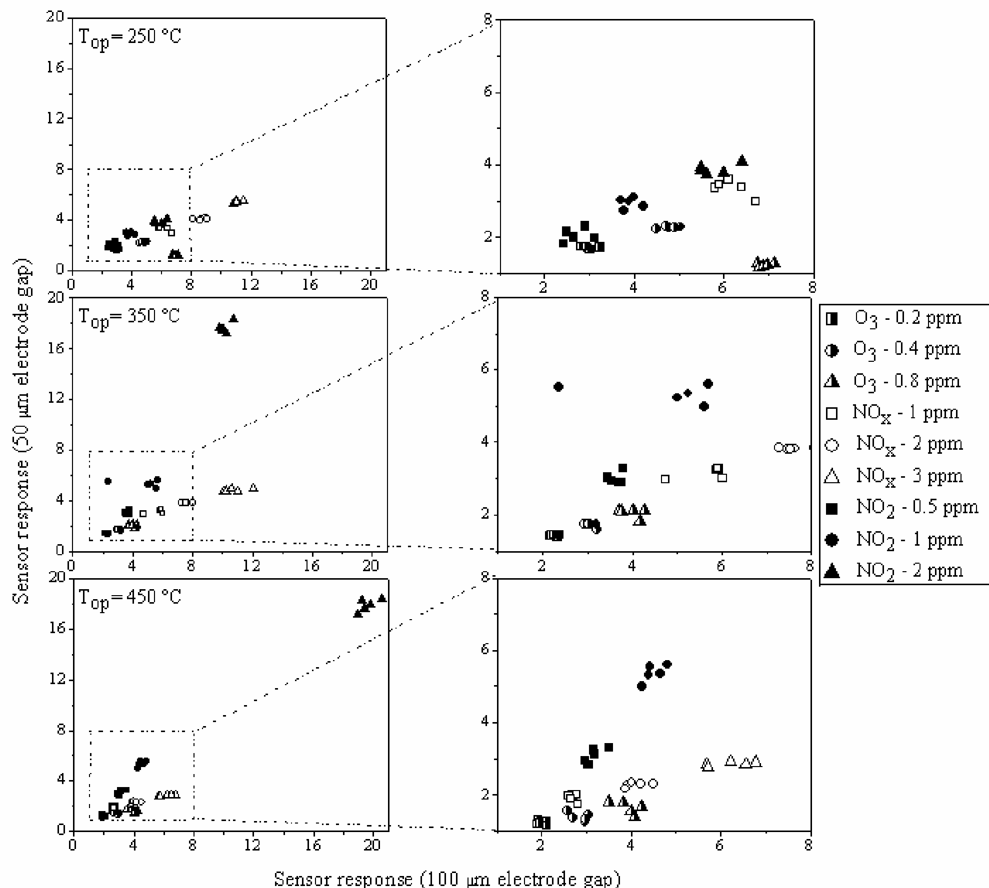

Figure 4.8. Sensor response spaces obtained for wide electrode gap and narrow electrode gap at various operating temperatures (a) 250 ºC, (b) 350 ºC, (c) 450ºC. Half full scatters belong to ozone, empty scatters to nitrogen oxide and full scatters to nitrogen dioxide. Corresponding concentrations to each gas are presented in the graphic label.

ISBN:978-84-691-9748-6 /DL:T-1249

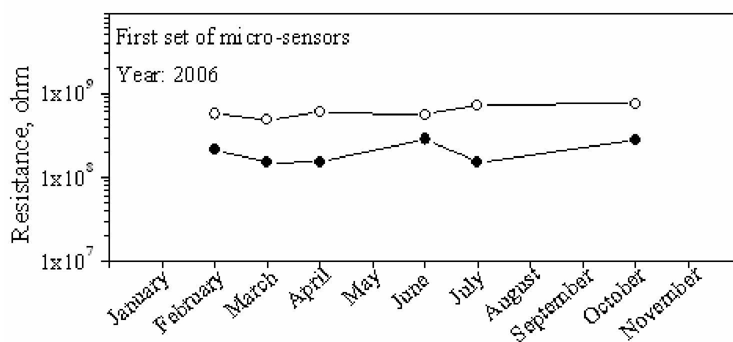

Figure 4.9. Resistance in air for the micro-sensors fabricated using interrupted regime over nine months. Sensors with electrode gap of 100 µm (○) and 50 µm (●).

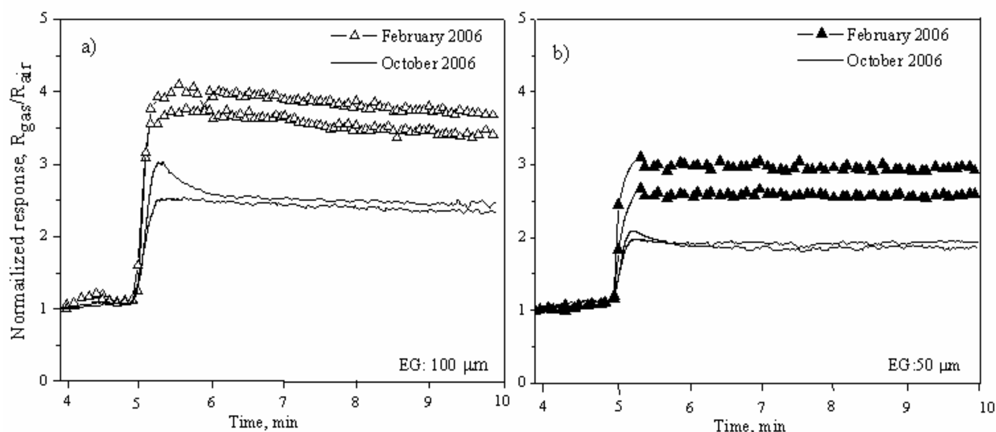

Figure 4.10. Comparison of the normalized sensor responses to 0.5 ppm of NO_2 in February 2006 and October 2006. Response acquired with electrodes of 100 µm (a) and 50 µm (a) gap.

4.1.1.4. Discussion

The results of this study show the role of interruptions in the enhancement of the sensitivity mainly to oxidizing gases such as O_3 and NO_2. The sensitivity of the micro-sensors fabricated with interruptions to NO_2 and O_3 is higher than the one obtained for the sensors prepared using the basic regime (Figure 4.11). Furthermore, it is observed a low cross-sensitivity of the micro-sensors to reducing gases. This effect is related to the grain size decrease in the metal oxide films and

ISBN:978-84-691-9748-6 /DL:T-1249

the increment of the number of free bonds on the sensing layer surface. Earlier it was shown that decreasing of grain size from 100 nm to 60 nm raised the sensor response to O_3 by a factor of 5 [6]. Similar results were presented in Ref. [8] where decreasing of grain size from 33 nm to 25 nm increased the sensor response to NO_2 by a factor of 3 approximately. In this dissertation, it is show that reducing grain size from 24 nm to 17 nm (see Chapter 3) promotes an increase of the sensor response to 0.8 ppm O_3 by a factor of 2.43. In the case of 1 ppm NO_2 decreasing of grain size promotes an increase in the sensor response more than 4 times.

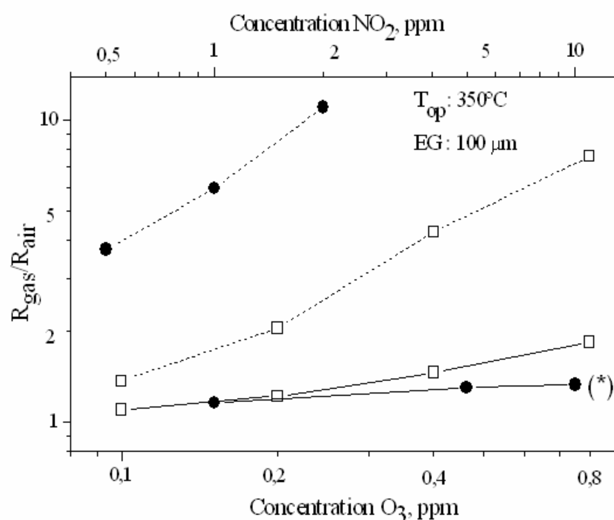

Figure 4.11. Sensor responses to various O_3 (□) and NO_2 (●) concentrations. WO_3 deposited without interruptions (——) and with interruptions (---). T_{op} is operation temperature. EG is electrode gap. The results (*) were adapted from Ref. [9].

In general the higher responses were observed for the micro-sensors with the electrode configuration of 100 μm. This behaviour was identical for the sensors fabricated with interrupted and basic regimes. Basically, the electrode geometry produces a different sensor signal depending on how the electrodes are positioned within the porous sensor body. If the electrode geometry implies that a narrow gap exists between the fingers, the resistance change of the sensing layer in the presence of oxidizing gases involves the volume of sensing film that lies between two interdigited electrode fingers only. In the case of wide gap electrode geometry, the resistance changes involve the whole sensing film [10, 11]. Figure

4.12 shows a schematic illustration of this effect. This effect can explain the differences in the responses of the micro-sensors with two types of the electrode configuration.

Figure 4.12. Schematic illustrations of a cross section of the micro-sensor membrane for two fingers of the electrode. The current flow through the active layer is represented in dashed lines for the electrodes with narrow (a) and wide gap (b).

The effect of the operating temperature on the sensor response reveals to be dependent on the nature of the gaseous species and their concentrations. For instance, in the case of ozone (from 0.2 ppm to 0.8 ppm) the highest sensor response is observed at the operating temperature of 350 ºC. In the case of NO_2 the highest sensor response is shifted depending on the operating temperature and gas concentration. For 0.5 ppm and 1 ppm of NO_2 the highest sensor response is observed at 350 ºC, while for 2 ppm of NO_2 the highest sensor response is observed at 450ºC.

Other studies showed that the optimal operating temperature for 0.8 ppm of O_3 [12, 13] and 5 ppm of NO_2 [14] is 250ºC. These studies remarked a similar behaviour of the sensor response respect to the operating temperature and gaseous species. The discrepancy in the optimal operating temperature obtained in this dissertation and in Ref. [12-14] could be linked with the differences in the grain size and geometry of the sensing layers deposited. The operating temperature dependency of the sensor response can be explained with the model of resistivity based on the existence of an accumulation or depletion layer induced by the surrounded atmosphere. In accordance with this model there is an optimal sensor operating temperature which provides the highest sensor response. This optimal operating temperature is linked to the temperature of the adsorption efficiency [15].

The characterizations carried out towards oxidizing (NO_x, NO_2 and O_3) and reducing gases (NH_3, CO, H_2S and C_2H_6O) gases show an evidence of the low cross sensitivity of the micro-sensors fabricated with interruptions to oxidizing gases. According to several reports the non-doped WO_3 films are sensitive to NO_2, O_3 and H_2S having high cross sensitivity of H_2S with NO_2 or O_3. However, in this study this behaviour was not observed. The gas micro-sensors fabricated with interruptions show negligible responses to H_2S. This result may be related with the fact that at high operating temperatures, like the ones used in this study, a layer containing W=S bonds could be formed on the sensing layer surface. This superficial layer decreases the amount of surface-adsorbed oxygen [14]. As a result the sensor response to H_2S is very low.

Finally, the sensor responses spaces built through the correlation of the responses obtained for the sensors with 100 μm and 50 μm electrode gap show that the micro-sensors fabricated with the interruptions could be used to monitor air pollutant gases. However, it is remarked that in order to improve the discrimination of the sensor response to the air pollutant gases some additives in the sensing layers could be used.

4.1.2. WO_3 thin films deposited using floating regime

4.1.2.1. Sensitivity

This section presents the results of the sensing characterization of the micro-sensors fabricated during the second set of experiments with micro-machined silicon substrates. In this case the WO_3 sensing layers were deposited using the interrupted and floating regimes. Table 4.3 shows the sensor response to NO_2 for the micro-sensors prepared with interrupted and floating regimes. As in previous study (section 4.1.1) two types of electrodes configurations were used for the micro-sensors. Consequently, four types of micro-sensors were studied. The maximum sensor responses for each operating temperature and concentration were chosen over four measured responses. Four chips containing eight types of the micro-sensors were used for the characterizations. The standard errors (S.E.) for each type of sensor are between ±1.638 and ±3.905. In general, higher responses were obtained by the WO_3 micro-sensors deposited with the floating regime in

comparison with the sensors fabricated with the interrupted regime. All types of sensors showed higher sensor responses at the operating temperature of 400 ºC.

Table 4.3. Maximum responses of the WO_3 micro-sensors to NO_2 as function of the operating temperature and concentration.

T(ºC)	**Interruption regime S_i**			**Floating regime S_f**		
Electrode gap: 100 µm						
	1	2	3	1	2	3
450	7.83	58.54	133.15	39.96	202.86	335.76
400	59.85	293.54	530.28	114.29	617.44	1213.27
350	44.88	148.64	244.07	47.80	160.01	283.93
300	19.32	49.89	67.72	34.26	78.19	116.61
250	8.39	16.97	23.71	13.34	24.90	32.91
Electrode gap: 50 µm						
	1	2	3	1	2	3
450	58.38	272.85	507.60	41.03	329.66	773.56
400	67.58	655.90	1293.74	59.68	583.44	1106.95
350	40.07	135.20	247.66	33.54	178.66	406.47
300	17.12	46.89	63.81	43.40	131.01	215.83
250	8.00	15.28	19.77	22.97	58.43	89.54

1, 2, 3 denote NO_2 concentrations (ppm). S_i and S_f represent the sensors deposited with interrupted and floating regimes. T(ºC) is the operating temperature of the sensor.

Figure 4.13 shows the isothermal responses of the micro-sensors fabricated with the interruption and floating regimes to various NO_2 concentrations, ranged from 1 ppm to 5 ppm at the operating temperature of 400 ºC. The WO_3-sensor responses displayed a sharp increase (response time t_s~30 s) of the resistance to NO_2 concentrations between 2 ppm and 5 ppm. At 1 ppm of NO_2 the response time was slower (t_s~200 s).

Figure 4.14 presents the dependence of the sensor response on the operating temperature for each type of micro-sensors and NO_2 concentrations. The sensor response profiles reveal a bell-shaped variation with sensor operating temperature. It is noticed that the sensor response increases slowly below 300 ºC. Then a fast increment of the response is observed to reach a maximum value at the operating temperature of 400 ºC. Above 400 ºC the sensor response drops off again.

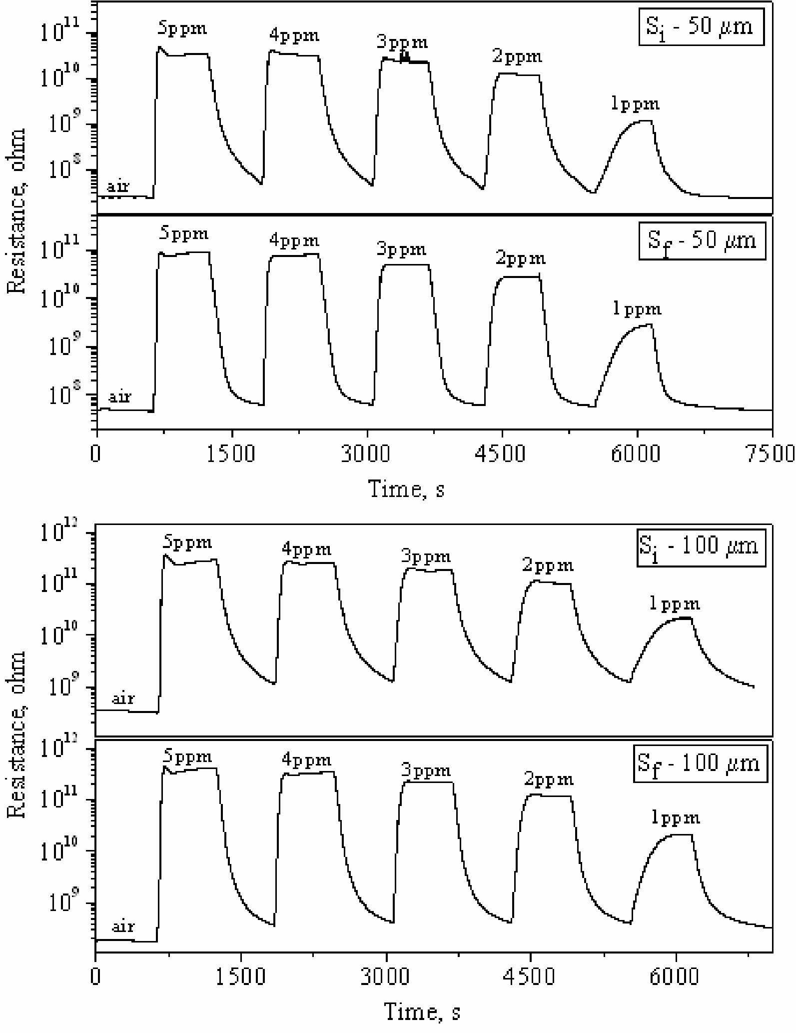

Figure 4.13. Isothermal responses of four types of the micro-sensors to NO_2 at 400 ºC. S_i – 50 µm and S_i – 100 µm represent the response of the sensors deposited with interruptions regime. S_f – 50 µm and S_f – 100 µm represent the response of the WO_3 sensors deposited with floating regime. The constant total flow during the measurements was 100 cm^3/min.

The results presented in Table 4.3 and Figure 4.14 show that the influence of the electrode configuration on the sensor response is opposite to the one observed in the first set of experiments with micro-machined substrates. The sensors constituted by narrow (50 µm) electrode gap present higher responses than the sensors with wide (100 µm) electrode gap.

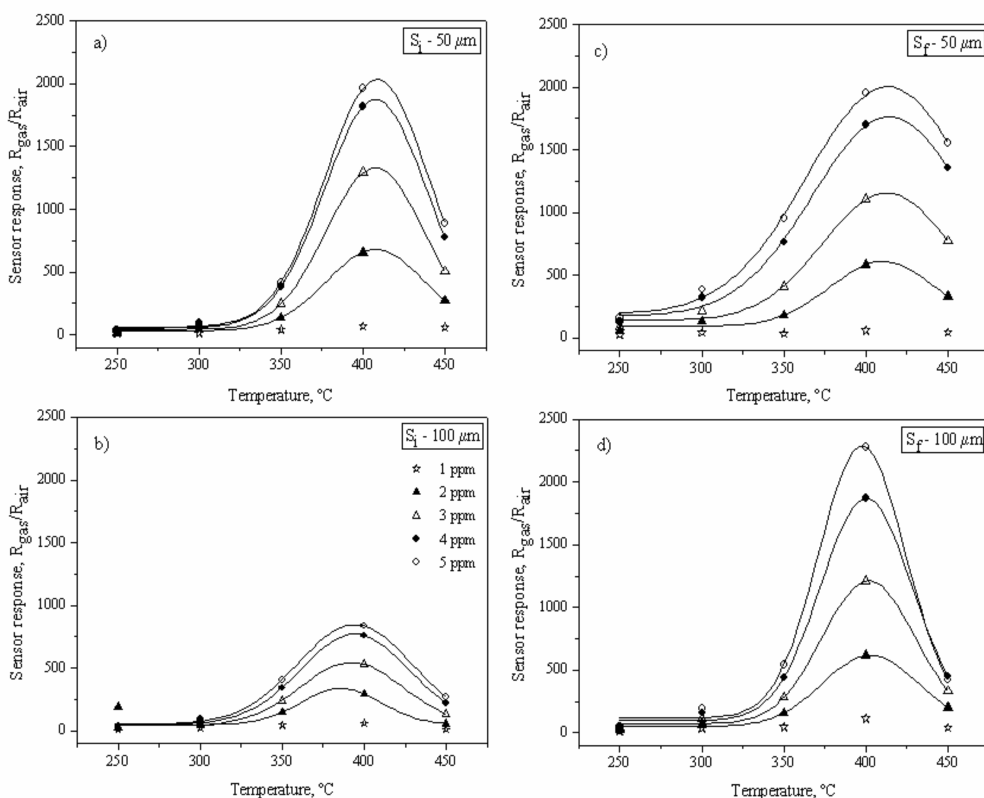

Figure 4.14. Sensor responses to various NO_2 concentrations as function of the operating temperature and regimen of fabrication. (a,b – interrupted regime; c,d – floating regime) 50 µm and 100 µm represent the electrode gap for each sensor.

4.1.2.2. Selectivity

The baseline normalized sensor responses to NO_2 (oxidizing gas) and some reducing gases (NH_3, CO, H_2S and C_2H_6O) at 400 ºC are presented in Figure 4.15. It is noticed that the micro-sensors fabricated both with interrupted and floating regimes have negligible responses to reducing gases in comparison with the ones achieved to NO_2. It is important to remark that the characterizations carried out at 250ºC and 350ºC reveal a similar behaviour. The results presented in Figure 4.15 show the low cross sensitivity of the micro-sensors at operating temperatures between 250ºC and 450ºC.

ISBN:978-84-691-9748-6 /DL:T-1249

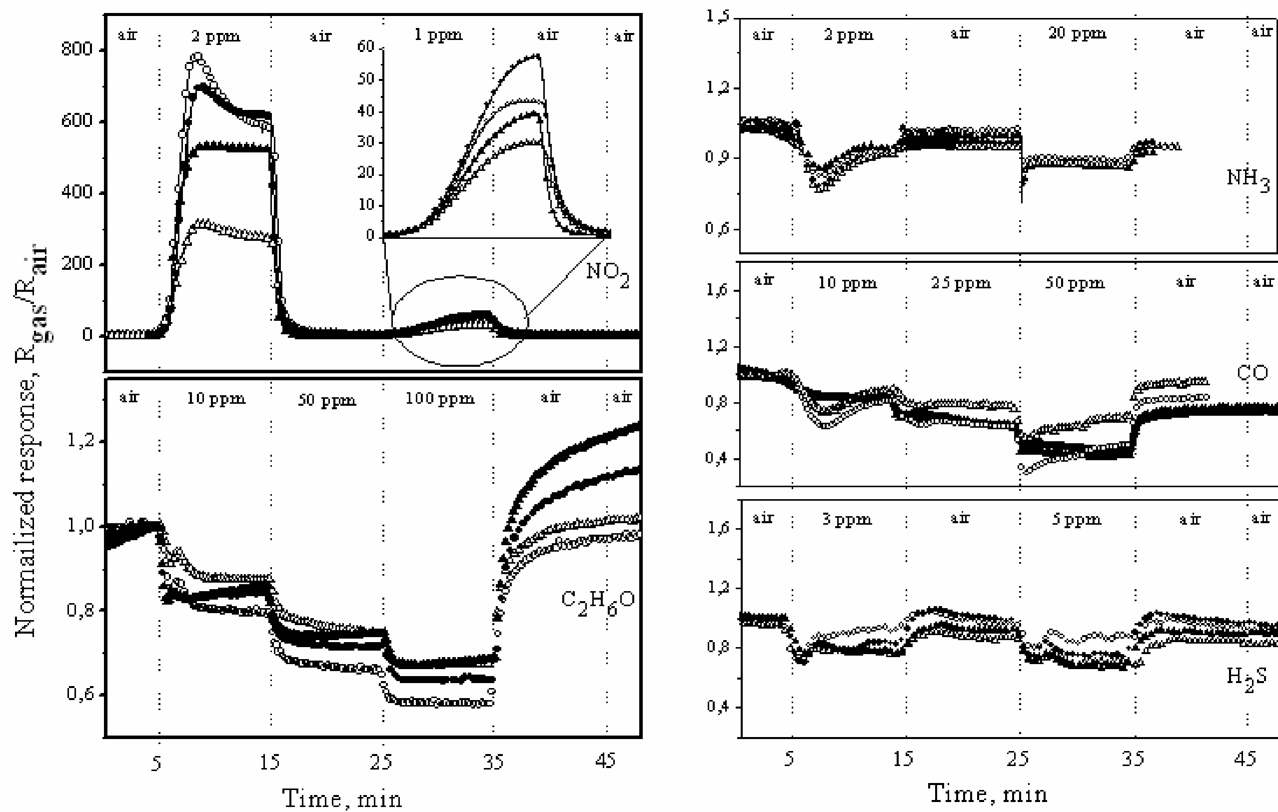

Figure 4.15. Baseline normalized sensor responses to NO_2 (oxidizing gas). NH_3. C_2H_6O. CO and H_2S (reducing gases) at 400ºC. Circle scatters: floating regime. Triangle scatters: interrupted regime. Full scatters (●)(▲) and empty scatters (○)(Δ) represent the response acquired with 100 μm and 50 μm electrode gap, respectively. The constant total flow during the measurements was 100 cm^3/min

4.1.2.3. Stability

Figure 4.16 shows the sensor resistances change in air over nine months. Similar resistance values are observed for the WO_3 films deposited with interrupted and floating regimes. These values were found to be ~ 200 MΩ for the sensors with 100 μm electrode gap and ~ 30 MΩ for the sensors with 50 μm electrode gap (slight changes are noticed over nine months). On the other hand Figure 4.17 presents a comparison of the sensor responses to 1 ppm of NO_2 after three months of the sensor use. It can be seen that for two types of the sensing layer deposition the decrement of the sensor response averages up to 15% and 8% for the sensors with 100 μm gap 50 μm electrode gap, respectively.

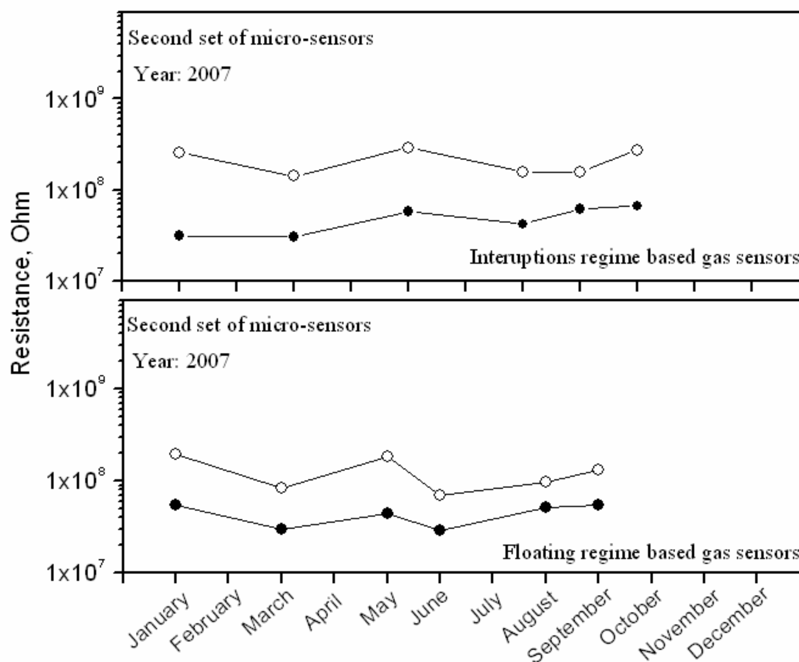

Figure 4.16. Resistance of the sensing layer in air over nine month. Sensors with electrode gap of 100 μm (○) and 50 μm (●).

ISBN:978-84-691-9748-6 /DL:T-1249

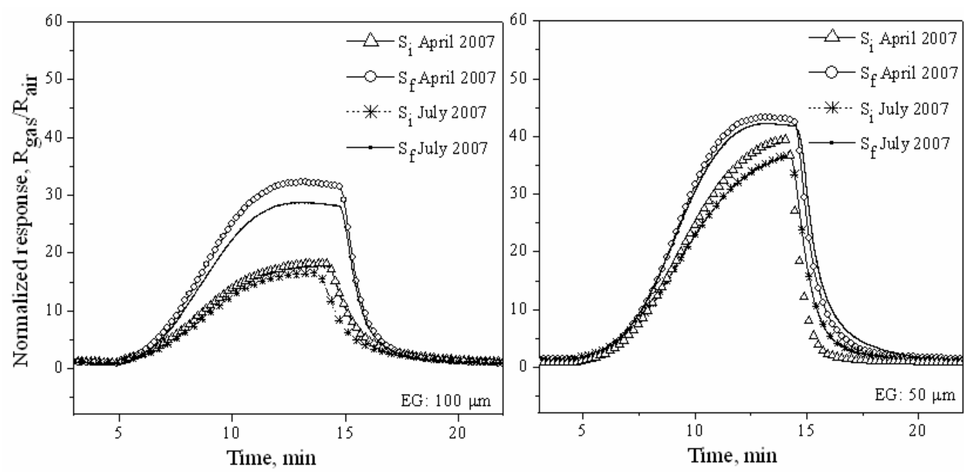

Figure 4.17. Comparison of the normalized sensor response to 0.5 ppm of NO_2 obtained in March 2007 and September 2007. Response obtained with electrodes of 100 µm (a) and 50 µm (a) gap.

4.1.2.4. Discussion

The results of this study show the effect of the sensing layer deposition with floating regime on the sensing properties of WO_3 thin films. The sensitivity of the WO_3 micro-sensors fabricated using floating regime to NO_2 is enhanced in comparison with the sensors fabricated with interruptions. Moreover, the gas sensor characterizations demonstrate that WO_3 films deposited using floating regime are selective to oxidizing gases as well. In this case the enhancement of the sensor sensitivity could not be related only to the grain size, since morphological and structural characterizations presented in Section 3.1.2.2 of Chapter 3 reveals similar grain size in WO_3 thin films deposited both with the interrupted and floating regimes. The enhancement of he sensor sensitivity could be related to the level of cleanness on the sensing layer surface which should be better in the films deposited using floating regime due to the higher rate of the superficial layer deposition. Basically, the films deposited by sputtering may trap some impurities or sputtered particles from the residual atmosphere. However, as the deposition rate increases the level of impurities in the film decreases because of resputtering most impurities that preferentially remove relative to the atoms of the main film [16].

Finally, the gas sensing characterizations at various operating temperatures reveal a maximum sensor response at 400 ºC. The results obtained by the first set of micro-sensor fabrication did not shown clear this behaviour since three operating temperatures were only characterized. On the base of the results obtained by the second set of micro-sensor fabrication we can conclude that the sensor response have a bell-shaped function with respect to the operating temperature. This behaviour shows correlation with the results obtained in Ref [15], where it was noted that such bell-shaped variations are the result of the cooperation of two opposite effects: an increasing probability of activated detection reactions when the operating temperature raises (in this case from 250ºC to 400ºC) and an increasing probability of adsorbed gas molecules to desorb when the sensor operating temperature increases (in this case over 400ºC).

Second set of micro-sensor fabrication showed higher sensor responses by the use of sensors composed with 50 μm electrode gap. On contrary, the first set of sensors showed an opposite behaviour. Analysing the sensor responses to NO_2 at 350ºC presented in Table 4.2, it is possible to observe that the responses of the sensors with 100 μm electrode gap are rather higher than the response of the sensors 50 μm electrode gap. The same is noted for the second set of micro-sensor fabrication (see Table 4.3, temperature at 350ºC). The characterizations carried out for the second set of micro-sensor fabrication at 250ºC, 300ºC, 350ºC, 400ºC, 450ºC give a better vision of the electrode dependency of the sensor response and reveals that the sensors with narrow (50 μm) electrode gap have better responses. It seems that the effect illustrated in Figure 4.12,b does not take place in the second set of micro-sensor fabrication due to the similar thickness of the electrodes (0.2 μm) and the sensing layer (0.2 μm). So that, both wide and narrow electrodes measure the resistance change in the whole sensing film.

The results of this study show an evident difference of the sensor responses obtained by the first and second set of micro-sensors fabrication. For instance, at 350ºC the first set of micro-sensors showed that the resistance of the film increases approximately 6 times by the action of 1 ppm of NO_2. At the same time for the same conditions the second set of micro-sensors showed that the change in the resistance of the film is approximately 40 times. These differences in the sensor response seem to be linked with the change in the baseline resistance (see Figure

UNIVERSITAT ROVIRA I VIRGILI
STUDY OF STRUCTURAL AND SENSING PROPERTIES OF TUNGSTEN TRIOXIDE THIN FILMS
DEPOSITED BY RF SPUTTERING
Stella Vallejos Vargas
ISBN:978-84-691-9748-6 /DL:T-1249

4.9 and Figure 4.16). According to Ref [17], the electrical equivalent circuit of the sensing layer could be regarded as a parallel circuit of the surface resistance and the bulk resistances. Thus, when the surface resistance is changed by the charges adsorbed onto the surface, if the reference bulk resistance is high, the relative change of the resistance is covered and poor sensor responses are observed. On the contrary when the reference bulk resistance is low, high relative change of the resistance is observed. The change in the baseline resistance of the sensors is part of a technological problem presented during the fabrication of the first set of micro-sensors (the photoresist was not removed properly afterwards the deposition of WO_3 sensing layers).

ISBN:978-84-691-9748-6 /DL:T-1249

4.2. Summary and outlook

On the base of the experimental results, it is concluded that gas micro-sensors fabricated with the interrupted and floating regimes have promising sensing characteristics. They show better sensitivity and selectivity to low concentrations of oxidizing gases such as NO_2 and O_3, in comparison to the gas micro-sensors fabricated using standard sputtering regime. These characteristics of the new gas micro-sensors allow suggesting them as good candidates to monitor air pollutant gases. Nevertheless, some typical problems of metal oxide based gas sensors such as the high operating temperature and the long term stability have to be investigated more thoroughly.

UNIVERSITAT ROVIRA I VIRGILI
STUDY OF STRUCTURAL AND SENSING PROPERTIES OF TUNGSTEN TRIOXIDE THIN FILMS
DEPOSITED BY RF SPUTTERING
Stella Vallejos Vargas
ISBN:978-84-691-9748-6 /DL:T-1249

Bibliography

[1] J. Hubálek, K. Malysz, P. J., X. Vilanova, P. Ivanov, E. Llobet, J. Brezmes, X. Correig, and Z. Svlatin, "Pt-loaded Al_2O_3 catalytic filters for screen-printed WO_3 sensors highly selective to benzene, ," *Sens. Actuators B*, vol. 101 pp. 277-283, 2004.

[2] V. Khatko, S. Vallejos, J. Calderer, E. Llobet, X. Vilanova, and X. Correig, "Gas sensing properties of WO_3 thin films deposited with interruptions," presented at 19th European Conference on Solid State Transducers, EUROSENSORS XIX Barcelona, Spain, 2005.

[3] V. Khatko, S. Vallejos, J. Calderer, E. Llobet, X. Vilanova, and X. Correig, "Gas sensing properties of WO_3 thin films deposited by rf sputtering " *Sens. Actuators B*, vol. 126 . pp. 400-405, 2007.

[4] V. Khatko, S. Vallejos, K. Aguir, K. Ngo, J. Calderer, I. Gràcia, C. Cané, E. Llobet, and X. Correig, "Ozone monitoring by micro-mashined sensors with WO_3 sensing films," presented at Proceedings of the 20th European Conference on Solid State Transducers, EUROSENSORS XX, Goteborg, Sweden, 17-20 September 2006.

[5] S. Vallejos, V. Khatko, K. Aguir, K. Ngo, J. Calderer, I. Gràcia, C. Cané, E. Llobet, and X. Correig, "Ozone monitoring by micro-mashined sensors with WO_3 sensing films," *Sens. Actuators B*, vol. 126, pp. 573-578., 2007.

[6] M. Gillet, K. Aguir, M. Bendahan, and P. Mennini, "Grain size effects in sputtered tungsten trioxide thin fims on the sensitivity to ozone " *Thin Solid Films*, vol. 2005, pp. 358-363, 2005.

[7] S. Vallejos, V. Khatko, J. Calderer, I. Gracia, C. Cané, E. Llobet, and X. Correig, "Micro-machined WO_3-based sensors selective to oxidizing gases," *Sens. Actuators B.* , 2007, submitted.

[8] J. Tamaki, Z. Zhang, K. Fujimori, M. Akiyama, T. Harada, N. Miura, and N. Yamazoe, "Grain size effects in tungsten oxide-based sensors for nitrogen oxides," *J. Electrochem. Soc.*, vol. 141, pp. 2207-2210, 1994.

[9] M. Stankova, X. Vilanova, J. Calderer, E. Llobet, J. Brezmes, I. Gràcia, C. Cané, and X. Correig, "Sensitivity and selectivity improvement of rf sputtered WO_3 microhotplate gas sensors," *Sens. Actuators B*, vol. 113, pp. 241-248, 2006.

[10] D. E. Williams, "Semiconducting oxides as gas-sensitive resistors," *Sens. Actuators B*, vol. 57, pp. 1-16, 1999.

[11] D. E. Williams, S. R. Aliwell, K. F. E. Pratt, D. J. Caruana, R. L. Jones, R. A. Cox, G. M. Hansford, and J. F. Halsall, "Modeling the response of a tungsten oxide semiconductor as gas sensor for the measurements of ozone," *Meas. Sci. Technol.*, vol. 13, pp. 923-931, 2002.

[12] M. Bendahan, R. Boulmani, J. L. Seguin, and K. Aguir, "Characterization of ozone sensors based on WO_3 reactively sputtered films: influence of O_2 concetration in the sputtering gas and working temperature," *Sens. Actuators B*, vol. 100, pp. 320-324, 2004.

[13] M. Bendahan, J. Guérin, R. Boulmani, and K. Aguir, "WO_3 sensor response according to operating temperature: experiments and modelling," *Sens. Actuators B*, vol. 124, pp. 24-29, 2007.

[14] L. F. Reyes, A. Hoel, S. Saukko, P. Heszler, V. Lantto, and C. G. Granqvist, "Gas sensor response of pure and activated WO_3 nanoparticle films made by advanced reactive gas deposition," *Sens. Actuators B*, vol. 117, pp. 128-134, 2006.

[15] S. Ahlers, G. Müller, and T. Doll, "A rate equation to the gas sensitivity of thin film metal oxide materials," *Sens. Actuators B*, vol. 107, pp. 587-599, 2005.

[16] L. Maissel, "Application of sputtering to the deposition of films " in *Hand book of thin film technology*, L. I. Maissel and R. Glang, Eds.: McGraw-Hill, 1970.

[17] N. Bârsan, D. Koziej, and U. Weimar, "Metal oxide-based gas sensor research: How to?," *Sens. Actuators B*, vol. 121, pp. 18-35, 2006.

UNIVERSITAT ROVIRA I VIRGILI
STUDY OF STRUCTURAL AND SENSING PROPERTIES OF TUNGSTEN TRIOXIDE THIN FILMS
DEPOSITED BY RF SPUTTERING
Stella Vallejos Vargas
ISBN:978-84-691-9748-6 /DL:T-1249

UNIVERSITAT ROVIRA I VIRGILI
STUDY OF STRUCTURAL AND SENSING PROPERTIES OF TUNGSTEN TRIOXIDE THIN FILMS
DEPOSITED BY RF SPUTTERING
Stella Vallejos Vargas
ISBN:978-84-691-9748-6 /DL:T-1249

Summary and conclusions

UNIVERSITAT ROVIRA I VIRGILI
STUDY OF STRUCTURAL AND SENSING PROPERTIES OF TUNGSTEN TRIOXIDE THIN FILMS
DEPOSITED BY RF SPUTTERING
Stella Vallejos Vargas
ISBN:978-84-691-9748-6 /DL:T-1249

In this dissertation, two special regimes of thin film deposition by rf sputtering were developed to deposit WO_3 gas sensing layers with nanometer size. The first regime consisted of a series of interruptions during the sputtering process – *interruption regime*, and the second regime consisted of a series of interruptions using two power densities of rf sputtering: the first one to deposit the initial interrupted layer within the bulk and the second one to deposit the superficial layer – *floating regime*.

The application of interruption regime during the thin film formation allowed depositing WO_3 sensing layers with nanometer grain size. The morphological characterizations of the samples deposited using this regime gave evidence of a reduction in WO_3 grain size comparing with the samples deposited using basic regime. The reduction in grain size from 24 nm to 17 nm was determined by AFM technique. On the other hand, the WO_3 thin films deposited with interruptions regime revealed a monoclinic structure with Pc symmetry. It was shown that the phase transformation of WO_3 structure from amorphous to crystalline has different activity in the films deposited with and without interruptions. Slower crystallization process was observed in films deposited with interruptions.

The sensing characterizations performed with the gas micro-sensors fabricated using interruption regime demonstrated enhancement of the sensitivity and selectivity to oxidizing gases such as nitrogen dioxide (NO_2) and ozone (O_3). On the base of this results it was noticed a good potential of this type of micro-sensors to monitor air pollutant gases. The enhancement of the sensitivity was determined to be connected with the decrease in grain size.

WO_3 sensing layers deposited using the floating regime did not show any differences in the phase composition or in the grain size in comparison with the films deposited using interruption regime. In this case the WO_3 films had a monoclinic phase with Pc symmetry and grain size of 11 nm.

WO_3 micro-sensors fabricated using floating regime showed higher sensitivities to NO_2. The enhancement of the sensitivity for this type of micro-sensors is not related only with decreasing in WO_3 grain size. The enhancement of the sensor sensitivity could be related with the level of cleanness on the sensing layer surface that is better in the films deposited at higher power density of rf sputtering.

UNIVERSITAT ROVIRA I VIRGILI
STUDY OF STRUCTURAL AND SENSING PROPERTIES OF TUNGSTEN TRIOXIDE THIN FILMS
DEPOSITED BY RF SPUTTERING
Stella Vallejos Vargas
ISBN:978-84-691-9748-6 /DL:T-1249

Appendix

I

Reprinted from Elsevier B.V.
Sensor and Actuators B: Chemical, 126 (2007) 400 - 405
Gas sensing properties of WO_3 thin films deposited by rf sputtering
V. Khatko, S. Vallejos, J. Calderer, E. Llobet, X. Vilanova, X. Correig

Available online at www.sciencedirect.com
ScienceDirect
Sensors and Actuators B 126 (2007) 400–405
SENSORS AND ACTUATORS B CHEMICAL
www.elsevier.com/locate/snb

Gas sensing properties of WO_3 thin films deposited by rf sputtering

Viacheslav Khatko [a,*], Stella Vallejos [a], Josep Calderer [b], Eduard Llobet [a], Xavier Vilanova [a], Xavier Correig [a]

[a] *Departament d'Enginyeria Electronica, Universitat Rovira i Virgili, Països Catalans 26, 43007 Tarragona, Spain*
[b] *Universitat Politecnica de Catalunya, Departament d'Enginyeria Electronica, Campus Nord 08034 Barcelona, Spain*

Received 22 December 2006; received in revised form 21 March 2007; accepted 22 March 2007
Available online 30 March 2007

Abstract

WO_3 thin films were deposited by reactive radio frequency (rf) sputtering from a pure tungsten target. The deposition process was conducted with three interruptions and the interruption time was 30, 90 and 300 s. On the basis of these films, sensing layers were prepared and their responses to NO_2, ammonia and ethanol were investigated. It was found that the sensing layers prepared with an interruption time of more than 90 s showed the best sensing properties.
© 2007 Elsevier B.V. All rights reserved.

Keywords: WO_3 thin film; Deposition with interruptions; Gas sensing properties

1. Introduction

Among metal oxide semiconductors, tungsten oxide is a promising material for gas sensing. Several studies have shown that it can be used for the detection of nitrogen oxide (NO and NO_2) [1,2], ozone [3,4], and other toxic gases [5,6]. Tungsten oxide films can be deposited by reactive radio frequency (rf) sputtering, thermal evaporation and other methods. The results obtained until the moment with tungsten oxide indicate that the characteristics of the sensor strongly depend on the conditions and methods used in their deposition.

Grain size reduction in metal oxide films is one of the key factors to enhance the gas sensing properties of semiconductor layers [7,8]. A way to create metal-oxide thin films with small grain size is to use a special regime of thin film deposition by the dc magnetron, ion-beam or rf sputtering of pure metal or metal oxide targets. This regime implies the deposition of the thin film with one or several interruptions during the deposition process [9–11]. In these articles the deposition process of WO_3 thin films was conducted without interruption and with one, two and three interruptions. Interruption time was always constant and set to 30 s. It was shown that the sensing layers prepared with the maximum number of interruptions showed the best sensing properties.

Earlier systematic investigations on growth kinetics of pure metals on amorphous carbon substrates have revealed that after interrupting a continuous deposition period by closing the beam shutter during vapour deposition, metal particles continued to grow for up to several minutes with decreasing speed [12–14]. At a constant temperature, after an interruption of deposition, particle growth resumed with a delay being similar to that during particle nucleation. On the basis of these results we can suggest that delayed resumption of particle growth after an interruption of the deposition could depend on the interruption time as well.

The aim of this work is to study the influence of interruption time on the morphology and gas sensing properties of WO_3 thin films deposited with three interruptions.

2. Experimental

WO_3 thin films were deposited on top of silicon wafers oxidised in dry oxygen by reactive rf magnetron sputtering using an ESM100 Edwards sputtering system. A tungsten target of 99.95% purity was used. The sputtering atmosphere consisted of Ar–O_2 mixed gas and its flow rate was controlled by separate gas flow-meters to provide an Ar:O_2 flow ratio of 1:1. The pressure in the deposition chamber during sputtering was

* Corresponding author. Tel.: +34 977558653; fax: +34 977559605.
E-mail address: vkhatko@urv.cat (V. Khatko).

0925-4005/$ – see front matter © 2007 Elsevier B.V. All rights reserved.
doi:10.1016/j.snb.2007.03.031

5×10^{-3} mbar. The rf sputtering power was 100 W. The film thickness was controlled by ellipsometry (PLASMOS 2000) at 50° and 60° of incidence angle. According to the results reported in [10], WO_3 thin films with three interruptions during the deposition process were prepared. A shutter was used to interrupt the deposition process. Unlike in [10], where the interruption time was constant (30 s), in the research reported in this article, the interruption time changed. The actual deposition time was up to 40 min for all thin films. These parameters of deposition process led to a total thickness of the WO_3 films in the range from 80 to 90 nm. Five sets of depositions were carried out. Each set included four depositions: without interruption and three-time interrupted depositions with interruption times of 30, 90, and 300 s. Four samples were simultaneously deposited at each deposition step. Therefore, the total number of silicon wafers with WO_3 films (i.e. samples) was 80. This allowed for estimating the reproducibility of the deposition method with interruptions. During each deposition the reproducibility of film thickness was better than ±1.0 nm.

The top contacts to the sensing layers were formed using air-dry silver paste (Heraeus AD1688-06) and annealing at 400 °C during 2 h for contact formation. The diameter of both point contacts was up to 1 mm and the distance between their centrums was up to 3 mm. Using this paste, the test samples were fixed on a ceramic heater prepared according to the method reported in [10]. The responses of the different films to nitrogen dioxide, ethanol and ammonia were investigated. The sensors (four replicate sensors were studied per sensing film) were kept in a temperature and moisture controlled test chamber. The sensors were operated in the temperature range from 150 to 300 °C to analyze the effect of working temperature on their response. The resistance of the sensing layers in the presence of either pure air (R_{air}) or different pollutants (R_{gas}) of different concentrations was monitored and stored in a PC.

XRD measurements were made using a Siemens D5000 diffractometer (Bragg-Brentano parafocusing geometry and vertical θ–θ goniometer) fitted with a curved graphite diffracted-beam monochromator, a Soller slit, a 0.2 mm receiving slit and a scintillation counter as a detector. The angular range was between 19° and 70° for 2θ. Data were collected with an angular step of 0.02° and 6 s per step and sample rotation. Cu Kα radiation was obtained from a Cu X-ray tube operated at 40 kV and 30 mA. To run XRD measurements at high temperature, an Anton-Paar HTK10 temperature chamber was attached to the diffractometer. Temperature patterns were collected at $\Delta T = 100$ °C. The time for X-ray pattern recording was up to 60 min at each definite temperature. A static air-atmosphere was used throughout the measurements.

Morphology of the WO_3 thin films was determined by atomic force microscopy from Molecular Imaging (PicoScan controller) in tapping mode. The estimation of grain size and image processing were achieved using MetaMorph 6.1 and WSxM 4.0 software, respectively. The mean grain diameter was calculated for population up to 100 elements. The standard error of the mean grain diameter (SEM) was calculated with the following expression: $SEM = SD/\sqrt{n}$, where SD is the standard deviation and n the number of elements.

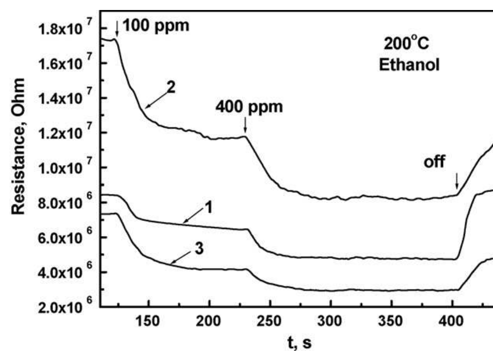

Fig. 1. Sensor response of WO_3 thin films to ethanol at 200 °C. 1, 2 and 3 are thin films prepared without (1) and with three interruptions (2, 3) of the deposition process and interruption time of 30 s (2) and 300 s (3).

3. Results and discussion

3.1. Gas sensitivity studies

The responses of the films with the interruption time up to 30, 90 and 300 s to nitrogen dioxide, ammonia and ethanol were analyzed at operating temperatures of 150, 200, 250 and 300 °C. Fig. 1 shows the response of the tungsten oxide thin films to ethanol at 200 °C. In this figure, the sensor response of the WO_3 thin film deposited without interruptions is presented as well. Table 1 shows the average responsiveness of the sensors to ethanol, calculated using the relation $S = |R_{gas} - R_{air}|/R_{air}$. It can be seen that the sensing layers prepared with an interruption time of at least 90 s show the best sensing properties. We can note that the differences in the sensor response of WO_3 thin films deposited with and without interruptions at a sputtering power of 200 W are higher [10].

Figs. 2 and 3 show the responses of WO_3 thin films deposited with interruptions to ammonia and nitrogen dioxide, respectively. Table 2 shows the average sensor responsiveness to these gases. It can be seen that WO_3 thin films deposited with interruption times equal or higher than 90 s have the best responsiveness both to ammonia and nitrogen dioxide.

Table 1
Sensor responsiveness (S) in the presence of ethanol as a function of interruption time and working temperature

Interruption time (s)	Concentration (ppm)	Working temperature (°C)	
		200	250
0	100	0.31	0.18
	500	0.48	0.31
30	100	0.32	0.21
	500	0.54	0.42
90	100	0.43	0.26
	500	0.55	0.44
300	100	0.44	0.28
	500	0.60	0.47

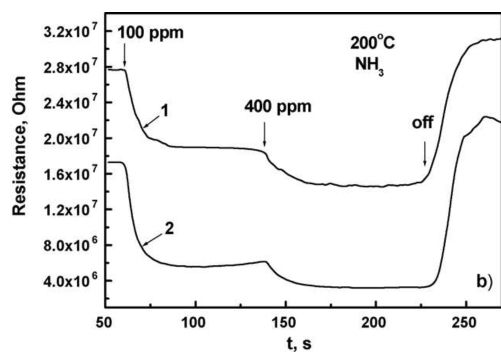

Fig. 2. Sensor response of WO_3 thin films to ammonia at 200 °C. 1 and 2 are thin films prepared with three interruptions of the deposition process and interruption time of 30 s (1) and 300 s (2).

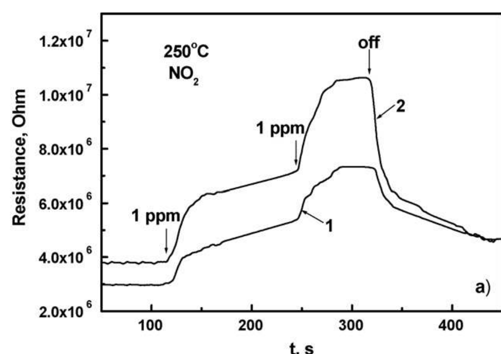

Fig. 3. Sensor response of WO_3 thin films to NO_2 at 250 °C. 1 and 2 are thin films prepared with three interruptions of the deposition process and interruption time of 30 s (1) and 300 s (2).

3.2. Structure of the WO_3 films

Fig. 4 shows the X-ray diffractograms of WO_3 thin films from $2\theta = 23.0°$ to 35°. The XRD data shows that the structure of as-deposited WO_3 films is amorphous. After annealing at 400 °C one monoclinic phase is present in the thin film that is described with the space group *Pc* (ICDD card no. 87-2386, cell parameters: $a = 5.277$ Å, $b = 5.156$ Å, $c = 7.666$ Å, $\beta = 91.742°$). The XRD patterns contain (1 1 0), (2 0 0) and (1 1 2) reflections from the monoclinic phase (*Pc*).

Table 2
Sensor responsiveness (*S*) in the presence of NH_3 (at 200 °C) or NO_2 (at 250 °C) as a function of interruption time

	Interruption time (s)		
	30	90	300
NH_3, 100 ppm	0.315	0.61	0.68
NH_3, 500 ppm	0.47	0.81	0.815
NO_2, 1 ppm	0.78	0.85	0.86
NO_2, 2 ppm	1.47	1.74	1.8

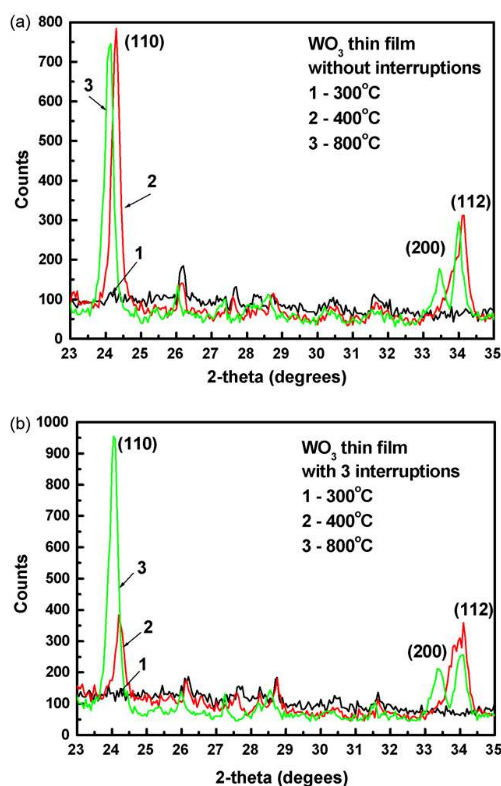

Fig. 4. X-ray diffractograms of WO_3 thin films deposited without (a) and with three interruptions (b). 1, 2 and 3 are the temperatures during XRD measurement.

It can be seen that the process of thin film crystallization has a different activity for both types of WO_3 thin films. The crystallization in the thin film prepared with three interruptions of deposition (Fig. 4b) is slower than in the films prepared without interruptions (Fig. 4a). This can be derived by comparing the intensities of (1 1 0) peaks and their full widths at half maximum. WO_3 thin films prepared without interruptions have the maximum intensity of (1 1 0) peak and minimal width at its half maximum. It is worth noting that the low-temperature monoclinic phase in WO_3 thin films was stable in a temperature range from 400 to 800 °C. The WO_3 thin films were sublimated at 900 °C.

3.3. Morphology of the WO_3 films

In this study we attempted to find a confirmation that interruption time influenced the morphology, roughness and mean grain size of the WO_3 surface layers during thin film growth. We analyzed $Si–SiO_2–WO_3$ structures as-deposited and annealed at 400 and 450 °C. Fig. 5 shows the surface morphology and roughness profiles of the WO_3 films as-deposited and annealed. It can be seen that tungsten oxide grains deposited without interruptions tend to reach an ordered distribution after annealing.

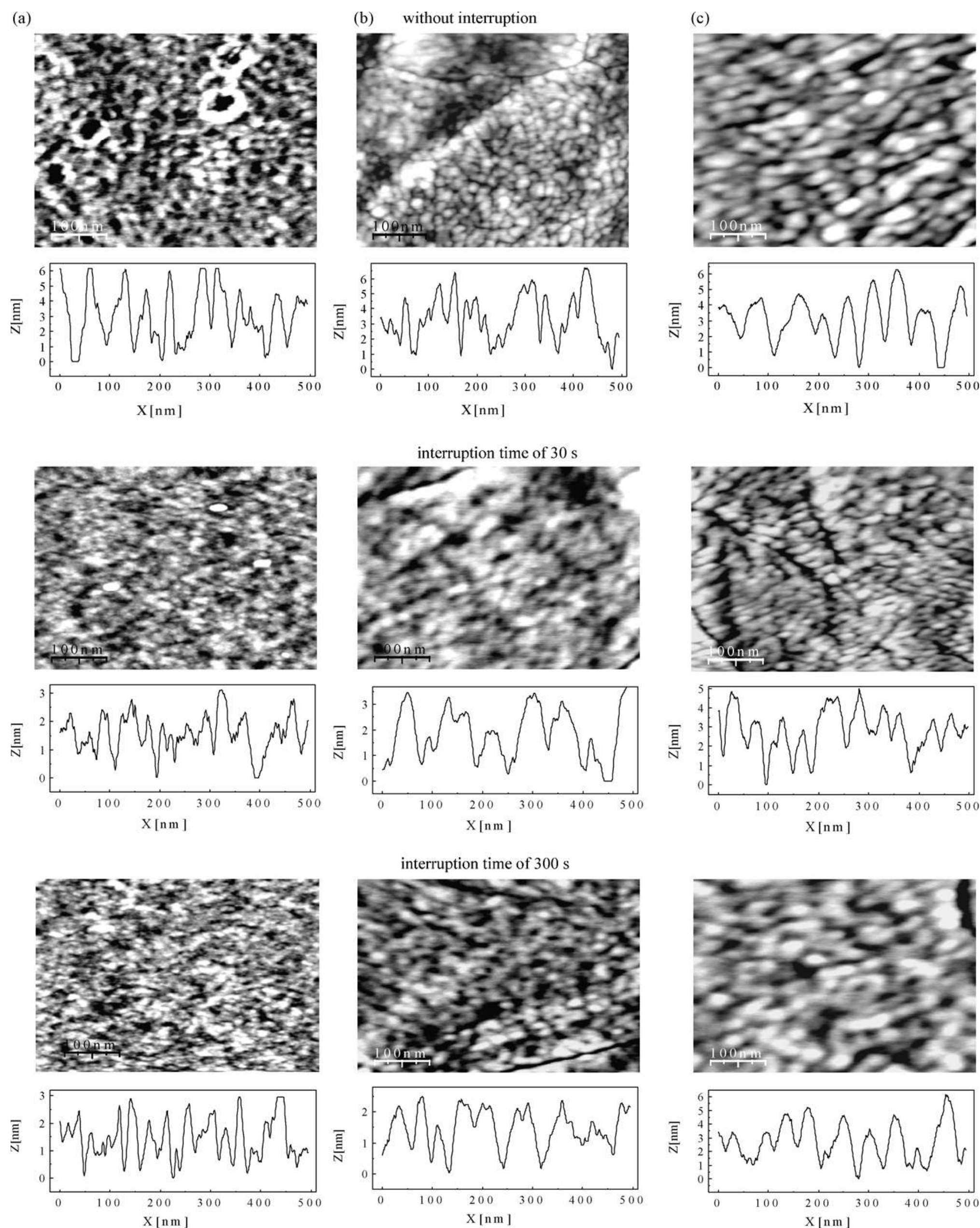

Fig. 5. AFM surface morphology and roughness profile of WO_3 thin films without interruptions and with three interruptions as deposited (a) and annealed at 400 °C (b) and 450 °C (c).

This is not clear for all the films deposited with three interruptions. The occurrence of an ordered distribution is correlated to the results obtained by XRD. The crystalline structure in the films prepared with three interruptions is not fully ordered as in the films prepared without interruptions. On the other hand, the roughness profile analysis along the horizontal lines of the AFM pictures shows that the sample deposited with three interruptions is smoother than the one deposited without interruption.

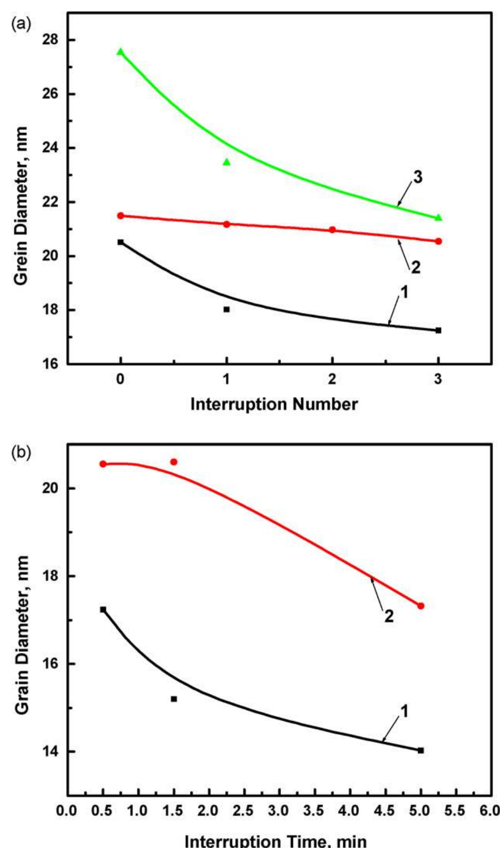

Fig. 6. Mean diameter of grains in WO_3 films as a function of the number of interruptions (a) and interruption time (b). 1, 2 and 3 are Si–SiO_2–WO_3 structures as deposited and annealed at 400 °C and 450 °C, respectively.

Fig. 6 shows the mean diameter of grains in the WO_3 films as a function of the number of interruptions and interruption duration. It can be seen the grain diameter decreases from 20.5 to 14.0 nm in as-deposited Si–SiO_2–WO_3 structures without interruptions and with three interruptions and interruption duration up to 300 s, respectively. When annealing at 400 °C the process of WO_3 film crystallization results in a slight increase in grain diameter.

3.4. Discussion

Analysis of the experimental data shows that the enhancement of the sensing properties observed for the WO_3 films deposited with three interruptions and interruption duration of more than 90 s is due to the decrease in grain size in the resulting metal oxide films. The decrease in grain size is the result of the features of thin film formation. The introduction of "extra" interfaces during interruptions influences the process of WO_3 crystallization and its surface morphology [10,11]. The prolongation of film growth on the "extra" interface involves a new nucleation of the metal oxide film that is the formation and growth of the metal oxide film with smaller grain size. Our experimental data shows that the duration of the interruptions influences the nucleation and growth of the film on the "extra" interface. We can conclude that the "extra" interface is formed as a result of the structural relaxation of the film surface during the interruption time.

4. Conclusions

WO_3 thin films were deposited by reactive rf sputtering from a pure tungsten target. The deposition process was conducted with three interruptions and the interruption time was 30, 90 and 300 s. On the basis of these films, sensing layers were prepared and their responses to NO_2, ammonia and ethanol were investigated. It was found that the sensing layers prepared with three interruptions and interruption duration of more than 90 s showed the best sensing properties. The increase in sensitivity is related to the decrease of grain size in the WO_3 thin films observed as the number of interruptions and interruption time were increased. These results are based on five different deposition batches, which resulted in 80 samples being produced and analyzed. It can be concluded that the reported deposition method leads to reproducible results.

References

[1] G. Sberveglieri, L. Depero, S. Groppelli, P. Nelli, WO_3 sputtered thin films for NO_x monitoring, Sens. Actuat. B, Chem. 26–27 (1995) 89–92.
[2] M. Penza, C. Martucci, G. Cassano, NO_x gas sensing characteristics of WO_3 thin films activated by noble metals (Pd, Pt, Au) layers, Sens. Actuat. B, Chem. 50 (1998) 52–59.
[3] M. Bendahan, R. Boulmani, J.L. Seguin, K. Aguir, Characterization of ozone sensors based on WO_3 reactively sputtered films: influence of O_2 concentration in the sputtering gas, and working temperature, Sens. Actuat. B, Chem. 100 (2004) 320–324.
[4] S.R. Utembe, G.M. Hansford, M.G. Sanderson, R.A. Freshwater, K.F.E. Pratt, D.E. Williams, R.A. Cox, L. Jones, An ozone monitoring instrument based on the tungsten trioxide (WO_3) semiconductors, Sens. Actuat. B, Chem. 114 (2006) 507–512.
[5] M.D. Antonik, J.E. Schneider, E.L. Wittman, K. Snow, J.F. Vetelino, R.J. Lad, Microstructural effects in WO_3 gas-sensing films, Thin Solid Films 26 (1995) 247–252.
[6] M. Stankova, X. Vilanova, E. Llobet, J. Calderer, M. Vinaixa, I. Gràcia, C. Cané, X. Correig, On-line monitoring of CO_2 quality using doped WO_3 thin film sensors, Thin Solid Films 500 (2006) 302–308.
[7] G.-J. Li, X.-H. Zhang, S. Kawi, Relationships between sensitivity, catalytic activity, and surface areas of SnO_2 gas sensors, Sens. Actuat. B, Chem. 60 (1999) 64–70.
[8] G. Zhang, M. Liu, Effect of particle size and dopant on properties of SnO_2 — based gas sensors, Sens. Actuat. B, Chem. 69 (2000) 144–152.
[9] V. Khatko, J. Calderer, E. Llobet, X. Correig, New technology of metal-oxide thin film preparation for chemical sensor application, in: Proceedings of the European Materials Conference E-MRS 2004 FALL MEETING, Warsaw (Poland), 6–10 September, 2004, p. 36.
[10] V. Khatko, J. Calderer, E. Llobet, X. Correig, New technology of metal-oxide thin film preparation for chemical sensor application, Sens. Actuat. B, Chem. 109 (2005) 128–134.
[11] V. Khatko, S. Vallejos, J. Calderer, E. Llobet, X. Vilanova, X. Correig, Gas sensing properties of WO_3 thin films deposited with interruptions, in: Proc. 19th European Conference on Solid State Transducers, EUROSENSORS XIX, Barcelona, Spain, 11–14 September 2005, 2005, TP20.

[12] A.A. Schmidt, R. Anton, Anomalous growth behaviour of Pd–Au and Ag–Au alloy particles during vapour deposition on carbon substrates at elevated temperatures, Surf. Sci. 322 (1995) 307–324.
[13] A.A. Schmidt, H. Eggers, K. Herwig, R. Anton, Comparative investigation of the nucleation and growth of fcc-metal particles (Rh, Ir, Ni, Pd, Pt, Cu, Ag, Au) on amorphous carbon and SiO_2 substrates during vapor deposition at elevated temperatures, Surf. Sci. 349 (1996) 301–316.
[14] R. Anton, A.A. Schmidt, Anomalous nucleation and growth of metal and allow particles during vapor deposition on amorphous substrates, Surf. Sci. 357–358 (1996) 835–839.

Biographies

Viacheslav Khatko graduated in nuclear physics from the Belarusian State University (Minsk, Belarus) in 1971. He received his PhD in materials science in 1986 and DrSc in solid-state electronics in 2001. In 1975–2003 he worked at the Physical Technical Institute of National Academy of Sciences of Belarus, Minsk, as a researcher, head of the Laboratory of Electronic Engineering Materials, head of the Thin Film Materials Department and then as Principal Investigator of the same institute. He was Ford SABIT Intern and Ford Visiting Scientist in 1998 and 1999, respectively. From April 2003 he is Ramón y Cajal professor in the Electronic Engineering Department of the Universitat Rovira i Virgili (Tarragona, Spain). His current research interests include the development and application of semiconductor thin and thick film gas sensors.

Stella Vallejos graduated in electrical engineering (2002) and electronic engineering (2003) from the Universidad Técnica de Oruro, Bolivia. She is currently a PhD student in the Electronic Engineering Department at the Universitat Rovira i Virgili, Spain. Her main areas of interest are in fabrication and characterization of solid-state gas sensors.

Josep Calderer obtained his degree in Physics in 1973 and the PhD in 1981 in the University of Barcelona. He has been working in technology and characterization of photovoltaic solar cells, heterojunction bipolar transistors and silicon-based integrated optical sensors. At present he is a staff member of the Department of Electronic Engineering (DEE) of the Polytechnic University of Catalonia (UPC, Barcelona). His main research activity focuses on resistive gas sensors using metal oxide compounds.

Eduard Llobet graduated in telecommunication engineering from the Universitat Politècnica de Catalunya (UPC), (Barcelona, Spain) in 1991, and received his PhD in 1997 from the same university. During 1998, he was a visiting fellow at the School of Engineering, University of Warwick (UK). He is currently an associate professor in the Electronic Engineering Department at the Universitat Rovira i Virgili (Tarragona, Spain). His main areas of interest are in the fabrication, and modelling of semiconductor chemical sensors and in the application of intelligent systems to complex odour analysis.

Xavier Vilanova graduated in telecommunication engineering from the Universitat Politècnica de Catalunya (UPC) (Barcelona, Spain) in 1991, and received his PhD in 1998 from the same university. He is currently an associate professor in the Electronic Engineering Department at the Universitat Rovira i Virgili (Tarragona, Spain). His main areas of interest are in semiconductor chemical sensors modelling and simulation.

Xavier Correig graduated in telecommunication engineering from the Universitat Politècnica de Catalunya (UPC) (Barcelona, Spain) in 1984, and received his PhD in 1988 from the same university. He is a full professor of Electronic Technology in the Electronic Engineering Department at the Universitat Rovira i Virgili (Tarragona, Spain). His research interests include heterojunction semiconductor devices and solid-state gas sensors.

UNIVERSITAT ROVIRA I VIRGILI
STUDY OF STRUCTURAL AND SENSING PROPERTIES OF TUNGSTEN TRIOXIDE THIN FILMS
DEPOSITED BY RF SPUTTERING
Stella Vallejos Vargas
ISBN:978-84-691-9748-6 /DL:T-1249

II

Reprinted from Elsevier B.V.
Surface and Coating Technology, 202 (2007) 453 - 459
Technology of metal oxide thin film deposition with interruptions
V. Khatko, J. Calderer, S. Vallejos, E. Llobet, X. Correig

Available online at www.sciencedirect.com
ScienceDirect
Surface & Coatings Technology 202 (2007) 453–459
SURFACE & COATINGS TECHNOLOGY
www.elsevier.com/locate/surfcoat

Technology of metal oxide thin film deposition with interruptions

V. Khatko [a,*], J. Calderer [b], S. Vallejos [a], E. Llobet [a], X. Correig [a]

[a] Departament d'Enginyeria Electronica, Universitat Rovira i Virgili, Campus Sescelades 43007 Tarragona, Spain
[b] Universitat Politecnica de Catalunya, Departament d'Enginyeria Electronica, Campus Nord 08034 Barcelona, Spain

Received 22 December 2006; accepted in revised form 5 June 2007
Available online 13 June 2007

Abstract

The idea to obtain metal-oxide films with small grain size is to use a special regime of thin film deposition by r.f. sputtering of pure metal or metal oxide targets. This regime includes the deposition of thin films with one or several interruptions during the deposition process. WO_3 films were r.f. sputtered onto pure and oxidized silicon wafers. Four types of films were prepared, i.e. using continual deposition, one, two and three interrupted depositions with an actual deposition time of 40 min. The interruption time changed from 0.5 min to 5.0 min for the different samples. It was found that the total thickness of WO_3 films decreased with the increase of the number of interruptions and the increase in interruption time. Phase composition and features of surface morphology of the films deposited and annealed in the temperature range from room temperature to 900 °C have been investigated by XRD and AFM, respectively. It is shown that grain size in the metal oxide films decreased essentially with the increase of the number of interruption during the deposition process.
© 2007 Elsevier B.V. All rights reserved.

PACS: 81.15.Cd; 68.55.Jk
Keywords: R.f. sputtering; Deposition with interruptions; Tungsten trioxide thin films properties

1. Introduction

Tungsten trioxide (WO_3) has interesting physical and chemical properties, which make it useful for a wide spectrum of technological applications. For example, tungsten trioxide is an important material for electrochromic [1] and photoelectrochemical devices [2], catalysts [3] and gas sensors [4,5]. Nowadays, WO_3-based films are considered as one of the most interesting materials for detecting nitrogen oxides and other species such as NH_3, CH_4 and CO [4-9]. Reducing the grain size of active layers is one of the key factors to enhance the gas sensing properties of semiconductor metal oxide sensors [10,11].

The idea to create metal-oxide films with small grain size consists of using a special regime of thin film deposition by the dc magnetron, ion-beam or r.f. sputtering of pure metal or metal oxide targets. This regime includes the deposition of thin films with one or several interruptions of the deposition process [12,13].

* Corresponding author. Tel.: +34 977558653; fax: +34 977559605.
E-mail address: vkhatko@urv.cat (V. Khatko).

0257-8972/$ - see front matter © 2007 Elsevier B.V. All rights reserved.
doi:10.1016/j.surfcoat.2007.06.007

Early systematic investigations of the growth kinetics of pure metals evaporated on amorphous carbon substrates have revealed that, after interrupting a continuous vapour deposition period by closing the beam shutter, the metal particles continued to grow for up to several minutes with decreasing speed [14-16]. At constant temperature, after re-opening the shutter, particle growth resumed with a delay being similar to that of particle nucleation. It was shown that there are at least two different mechanisms of adatom diffusion. There exist at least two binding states for the metal atoms with energies of about 1 eV for regular states and in the range from 1.5 to 1.7 eV with abundance of 10^{13} to 10^{14} cm^{-2} [14,16]. The occurrence of growth transients after closing the beam shutter requires re-emission of adatoms from the sites with higher energy in an activated process of particle growth. Porosities in the substrate surface could be responsible for temporarily trapping of adatoms in states with higher energy.

The detailed evolution of stress in thin films that grow by the Volmer–Weber (VW) mechanism during ultra-high vacuum deposition and growth interrupts was explored using real-time wafer curvature measurements [17–19]. It was shown that reversible stress changes during the interruption of thin film

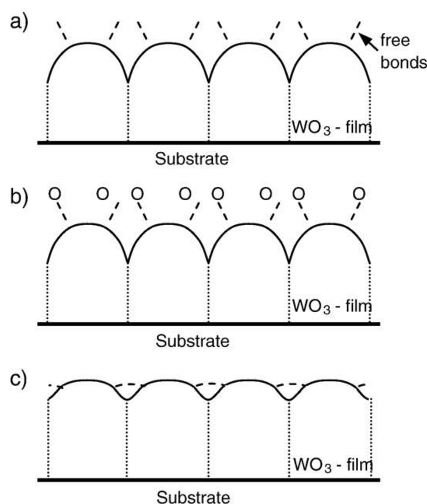

Fig. 1. Schematic illustrations of the manner of a film growth (a) and an equilibrium surface formation during interruption processes (b,c). Subplots b and c show the saturation of surface free bonds by oxygen atoms (b) and the structural relaxation of the surface (c).

growth are phenomenologically similar in the pre-coalescence and post-coalescence growth regimes. It was suggested that the reversible stress changes are associated with changes in the concentration of atomic defects on the substrate and film surface [19]. At the pre-coalescence stages of growth initiation, the dominant defects are isolated adatoms. At the post-coalescence stages, film surface is likely to be atomically rough, with excess adatoms, ledges and other defects. When film growth is interrupted, the defect population decays to the equilibrium value as excess adatoms diffuse to incorporation sites and excess defects are eliminated [19].

During the interruption of the deposition process at the post-coalescence stages of film growth, an equilibrium film surface can be formed due to the free surface bond saturation by the atoms from the residual atmosphere and/or the structural relaxation of the interface. Fig. 1 illustrates, for the two possible cases, the way in which the equilibrium surface is formed during an interruption process. The saturation of metal films by oxygen atoms from the residual atmosphere has been shown earlier by the investigation of sputtering-deposited molybdenum films [20]. It could be realized by the formation of bonds between metal atoms and O^- ions accelerated from the target (Fig. 1b). It is known that a deposited thin film tries to minimize its total energy by keeping its surface area as small as possible to obtain an ideally flat surface. Surface diffusion of the adatoms makes possible the occupancy of empty sites in the film lattice and can lead to less surface area by filling in the valleys and leveling the atom peaks to give a lower surface energy [19,21,22] (Fig. 1,c).

Thus, the surface diffusion of adatoms during interruption of the deposition could promote both film growth continuation [14-16] and structure relaxation of the film surface [19,21,22].

For the subsequent prolongation of the deposition process, film growth begins over again on the new “extra” equilibrium surface (relaxed surface) and the average grain size of the film at the surface could be smaller than in the original film. The equilibrium surface is sufficiently rough and there can be coalescence between both new islands and a new island and an existing film grain [22]. Fig. 2 shows a qualitative representation of the influence of the deposition interruptions on thin film thickness and grain size growth. The qualitative views of the dependencies of film thickness and grain size on deposition time were built on the base of theoretical and experimental data presented in Ref. [21]. So, Fig. 2,a sketches out the change in film thickness after each interruption. Lines 0, 1 and 2 present the change in film thickness as a function of deposition time for the film deposited without interruptions (line 0) and with one (line 1) and two (line 2)interruptions, respectively. Lines 1 and 2 show the time delay necessary for the nucleation of new particles [14]. The points 0, 1 and 2 define the film thickness after the end of the deposition process. Fig. 2,b shows a reiteration of the nucleation of grains on each new “extra” equilibrium surface formed after the interruption of the deposition process. Lines 0′, 1′ and 2′ present grain growth in the film as a function of deposition time for the film deposited without interruption (line 0′) and with one (line 1′) and two (line 2′) interruptions, respectively. The points 0′, 1′ and 2′ define grain size in the films after the end of the deposition process. The differences in grain size after the first and second interruption are related to the coalescence between both new islands and a new island and an existing grain in the film [14,22].

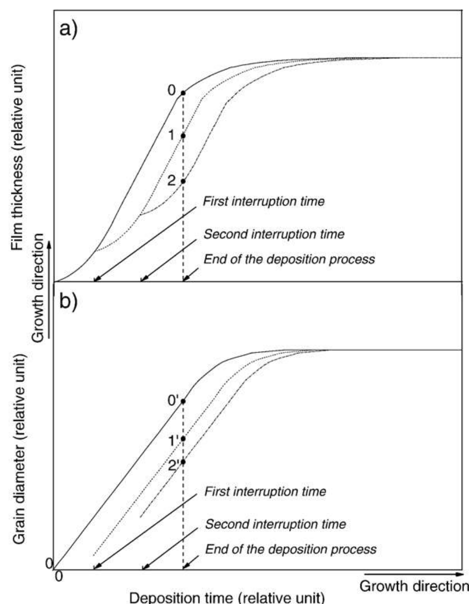

Fig. 2. Qualitative views of the dependencies of film thickness (a) and grain size (b) on deposition time. Labels 0, 1 and 2 correspond to deposition processes without and with one and two interruptions, respectively.

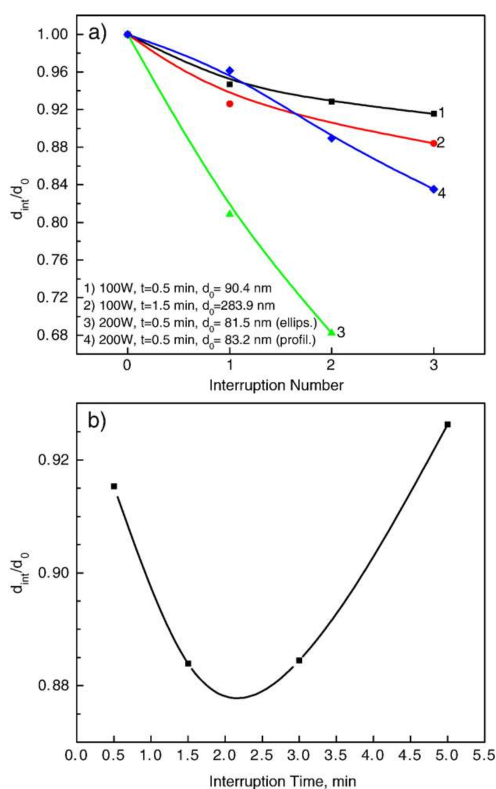

Fig. 3. Relative change of the metal oxide film thickness (d_{int}/d_0) as a function of the number of interruptions (a) and interruption time (b). For reference, the experimental data obtained at the sputtering power of 200 W [Ref. [13]] are presented as well.

In previous studies it has been shown that using a deposition process with interruptions leads to WO_3 films with a decreased average grain size and better sensitivity to toxic gases [12,13]. The aim of this paper is to study the influences of interrupting the deposition process and interruption time on the changes in film thickness, chemical composition, structure and surface morphology of WO_3 thin films.

2. Experimental

Tungsten oxide films were deposited onto boron-doped (1-10 Ω cm) Si(100) wafers by reactive r.f. magnetron sputtering using an ESM100 Edwards sputtering system. A metal target of 99.95% purity with a diameter of 100 mm and thickness of 3.175 mm was used. The target to substrate distance was set to 70 mm [13]. One part of the silicon wafers used was oxidized in dry oxygen at 1100 °C. The thickness of the SiO_2 films was about 150 nm. All wafers were held in thermal contact with a holder during the deposition process. The substrate temperature was kept constant during film deposition at room temperature. The base pressure in the sputtering chamber was 6×10^{-3} mbar. The sputtering atmosphere consisted of $Ar–O_2$ mixed gas and its flow rate was controlled by separate gas flow-meters to provide an $Ar:O_2$ flow ratio of 1:1. The pressure in the deposition chamber during sputtering was 5×10^{-3} mbar. The r.f. sputtering power was 100 W.

Four types of tungsten oxide films were prepared. For the first type a non-interrupted sputtering process was used. In the deposition of films type 2, 3 and 4, the sputtering process was interrupted once, two and three times, respectively. A shutter was used to interrupt the deposition process. As a rule, the actual deposition time without interruption was 40 min. Nevertheless, for several tungsten oxide films deposited with interruptions, the deposition time was up to 2 h. The interruption time changed from 0.5 min to 5.0 min for the different samples. The film thickness and refractive index were measured by ellipsometry (PLASMOS 2000) at 50° and 60° of incidence angle. As-deposited and annealed tungsten oxide films had refractive index of 2.08–2.13 that corresponded to those obtained in Ref.[23].

X-ray diffraction (XRD) measurements were made using a Siemens D5000 diffractometer (Bragg–Brentano parafocusing geometry and vertical θ–θ goniometer) fitted with a curved graphite diffracted-beam monochromator and Soller slit, 0.2 mm

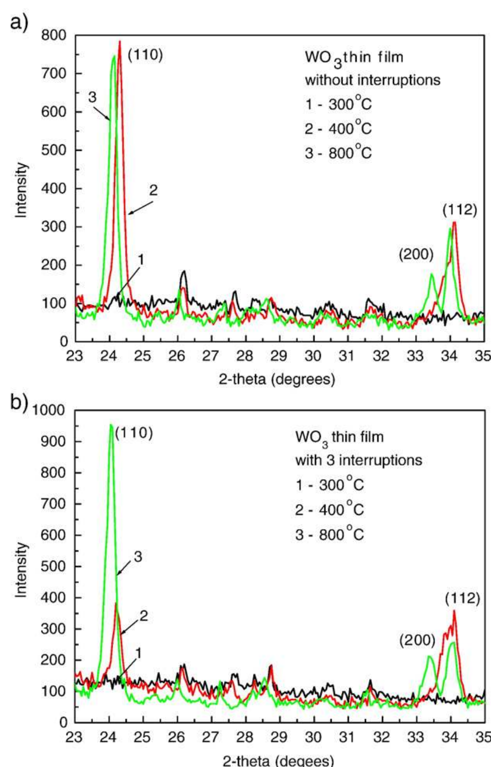

Fig. 4. X-ray diffractograms of WO_3 thin films deposited without (a) and with three interruptions (b). 1, 2 and 3 correspond to the temperature of the XRD measurement.

receiving slit and scintillation counter as detector. The angular range was between 19° and 70° for 2θ. Data were collected with an angular step of 0.02° and 6 s per step and sample rotation. CuK_α radiation was obtained from a Cu X-ray tube operated at 40 kV and 30 mA. To run XRD measurements at high temperature, an Anton-Paar HTK10 temperature chamber was attached to the diffractometer. Temperature patterns were collected at $\triangle T = 100$ °C. The time for X-ray pattern recording was up to 60 min at each definite temperature. A static air-atmosphere was used throughout the measurements.

As-deposited tungsten oxide films were studied by Auger spectrometry to investigate oxygen segregation on the equilibrium surface built up during deposition interruption. The tungsten oxide layer surface and the chemical element distribution in the samples were examined with a PHI-660 Auger spectrometer operating at 3 kV and using a probe diameter up to 1 μm. Auger electron collection depth was up to 2.0 nm. The layer thickness removed during each step of argon ion etching was up to 0.9–1.0 nm.

The morphology of the WO_3 thin films was determined by Atomic Force Microscopy (AFM) from Molecular Imaging

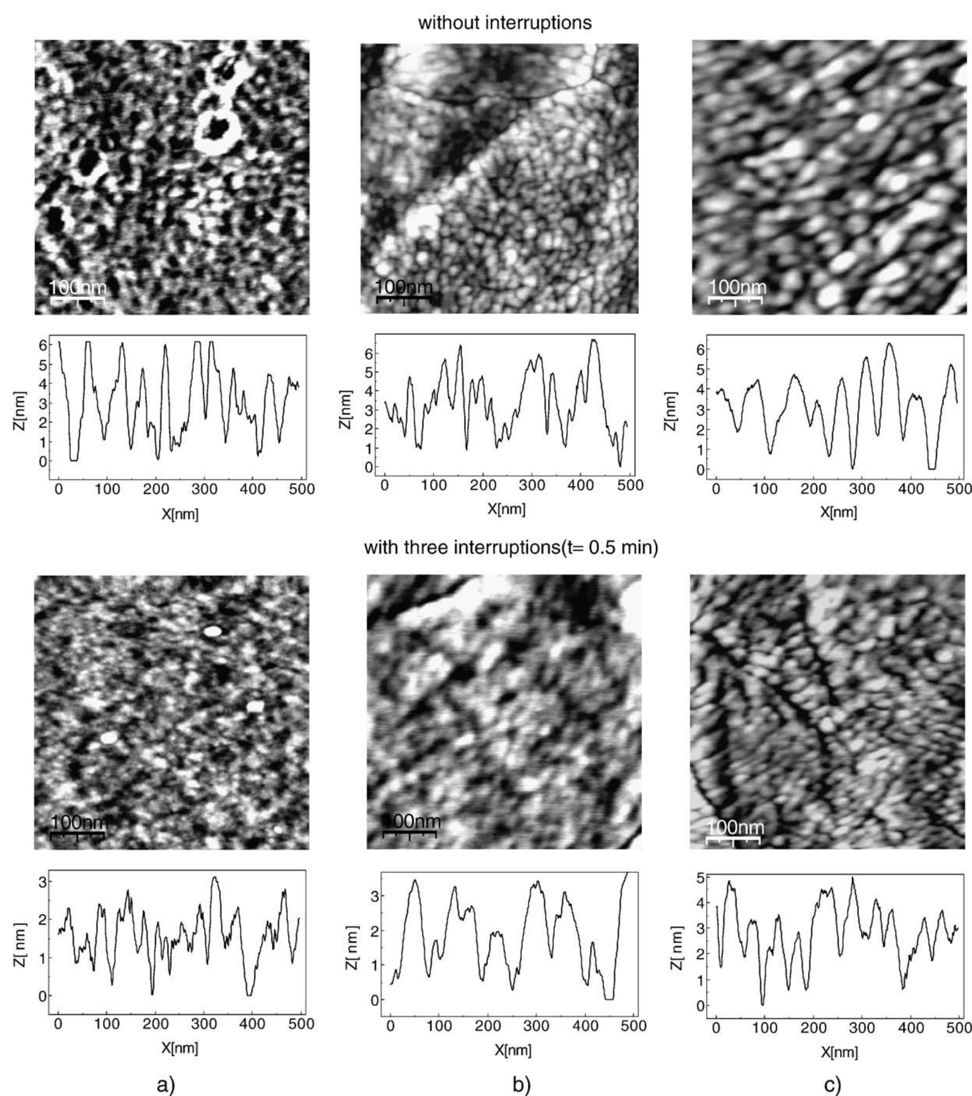

Fig. 5. AFM surface morphology and roughness profile of WO_3 thin films without interruptions and with three interruptions. (a) as deposited, (b) annealed at 400 °C and (c) annealed at 450 °C.

ISBN:978-84-691-9748-6 /DL:T-1249

(PicoScan controller) in tapping mode. The estimation of grain size and image processing were achieved using MetaMorph 6.1 and WSxM 4.0 software respectively. The mean diameter of grains was calculated for a population of one hundred elements. The standard error of the mean diameter of grains (SEM) was calculated with the following expression: $SEM = \frac{SD}{\sqrt{n}}$, where SD is the standard deviation and n the number of elements. The standard error of the mean diameter of grains was between ±0.14-±0.52 nm in each case.

3. Results and discussion

3.1. Measurement of film thickness

Fig. 3 shows the relative change of the metal oxide film thickness (d_{int}/d_0) as a function of the number of interruptions (Fig. 3,a) and interruption time (Fig. 3,b). Here, d_{int} and d_0 are the thickness of WO_3 thin films deposited with a definite number of interruptions (int=0, ..., 3) and without interruptions (int=0), respectively. For comparison, the experimental data obtained at the r.f. sputtering power of 200 W taken from Ref. [13] is presented in Fig. 3,a as well.

It can be seen that the total thickness (d_{int}) of WO_3 thin films deposited with interruptions decreases when the number of interruptions during the deposition process increases (Fig. 3,a). This result is verified for the different total thickness of WO_3 thin films and the different r.f. sputtering power of the deposition process. The relative change in the metal oxide film thickness decreases when the total thickness of WO_3 thin films and r.f. sputtering power are increased. In the latter case, using higher sputtering power (200 W) has an extremely strong influence on the properties and total thickness of the WO_3 thin films [13]. There is a difference in the thickness measured by profilometry and ellipsometry for the tungsten oxide thin films deposited with interruptions during the deposition process. For examples, the relative changes in the thickness of the films deposited with two interruptions have values of 0.89 and 0.68 measured by profilometry and ellipsometry, respectively (Fig. 3,a). This result shows that “extra” interfaces are introduced into the body of a thin film during each interruption of the deposition process. At this point we can conclude that the features of the surface relaxation process influence on the formation of “extra” interfaces.

This is confirmed by a stress relaxation study [17–19] and the experimental data presented in Fig. 3, b. It can be seen that the duration of interruption influences on the total thickness and the relative change of the metal oxide film thickness. For explaining this functional dependence we will use the experimental data obtained in [14,15] and presented above. It can be assumed that there is some relation between the time in which a film continues to grow after the shutter has been closed and the time delay for the film to resume its growth after re-opening the shutter. Increasing the time in which the film continues to grow could decrease the time delay before resuming its growth. In this case, the relative change of the metal oxide film thickness can have a minimum at a definite value of the interruption time, just as Fig. 3,b shows. We can conclude that the process of film surface relaxation has a definite time (the time for the connection of all free bonds).

3.2. Structure of the WO_3 films

Fig. 4 shows the X-ray diffractograms of WO_3 thin films deposited onto a silicon substrate from 2θ=23.0° to 35°. XRD data showed that the structure of as deposited WO_3 films is amorphous. After annealing at 400 °C one monoclinic phase is present in the thin film that is described with the space groups *Pc* (ICDD card no. 87-2386, cell parameters: a=5.277 Å, b=5.156 Å, c=7.666 Å, β=91.742°). XRD patterns contain (110), (200) and (112) reflections from the monoclinic phase (*Pc*).

It can be seen that the process of thin film crystallization has a different activity for the different types of WO_3 thin films. The crystallization in the thin film prepared with three interruptions during its deposition (Fig. 4b) is slower than in films prepared without interruptions (Fig. 4a). This can be derived by comparing the intensities of (110) peaks and their full widths at half maximum. WO_3 thin films prepared without interruptions have maximum intensity of (110) peak and full width at half maximum of this peak is minimal. It its worth noting that the low-temperature monoclinic phase in WO_3 thin films was

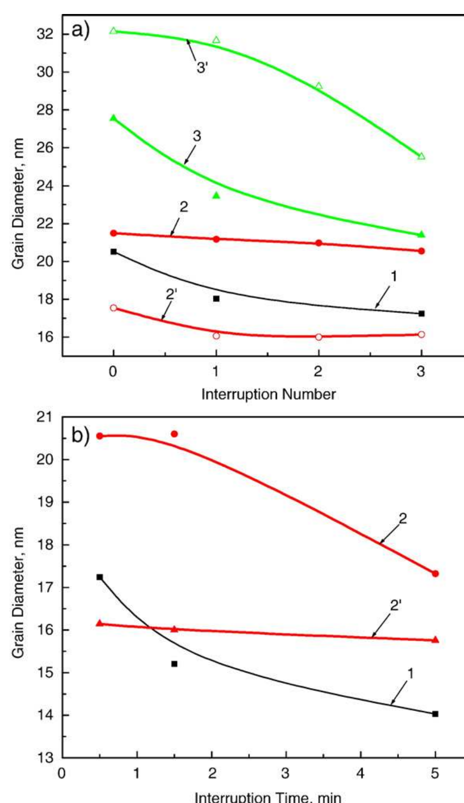

Fig. 6. Mean diameter of grains in WO_3 films as a function of the number of interruptions (a) and interruption time (b). 1, 2 and 3 are labels for $Si–SiO_2–WO_3$ structures as-deposited and annealed at 400 °C and 450 °C, respectively. 2′ and 3′ are labels for $Si–WO_3$ structures annealed at 400 °C and 450 °C, respectively.

stable in a temperature range from 400°C to 800°C. WO_3 thin films were sublimated at 900°C. The same result was obtained for WO_3 thin films deposited onto oxidized silicon wafers.

The fact that the monoclinic phase with *Pc* symmetry exists in WO_3 thin film deserves some comments. The existence of low-temperature *Pc* phases has been reported in gas-evaporated WO_3 microcrystals analyzed by Raman spectroscopy [24,25]. The reason for the existence of *Pc* phase in these microcrystals could be either high compression stresses or surface effects on the grains or interfaces [26]. In our case the basic reason for the existence of a *Pc* phase in WO_3 thin films could be compressive stresses into the layers.

3.3. Morphology of the WO_3 films

In this section we tried to find a confirmation that the “extra” interfaces influence on the morphology, roughness and mean grain size formed in WO_3 surface layers during thin film growth. We analyzed $Si–SiO_2–WO_3$ structures as deposited and annealed at 400 °C and 450 °C since these structure are used very intensively in the preparation of gas sensors [4,5,12,13]. The results obtained were compared with the experimental data for $Si–WO_3$ structures annealed at 400 °C.

Fig. 5 shows the surface morphology and roughness profiles of the WO_3 films as deposited and annealed. It can be seen that tungsten oxide grains in the films deposited without interruptions try to reach an ordered distribution after annealing. That is not so clear for all of the films with three interruptions. The occurrence of an ordered distribution is correlated to the results obtained by XRD. The crystalline structure in the films prepared with three interruptions is not fully ordered as in the films prepared without interruptions. On the other hand, the roughness profile analysis along the horizontal lines of the AFM pictures shows that the samples deposited with three

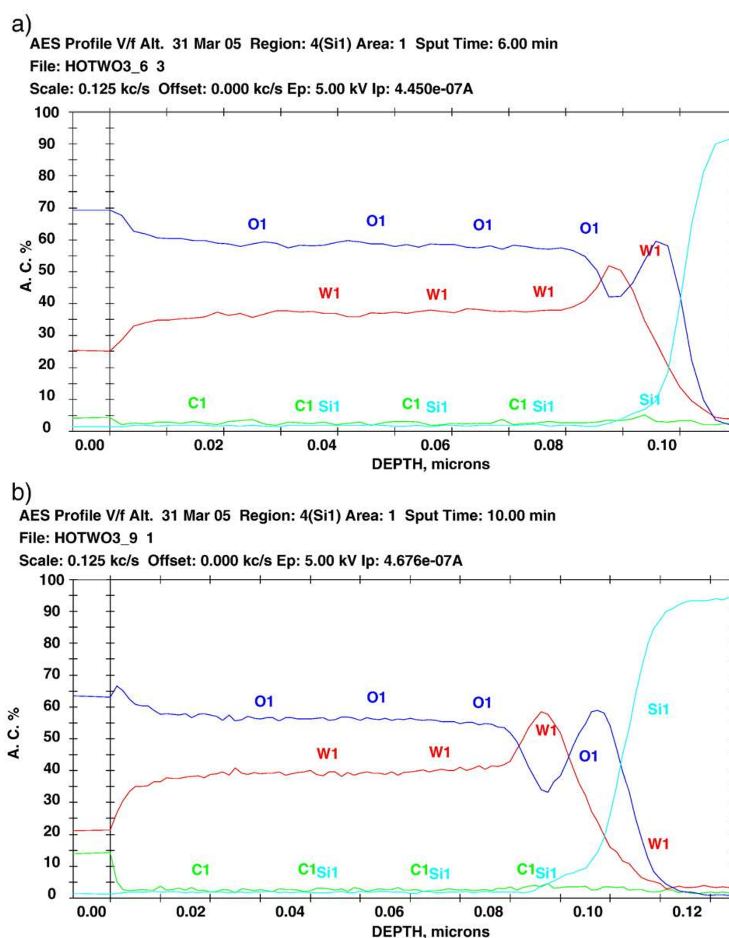

Fig. 7. Auger profiles of chemical elements into WO_3 thin films prepared without (a) and with three interruptions (b) during the deposition process. A.C. stands for atomic concentration in %.

interruptions are smoother than the ones deposited without interruptions.

Fig. 6 shows the mean diameter of grains in WO_3 films as a function of the number of interruptions and their duration. It can be seen that grain diameter decreases from 20.5 nm down to 17.0 nm in as deposited $Si–SiO_2–WO_3$ structures without and with 3 interruptions respectively. Increasing the interruption time from 30 s up to 5 min results in a further reduction of grain size from 17.0 nm down to 14.0 nm. When annealing at 400 °C, the process of WO_3 film crystallization results in a slight increase in the diameter of the grains. There is a tendency showing that the higher the number of interruptions is, the lower the increase in grain size during the annealing process is.

3.4. Discussion

On the base of the experimental results obtained we can summarize that the introduction of the “extra” interfaces during the deposition interruptions influences the process of WO_3 film crystallization retarding it.

Fig. 7 shows Auger profiles for two types of as-deposited WO_3 thin films on silicon wafers. It can be seen that the chemical element composition on the surface of tungsten oxide film corresponds to stoichiometric WO_3. The change in the ratio of tungsten to oxygen atoms observed after argon ion etching of the film surface is due to the difference in the scattering coefficient of oxygen and tungsten [27]. The existence of a narrow area (up to 20 nm) close to the film-substrate interface containing a high amount of tungsten atoms could be explained by the formation of WO_{3-x} (Magneli phases) [28]. Nevertheless WO_{3-x} phases were not detected by the XRD method.

The basic conclusion from Fig. 7 is that there is no heterogeneity at the profiles of tungsten and oxygen atoms. The absence of any segregation of oxygen or tungsten atoms into the thin film body evidences that the process of free bond saturation by the atoms from residual atmosphere on the “extra” interface is not clearly realized or can not be detected by Auger spectroscopy. This result is similar the one presented in Ref. [17] where oxide layers were not observed in Al films deposited with two interruptions. The tendency to obtain smoother surfaces in WO_3 films deposited with several interruptions shows that the process of minimization of film surface energy was repeated several times during interruptions. It could be suggested that the “extra” interface is formed due to the structural relaxation of the additional interface during the interruption time.

4. Conclusions

The properties and structural features of WO_3 thin film layers deposited with interruptions have been studied by XRD, Auger spectroscopy and AFM. The WO_3 films were deposited by r.f. sputtering onto pure and oxidized silicon wafers at an argon/oxygen flow ratio of 50/50, r.f. power of 100 W and a total pressure of 5×10^{-3} mbar. Four types of films were prepared, i.e. using continual deposition, one, two and three interrupted depositions with an actual deposition time of 40 min. The total thickness of WO_3 thin films deposited with interruptions decreases when the number of interruptions during the deposition process increases. All as-deposited WO_3 films have an amorphous structure. After annealing at 400 °C, a low-temperature monoclinic phase with *Pc* symmetry is present in the films. This phase was very stable up to 800 °C and the interruption of deposition influenced on WO_3 film crystallization by retarding it. On the base of the experimental data obtained and the references analyzed it could be suggested that the “extra” interface is formed into the body of the film due to surface structural relaxation during its interrupted growth. At the same time, the experimental data obtained by Auger spectroscopy did not show any segregation of oxygen or tungsten atoms into the WO_3 film body.

References

[1] G.G. Granqvist, Sol. Energy Mater. Sol. Cells 60 (2000) 201.
[2] A. Di Paola, L. Palmisano, A.M. Venezia, V. Augugliano, J. Phys. Chem. B103 (1999) 8236.
[3] A. Löfbeg, A. Frennet, G. Leclercq, L. Leclercq, J.M. Giraudon, J. Catal. 189 (2000) 170.
[4] P. Shaver, Appl. Phys. Lett. 11 (1967) 255.
[5] D.G. Dwyer, Sens. Actuators, B, Chem. 5 (1991) 155.
[6] A.A. Tomchenko, V.V. Khatko, I.L. Emelianov, Sens. Actuators, B, Chem. 46 (1998) 8.
[7] A.A. Tomchenko, I.L. Emelianov, V.V. Khatko, Sens. Actuators, B, Chem. 57 (1999) 166.
[8] Y.K. Chung, M.H. Kim, W.S. Um, H.S. Lee, J.K. Song, S.C. Choi, K.M. Yi, M.J. Lee, K.W. Chung, Sens. Actuators, B, Chem. 60 (1999) 49.
[9] D.S. Lee, S.D. Han, J.S. Huh, D.D. Lee, Sens. Actuators, B, Chem. 60 (1999) 57.
[10] I. Jimenez, J. Arbiol, G. Dezanneau, A. Cornet, J.R. Morante, Sens. Actuators, B, Chem. 93 (2003) 343.
[11] S.-H. Wang, T.-C. Chou, C.-C. Liu, Sens. Actuators, B, Chem. 94 (2003) 475.
[12] V. Khatko, J. Calderer, E. Llobet, X. Correig, Proceedings of the European Materials Conference E-MRS 2004 FALL MEETING, Warsaw (Poland), Sept. 6–10 2004, p. 36.
[13] V. Khatko, J. Calderer, E. Llobet, X. Correig, Sens. Actuators, B, Chem. 109 (2005) 128.
[14] A.A. Schmidt, R. Anton, Surf. Sci. 322 (1995) 307.
[15] A.A. Schmidt, H. Eggers, K. Herwig, R. Anton, Surf. Sci. 349 (1996) 301.
[16] R. Anton, A.A. Schmidt, Surf. Sci. 357-358 (1996) 835.
[17] J.A. Foro, S.J. Hearne, J.A. Hunter, P. Kotula, E. Chason, S.C. Seel, C.V. Thompson, J. Appl. Phys. 89 (2001) 4886.
[18] C. Friesen, C.V. Thompson, Phys. Rev. Lett. 89 (2002) 126103.
[19] C. Friesen, S.C. Seel, C.V. Thompson, J. Appl. Phys. 95 (2004) 1011.
[20] T.T. Bardin, J.C. Pronko, R.C. Budhan, et al., Thin Solid Films 165 (1988) 243.
[21] C.A. Neugebauer, in: L.I. Maissel, R. Glang (Eds.), Condensation, nucleation, and growth of thin films, Handbook of thin film technology Chapter 8, McGraw-Hill, N.Y., 1983.
[22] F. Spaepen, Acta Mater. 48 (2000) 31.
[23] D.J. Taylor, J.P. Cronin, L.F. Allard Jr, D.P. Birnie III, Chem. Mater. 8 (1996) 1396.
[24] M. Arai, S. Hayashi, K. Yamamoto, S.S. Kim, Solid State Commun. 75 (1990) 613.
[25] S. Hayashi, H. Sugano, H. Arai, K. Yamamoto, J. Phys. Soc. Jpn. 61 (1992) 916.
[26] A.G. Souza Filho, P.T.C. Freire, O. Pilla, A.P. Ayala, J. Mendes Filho, F.E.A. Melo, V.N. Freire, V. Lemos, Phys. Rev. 62 (2000) 3699.
[27] D. Briggs, M.P. Seach (Eds.), Practical surface analysis by Auger and X-ray photoelectron spectroscopy, MIR, Moscow, 1987, 600 pp. (in Russian).
[28] A. Al Mohammad, M. Gillet, Thin Solid Fims 408 (2002) 302.

Reprinted from Elsevier B.V.
Sensors and Actuators B: Chemical, 126 (2007) 573 - 578
Ozone monitoring by micro-machined sensors with WO_3 sensing films
S. Vallejos, V. Khatko, K. Aguir, K.A. Ngo, J. Calderer, I. Gràcia, C. Cané,
E. Llobet, X. Correig

ELSEVIER

Available online at www.sciencedirect.com
ScienceDirect

Sensors and Actuators B 126 (2007) 573–578

SENSORS AND ACTUATORS B CHEMICAL
www.elsevier.com/locate/snb

Ozone monitoring by micro-machined sensors with WO_3 sensing films

S. Vallejos [a], V. Khatko [a,*], K. Aguir [b], K.A. Ngo [b], J. Calderer [c], I. Gràcia [d], C. Cané [d], E. Llobet [a], X. Correig [a]

[a] *Universitat Rovira i Virgili, Països Catalans 26, 43007 Tarragona, Spain*
[b] *L2MP-UMR CNRS, FST Saint Jérôme, Université Paul Cézanne, Marseille, France*
[c] *Universitat Politècnica de Catalunya, Campus Nord 08034 Barcelona, Spain*
[d] *National Center of Microelectronics, 08193 Bellaterra-Barcelona, Spain*

Received 22 December 2006; received in revised form 4 April 2007; accepted 5 April 2007
Available online 13 April 2007

Abstract

Tungsten trioxide sensing films were deposited by rf sputtering onto silicon micro-machined substrates. The sensor substrate consisted of four-element integrated micro-hotplate arrays constructed using micro-systems technology. The sensing films were deposited using two sputtering technologies. The first one was a standard deposition without interruption of film deposition process. The second one included three interruptions of the process. It is shown that the sensor response to ozone is enhanced by the use of the second approach. Moreover, the features of sensor response to ozone demonstrate that fast responses and good sensor stability at low ozone concentrations are achieved using the micro-sensors.
© 2007 Elsevier B.V. All rights reserved.

Keywords: Micro-machined sensor; Response to ozone; Deposition with interruptions

1. Introduction

In the last decade, tungsten trioxide has been used as one of the most attractive and promising materials for semiconductor gas sensors. The main advantage of this wide band-gap n-type semiconductor certainly lies on its sensitivity to various air pollutants; for instance, NO_x [1–3], O_3 [4,5], H_2S, and SO_2 [6].

Ozone (O_3) is one of the gases that are naturally present in our atmosphere due to the interaction of sunlight with certain chemicals emitted to the environment (e.g., automobile emissions and chemical emissions of industrial plants). The negative role of ozone in the atmosphere which we breathe is to reach concentrations that can be harmful to our health. Severe exposure to this gas can cause problems such as inflammation and congestion of the respiratory tract [7]. Thus, harmful levels of ozone can be produced by the interaction of sunlight with certain chemicals emitted to the environment. These harmful concentrations of ozone in the atmosphere are often accompanied by high concentrations of other pollutants, including nitrogen dioxide, fine particles, and hydrocarbons. The international standards in the areas of safety and health recommend that the average of ozone concentration in the air should not exceed values of 0.05–0.10 ppm [8]. For this reason, monitoring pure ozone in the atmosphere or its mixtures with other chemicals is a very important task.

An ozone measuring device based on metal oxide semiconductor sensors shows a lot of potential as compared with conventional ozone measuring instruments [4,9]. The main advantage of solid-state sensors lies on their inexpensive production and portability. Metal oxides such as WO_3 [4,5], In_2O_3 [10,11] and SnO_2 [12] have been used for detecting ozone. However, among the materials mentioned before, WO_3 shows better sensitivity and selectivity to ozone at concentrations for atmospheric monitoring than other materials. Moreover, humidity interference, which has a strong effect in SnO_2-based gas sensors is moderate in WO_3 [4,13] sensors. In this work, we analyzed the experimental sensing features of WO_3 micro-machined sensors deposited both with and without interruptions in order to find the optimal parameters for their good performance in the detection of ozone. These results are important for evaluating the potential of our active layer deposited

* Corresponding author. Tel.: +34 977558653; fax: +34 977559605.
E-mail address: vkhatko@urv.cat (V. Khatko).

0925-4005/$ – see front matter © 2007 Elsevier B.V. All rights reserved.
doi:10.1016/j.snb.2007.04.012

ISBN:978-84-691-9748-6 /DL:T-1249

with interruptions in the area of atmospheric pollutant monitoring.

2. Experimental

2.1. Micro-machined substrate

The sensor substrates consisted of four-element integrated micro-hotplate arrays constructed using micro-systems technology. The devices were fabricated on double-side polished p-type ⟨1 0 0⟩ Si substrates with a 300 μm thickness. Thus, each chip had four membranes of 1 mm × 1 mm, the membranes consisted of a 0.3 μm thick Si_3N_4 layer grown by LPCVD, a $POCl_3$-doped polysilicon heating meander and sputtered interdigited Pt electrodes. The electrodes had different spacing between fingers. Two of the four micro-sensors had a 50 μm gap and the other two had a 100 μm gap. The electrode area in all cases was 400 μm × 400 μm. The layout of the sensor arrays is presented in Fig. 1. More detailed information about substrate fabrication is presented in Ref. [14].

2.2. Thin film deposition

An ESM100 Edwards sputtering system was used for depositing of tungsten oxide gas sensing layers. The sputtering atmosphere consisted of Ar–O_2 mixed gas with an Ar:O_2 flow ratio of 1:1. The pressure in the deposition chamber during sputtering was 5×10^{-3} mbar. A tungsten target of 99.95% purity was used. The radio frequency sputtering power was 100 W and the distance between the target and substrate holder was up to 7 cm. The sensing films were deposited onto silicon micro-machined substrates by reactive rf magnetron sputtering using two sputtering technologies. The first one was a standard deposition without interruption of film deposition process (S_R). The second one included three interruptions of the standard deposition process (S_A) [15]. A shutter was used to carry out the interruptions. The interruption time was up to 1.5 min. The use of this last procedure caused a reduction of thin film grain size from 24 to 17 nm [16]. The actual deposition time was 2 h in both cases. Then, the active layer area was defined using a lift-off process. These deposition conditions allowed obtaining WO_3 films with a thickness up to 0.25–0.27 μm. After that, the silicon micro-machined substrates and sensing films were annealed at 400 °C during 2 h in ambient atmosphere. Finally, the four-element gas sensor micro-arrays were ready for backside etching, dicing and packaging in a standard TO-8 package.

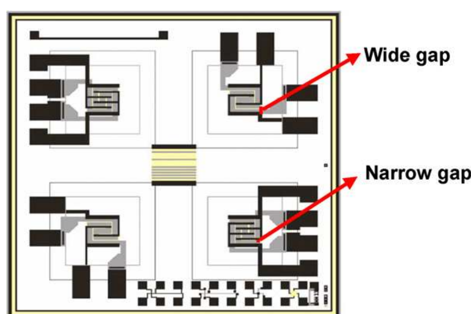

Fig. 1. Layout of the sensor micro-system. The four-element integrated micro-hotplate arrays are represented. Two micro-sensors have electrodes with a 100 μm gap (wide) and the other two have a 50 μm electrode gap (narrow).

2.3. XRD characterization

X-ray diffraction (XRD) measurements were made using a Siemens D5000 diffractometer (Bragg–Brentano parafocusing geometry and vertical θ–θ goniometer) fitted with a curved graphite diffracted-beam monochromator, a Soller slit, a 0.2 mm receiving slit and a scintillation counter as a detector. The angular range was between 19° and 70° for 2θ. Data were collected with an angular step of 0.02°, 6 s per step and sample rotation. Cu K_α radiation was obtained from a Cu X-ray tube operated at 40 kV and 30 mA.

Fig. 2 shows the X-ray diffractograms of WO_3 thin films from $2\theta = 20.0°$ to 38.0°, where important differences can be observed. The XRD data showed that the structure of as-deposited WO_3 films is amorphous. After annealing at 400 °C one monoclinic phase is present in the thin film that is described

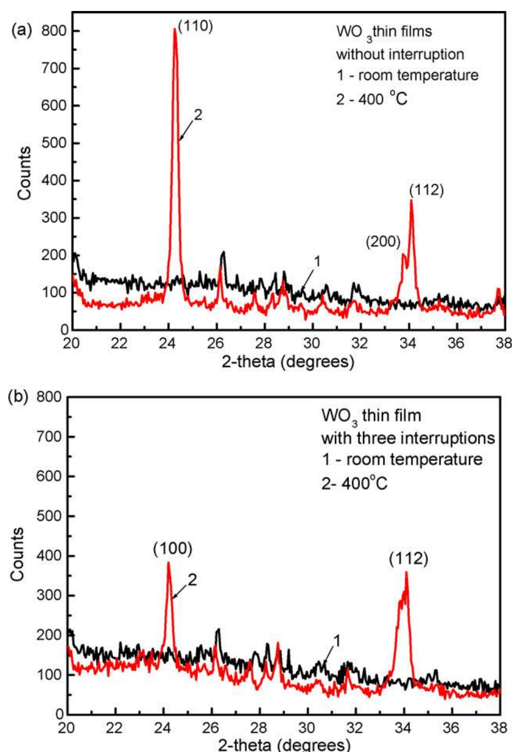

Fig. 2. X-ray diffractograms of WO_3 thin films deposited without (a) and with three interruptions (b). 1 and 2 are temperatures of WO_3 thin films as-prepared and annealed, respectively.

Table 1
Mean responses of the WO_3 micro-sensors to ozone as a function of the operating temperature

T (°C)	With interruptions S_A					Without interruptions S_R				
Electrode gap: 100 μm										
	0.1	0.2	0.4	0.6	0.8	0.1	0.2	0.4	0.6	0.8
450	1.22	1.69	2.81	4.10	4.26	1.01	1.03	1.07	1.08	1.18
350	1.34	1.85	3.01	4.21	4.48	1.10	1.24	1.49	1.73	1.84
250	1.03	1.08	1.12	1.17	1.39	1.05	1.09	1.19	1.27	1.35
Electrode gap: 50 μm										
	0.1	0.2	0.4	0.6	0.8	0.1	0.2	0.4	0.6	0.8
450	1.05	1.15	1.33	1.50	1.75	1.03	1.05	1.10	1.14	1.19
350	1.16	1.36	1.76	2.15	2.39	1.08	1.17	1.35	1.48	1.52
250	1.05	1.14	1.21	1.25	1.41	1.04	1.09	1.18	1.28	1.32

0.1, 0.2, 0.4, 0.6, 0.8 denotes the ozone concentration (ppm). S_A represent the sensors deposited with interruption regime and S_R the sensors deposited with basic regime. T is the operating temperature of the sensor.

with the space group Pc (ICDD card no. 87–2386, cell parameters: $a = 5.277$ Å, $b = 5.156$ Å, $c = 7.666$ Å, $\beta = 91.742°$). The XRD patterns contain (1 1 0), (2 0 0) and (1 1 2) reflections from the monoclinic phase (Pc). It can be seen that the process of thin film crystallization has a different activity for both types of WO_3 thin films. The crystallization in the thin film prepared with three interruptions of deposition (Fig. 2b) is slower than in the films prepared without interruptions (Fig. 2a).

2.4. Gas sensing characterization

To investigate their gas-sensing properties, the response of the sensors to ozone was measured using a continuous flow system where dry air was used as a reference gas [5]. Ozone was produced by an ozone generator made by UVP, Inc. [17]. The generator consists of a stable source of 185 nm radiation, a quartz reaction duct and radiation housing. This system provides a stable source of ozone for 100 h of operation. The different ozone concentrations were obtained in the range of 0.1–0.8 ppm in accordance with the calibration curves of the generator [17].

Two experimental sets were carried out. The first one was realized with a total flow of 200 cm^3/min. In this case the micro-machined sensors were exposed to the different ozone concentrations for 10 s (the sensor response reached approximately 90% of its maximum value during this period) and then ozone circulation was interrupted for 5 min before the next gas exposure started. These experimental conditions were selected to compare the response of micro-machined sensors prepared in this work with the response of gas sensors developed by other research group [5]. A second set of experiments was performed with a total flow of 100 cm^3/min. We tried to avoid the effect of ozone decomposition on the wall of the test chamber by the investigation of sensor response stability [13]. In this case the exposure time for each concentration was up to 5 min in order to reach a stable sensor response at a specific concentration. These measurements were carried out under isothermal conditions.

3. Results and discussion

Table 1 shows the mean responses of the WO_3 sensors fabricated to the different concentrations of ozone tested. The sensors were operated at different temperatures. The responses of four different types of sensors are reported in this table, which correspond to the films prepared with interruptions (S_A) or without them (S_R) and deposited onto narrow gap (50 μm) or wide gap (100 μm) electrodes. The sensing response was calculated by using the relationship: R_{gas}/R_{air}. The sensor response measure-

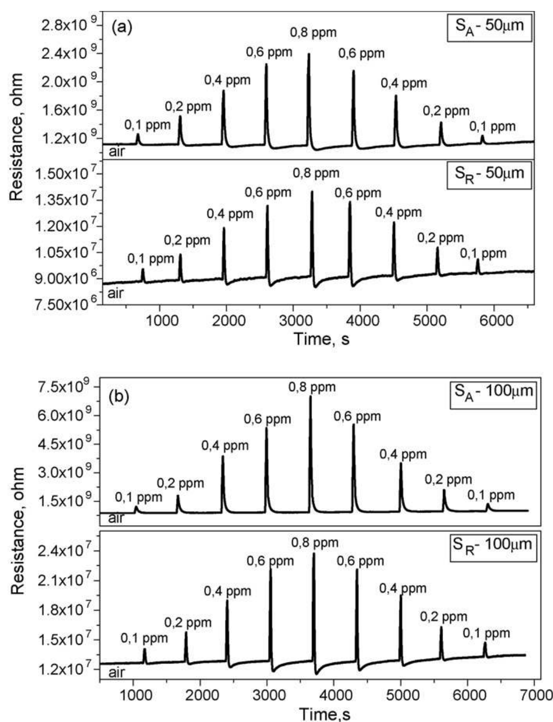

Fig. 3. Isothermal response of the two types of the sensing layers and electrode configurations to a series of ozone exposures at 350 °C. S_A-50 μm and S_A-100 μm represent the response of the WO_3 sensors deposited with interruptions (a). S_R-50 μm and S_R-100 μm represent the WO_3 sensors deposited with basic technology (b). The constant total flow during the measurement was 200 cm^3/min.

ments for each ozone concentration and operating temperature were carried out eight times. The S.E. of the mean response (S.E.M.) for the WO_3 sensors deposited with interruptions were below ±0.054 and ±0.771 in the case of the sensors with the electrode gap of 50 and 100 μm, respectively. These values were calculated using the responses obtained for each pair of two different sensors on the chip. The SEM was defined as follows:

$$\text{S.E.M.} = \frac{\text{S.D.}}{\sqrt{n}} \quad (1)$$

where S.D. denotes the standard deviation and $n = 8$.

From Table 1, it can be noted that two types of active layers and electrode configurations present the higher responses at the operating temperature of 350 °C. On the other hand, it is possible to see that the response of the sensors deposited with interruption is higher than that of the sensors deposited without interruptions. This effect is related to the grain size decrease in the metal oxide film, which is related to the fact that an "extra" interface is introduced into the body of the thin film at each interruption of the deposition process [15,16]. Grain size reduction in metal oxide films is one of the key factors to enhance the gas sensing properties of semiconductor layers [3,18]. The influence of grain size on the WO_3 film sensitivity to ozone was observed in Ref. [5] as well, where a change in the mean grain size from 100 to 60 nm (decreasing up to 40%) increased the response of the sensor by a factor of 5. In our case, the decrease of grain size from 24 to 17 nm (decreasing up to 30%) promoted an increase in sensor response by a factor of 2.43 (for 100 μm electrode gap) and 1.57 (for 50 μm electrode gap).

Fig. 3 presents the isothermal response of the micro-machined sensors to ozone at 350 °C, where the sensor response is maximum for all ozone concentrations measured and the two types of electrode configurations used. It can be seen that the response of the micro-machined sensors to ozone is completely reversible for the four types of sensors, as it was observed in previous studies for WO_3 sensing films [5]. Our results can be explained using a model of resistivity based on the existence of an accumulation or a depletion layer induced by the surrounding atmosphere which was developed in Ref. [19]. In accordance with this model, there is an optimal sensor operating temperature which provides the highest sensor response. In our case the maximal operating temperature is 350 °C. This temperature is higher than the temperature (250 °C) calculated in Ref. [19]. The differences in the optimal operating temperature could be linked with the differences in grain size and geometry of sensing layers between the WO_3 films deposited in our work and in Ref. [19].

A comparison of the sensor response trends obtained for the different types of electrodes and deposition technologies is represented in Fig. 4. The results show that the response of the films deposited both with and without interruptions is higher in

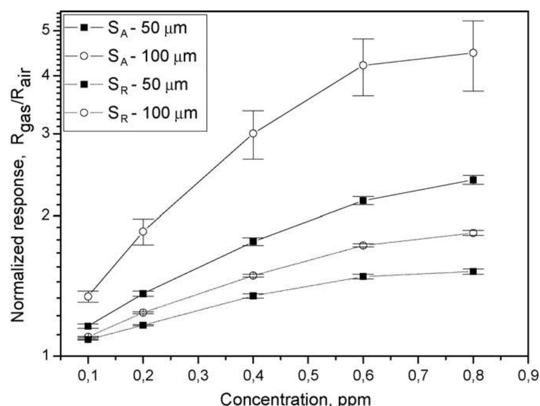

Fig. 4. Response of the sensors as a function of ozone concentration. S.E. of the measurements are presented.

the sensors with a 100 μm electrode gap. Basically, the electrode geometry produces a different sensor signal depending on how the electrodes are positioned within the porous sensor body. If the electrode geometry implies that a narrow gap exists between the fingers, the resistance change of the sensing layer in the presence of ozone involves the volume of sensing film that lies between two interdigited electrode fingers only. In the case of wide gap electrode geometry, the resistance changes involve the whole sensing film [13,20]. Fig. 5 presents a schematic illustration of this effect.

The S.E. for each type of sensor, the one for each pair of the similar sensors presented on the one micro-system chip and the one for the four similar sensors from two different chips were calculated. Eight measurements were used for each calculation. Measurements performed at the same flow rates and exposure time at an operating temperature of 350 °C were employed in these calculations. The calculation of the S.E. was done using Eq. (1). Fig. 6 presents a comparison of these S.E. We can notice that the sensors with a narrow electrode gap (50 μm) have better reproducibility than the sensors with a wide gap (100 μm).

During a second set of measurements the stability of the response when the sensors were exposed to ozone for 5 min was studied. Fig. 7 presents a normalized response of the sensors as a function of measurement time and ozone concentration. The sensor signal shows good stability and fast response at low ozone concentrations of 0.2 and 0.4 ppm. The signal has not sufficient stability at ozone concentrations of 0.8 ppm. This effect could be caused by the decomposition of ozone both on the wall of the measurement chamber and the active layer [13]. The response (τ_S) and recovery (τ_R) times of the sensors as a function of the operating temperature are presented in Fig. 8. The parame-

Fig. 5. Schematic illustrations of a cross section of the micro-sensor membrane for two fingers of the electrode. The current flow through the active layer is represented in dashed lines for the electrodes with narrow (a) and wide gap (b).

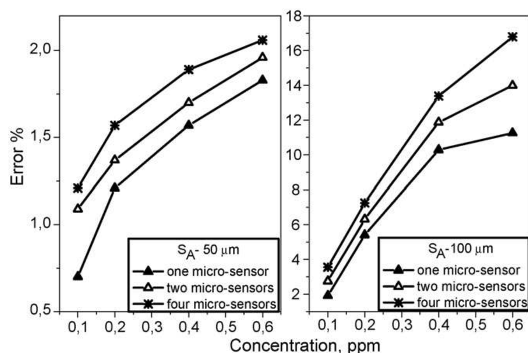

Fig. 6. S.E. of the measurements for the WO_3 sensors deposited with interruptions. The constant total flow was 200 cm^3/min. The filled triangles represent the S.E. of one micro-sensor from the sensor array. The open triangles represent the S.E. estimated for two micro-sensors with the same electrode geometry from the sensor array. The stars represent the S.E. estimated for four micro-sensors from two sensor arrays.

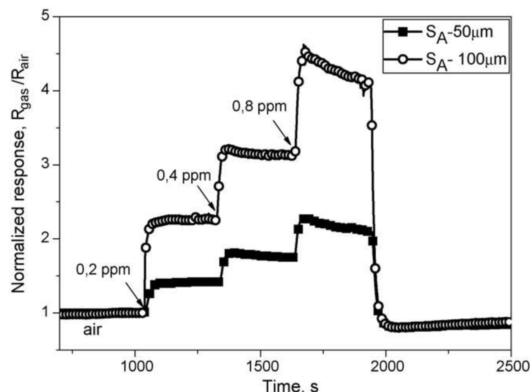

Fig. 7. Normalized sensor response to 0.2, 0.4 and 0.8 ppm of ozone. The time exposure of the sensors to ozone for each concentration was 5 min. Constant total flow during measurement was set 100 cm^3/min.

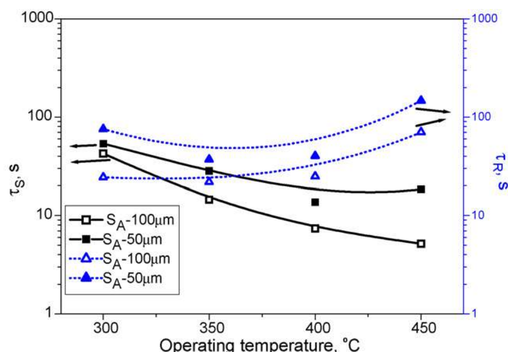

Fig. 8. Response time (τ_S) and recovery (τ_R) time of the WO_3 sensor response to 0.2 ppm of ozone.

ters were defined as the elapsed time from 10% to 90% of the response measured from the baseline resistance. It can be seen that the gas micro-sensors prepared with an electrode gap of 100 μm have the faster response and recovery.

The results of the study show the role of interruptions in the enhancement of the sensitivity to ozone. The reduction of the grain size and the increment of the number of free bonds on the sensing layer surface are the effects that characterize the sensing films deposited with interruptions [15,16]. The difference in the responses of the micro-sensors with two different electrode configurations is not very high for the sensing films that were deposited using standard technology in comparison with the films deposited with interruptions. Finally, the results obtained in this work show that the gas micro-sensors prepared using silicon micro-machined substrates show good potential for ozone monitoring.

4. Conclusions

Tungsten trioxide sensing films were deposited by rf sputtering onto silicon micro-machined substrates developed by CNM (Barcelona). Two regimes of the sensing film deposition without and with three interruptions were used. A clear enhancement of the sensor response to ozone was noticed for the WO_3 films deposited with interruptions in comparison with the ones deposited without interruptions. This effect is related to the decrease in grain size in the metal oxide films. The good stability, reversibility and reproducibility of the micro-sensors were observed in this study.

References

[1] Y.G. Choi, G. Sakai, K. Shimanoe, N. Yamazoe, Wet process-based fabrication of WO_3 thin film for NO_2 detection, Sens. Actuators B, Chem. 101 (2004) 107–111.
[2] S.H. Wang, T.C. Chou, C.C. Liu, Nano-crystalline tungsten oxide NO_2 sensor, Sens. Actuators B, Chem. 94 (2003) 343–351.
[3] J. Tamaki, A. Hayashi, Y. Yamamoto, M. Matsuoka, Detection of dilute nitrogen dioxide and thickness effect of tungsten oxide thin film sensors, Sens. Actuators B, Chem. 95 (2003) 111–115.
[4] S.R. Utembe, G.M. Hansford, M.G. Sanderson, R.A. Freshwater, K.F.E. Pratt, D.E. Williams, R.A. Cox, R.L. Jones, An ozone monitoring instrument based on the tungsten trioxide (WO_3) semiconductors, Sens. Actuators B, Chem. 114 (2006) 507–512.
[5] M. Gillet, K. Aguir, M. Bendahan, P. Mennini, Grain size effect in sputtered tungsten trioxide thin films on the sensitivity to ozone, Thin Solid Films 484 (2005) 358–363.
[6] M. Stankova, X. Vilanova, J. Calderer, E. Llobet, P. Ivanov, I. Gràcia, C. Cané, X. Correig, Detection of SO_2 and H_2S in CO_2 stream by means of WO_3-based micro-hotplate sensors, Sens. Actuators B, Chem. 102 (2004) 219–225.
[7] http://www.greenfacts.org/air-pollution/ozone-o3/index.htm.
[8] http://www.epa.gov/air/criteria.htm.
[9] http://www.ecosensors.com.
[10] G. Flagia, B. Allieri, E. Comini, L. El Depero, L. Sangaletti, G. Sberveglieri, Electrical and structural properties of RGTO-In_2O_3 sensors for ozone detection, Sens. Actuators B, Chem. 57 (1999) 188–191.
[11] G. Korotcenkov, A. Cerneavschi, V. Brinzari, A. Vasiliev, M. Ivanov, A. Cornet, J. Morante, A. Cabot, J. Arbiol, In_2O_3 films deposited by spray pyrolisis as a material for ozone gas sensors, Sens. Actuators B, Chem. 99 (2004) 297–303.

[12] G. Korotcenkov, I. Blinov, M. Ivanov, J.R. Stetter, Ozone sensors on the base of SnO_2 films deposited by spray pyrolisis, Sens. Actuators B, Chem. 120 (2007) 679–686.
[13] D.E. Williams, Semiconducting oxides as gas-sensitivite resistors, Sens. Actuators B, Chem. 57 (1999) 1–16.
[14] M. Stankova, X. Vilanova, J. Calderer, E. Llobet, J. Brezmes, I. Gràcia, C. Cané, X. Correig, Sensitivity and selectivity improvement of rf sputtered WO_3 microhotplate gas sensors, Sens. Actuators B, Chem. 113 (2006) 241–248.
[15] V. Khatko, J. Calderer, E. Llobet, X. Correig, New technology of metal oxide thin film preparation for chemical sensor application, Sens. Actuators B, Chem. 109 (2005) 128–134.
[16] V. Khatko, S. Vallejos, J. Calderer, E. Llobet, X. Vilanova, X. Correig, Gas sensing properties of WO_3 thin films deposited with interruptions, in: Proceedings of the 19th European Conference on Solid State Transducers, EUROSENSORS XIX, Barcelona, Spain, 2005, 11–14 September, p. TP20.
[17] http://uvp.com.
[18] G.-J. Li, X.-H. Zhang, S. Kawi, Relationships between sensitivity, catalytic activity, and surface areas of SnO_2 gas sensors, Sens. Actuators B, Chem. 60 (1999) 64–70.
[19] M. Bendahan, J. Guérin, R. Boulmani, K. Aguir, WO_3 sensor response according to operating temperature: experiment and modeling, Sens. Actuators B, Chem., in press.
[20] D.E. Williams, S.R. Aliwell, K.F.E. Pratt, D.J. Caruana, R.L. Jones, R.A. Cox, G.M. Hansford, J. Halsall, Modeling the response of a tungsten oxide semiconductor as gas sensor for the measurement of ozone, Meas. Sci. Technol. 13 (2002) 923–931.

Biographies

Stella Vallejos was graduated in electrical engineering (2002) and electronic engineering (2003) from the Universidad Técnica de Oruro, Bolivia. She is currently a PhD student in the Electronic Engineering Department at the Universitat Rovira i Virgili, Spain. Her main areas of interest are fabrication and characterization of solid state gas sensors.

Viacheslav Khatko graduated in nuclear physics from the Belarusian State University (Minsk, Belarus) in 1971. He received his PhD in materials science in 1986 and Dr.Sc. in solid state electronics in 2001. In 1975–2003 he worked at the Physical Technical Institute of National Academy of Sciences of Belarus, Minsk, as a Researcher, Head of the Laboratory of Electronic Engineering Materials, head of the Thin Film Materials Department and then as Principal Investigator of the same institute. He was Ford SABIT Intern and Ford Visiting Scientist in 1998 and 1999, respectively. From April 2003 he is Ramón y Cajal professor in the Electronic Engineering Department of the Universitat Rovira i Virgili (Tarragona, Spain). His current research interests include the development and application of semiconductor thin and thick film gas sensors.

Khalifa Aguir is a professor at Paul Cezanne Aix-Marseille University (France). He was awarded his Doctorat d'Etat en Sciences degree from the Paul Sabatier University Toulouse (France) in 1987. He is currently head of Sensors Group at Laboratoire Materiaux & Microelectronique (L2MP–CNRS) Marseille (France). His scientific interests are thin films preparation and characterization for micro-systems. Since 1998, he is interested in gas micro-sensors and multisensors, electronic noses, selectivity by signal treatment strategies and noise spectroscopy. He currently works on WO_3 gas sensors, flexible polymeric sensors, and modelling of sensor responses.

Kieu An Ngo was graduated in electronic engineering from the Saint Etienne University in 2002 and he obtained his PhD degree in micro-electronic from the Paul Cézanne University (France) in 2006. His work focuses on the selectivity enhancement of gas sensor by using sensor arrays, temperature programming and multivariate analysis methods.

Josep Calderer received his degree in Physics in 1973 and the PhD in 1981 in the University of Barcelona. He has been working in technology and characterization of photovoltaic solar cells, heterojunction bipolar transistors and silicon-based integrated optical sensors. At present he is a staff member of the Department of Electronic Engineering (DEE) of the Polytechnic University of Catalonia (UPC, Barcelona). His main research activity focuses on resistive gas sensors using metal oxide compounds.

Isabel Gràcia received the PhD degree in physics in 1993 from the Autonomous University of Barcelona, Spain, working on chemical sensors. Currently she is a full time senior researcher in the micro-nano systems department of the National Microelectronics Center (Barcelona, Spain). Her work is focused on gas sensing technologies and MEMS reliability.

Carles Cané received the PhD in 1989. Since 1990 he is a full time senior researcher at the National Microelectronics Center (Barcelona, Spain). He works on the development of CMOS technologies, mechanical and chemical sensors micro-systems. He is a member of the technical committee of EURIMUS-EUREKA programme since 1999. Over the last years he has been a co-ordinator of several R&D projects, both at national and international level in the MST field. He has performed management activities as well, as head of the Microsystems and Silicon Technologies Department of CNM and as vice-director of CNM Barcelona site. He is the co-ordinator of the GoodFood Integrated Project from the 6th Framework Programme (FP6-IST-508774-IP).

Eduard Llobet was graduated in telecommunication engineering from the Universitat Politècnica de Catalunya (UPC), (Barcelona, Spain) in 1991, and received his PhD in 1997 from the same university. During 1998, he was a visiting fellow at the School of Engineering, University of Warwick (UK). He is currently an associate professor in the Electronic Engineering Department at the Universitat Rovira i Virgili (Tarragona, Spain). His main areas of interest are in the fabrication, and modelling, of semiconductor chemical sensors and in the application of intelligent systems to complex odour analysis.

Xavier Correig was graduated in telecommunication engineering from the Universitat Politècnica de Catalunya (UPC), (Barcelona, Spain) in 1984, and received his PhD in 1988 from the same university. He is a full professor of Electronic Technology in the Electronic Engineering Department at the Universitat Rovira i Virgili (Tarragona, Spain). His research interests include heterojunction semiconductor devices and solid-state gas sensors.

ISBN:978-84-691-9748-6 /DL:T-1249

IV

Reprinted from Elsevier B.V.
Sensors and Actuators B: Chemical, in press

Micro-machined gas sensors selective to oxidizing gases

S. Vallejos, V. Khatko, J. Calderer, I. Gràcia, C. Cané, E. Llobet, X. Correig

Accepted Manuscript

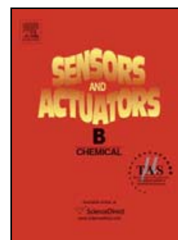

Title: Micro-machined WO_3-based sensors selective to oxidizing gases

Authors: S. Vallejos, V. Khatko, J. Calderer, I. Gracia, C. Cané, E. Llobet, X. Correig

PII: S0925-4005(08)00066-X
DOI: doi:10.1016/j.snb.2008.01.044
Reference: SNB 10623

To appear in: *Sensors and Actuators B*

Received date: 26-7-2007
Revised date: 11-1-2008
Accepted date: 16-1-2008

Please cite this article as: S. Vallejos, V. Khatko, J. Calderer, I. Gracia, C. Cané, E. Llobet, X. Correig, Micro-machined WO_3-based sensors selective to oxidizing gases, *Sensors and Actuators B: Chemical* (2007), doi:10.1016/j.snb.2008.01.044

This is a PDF file of an unedited manuscript that has been accepted for publication. As a service to our customers we are providing this early version of the manuscript. The manuscript will undergo copyediting, typesetting, and review of the resulting proof before it is published in its final form. Please note that during the production process errors may be discovered which could affect the content, and all legal disclaimers that apply to the journal pertain.

ACCEPTED MANUSCRIPT

Micro-machined WO_3-based sensors selective to oxidizing gases

S. Vallejos[a], V. Khatko*[a], J. Calderer[b], I. Gracia[c], C. Cané[c], E. Llobet[a], X. Correig[a]

[a]Departament d'Enginyeria Electronica, Universitat Rovira i Virgili,

Campus Sescelades 43007 Tarragona, Spain

[b]Universitat Politecnica de Catalunya, Departament d'Enginyeria Electronica,

Campus Nord 08034 Barcelona, Spain

[c]Centro Nacional de Microelectronica

Bellaterra 08193 Barcelona, Spain

Abstract

Tungsten trioxide sensing films were deposited with interruptions by rf sputtering onto silicon micro-machined substrates. The use of a deposition process with several interruptions allowed decreasing grain size in the WO_3 films. The decrease in grain size is a result of the thin film formation features. It is shown that the gas sensing properties observed for the WO_3 films deposited with three interruptions are highly enhanced to oxidizing gases in comparison with those sensing films prepared without interruptions. For instance, the response of the fabricated micro-sensors to nitrogen dioxide and ozone is up to 4 times higher than that of the micro-sensors prepared using the basic technology.

Keywords: Micro-machined gas sensor, air pollutant oxidizing gases, selectivity

*Corresponding author. Tel.: +34 977558653; fax: +34 977559605;

E-mail address: vkhatko@urv.cat; viacheslav.khatko@gmail.com (V. Khatko).

Accepted Manuscript

ISBN:978-84-691-9748-6 /DL:T-1249
ACCEPTED MANUSCRIPT

1. Introduction

Poor quality of air has negative effects on the environment in which we live. The air which we daily breathe is continuously polluted by activities such as driving cars and trucks; burning coal, oil, and other fossil fuels; and manufacturing chemicals. According to the Environment Protection Agency of United States (EPA), the most important air pollutants are nitrogen dioxide (NO_2), ozone (O_3), sulfur dioxide (SO_2), particulate matter (PM), carbon monoxide (CO), and lead (Pb). Generally, NO_2, CO, SO_2, and Pb are emitted directly from a variety of sources. Ozone is not directly emitted, but is formed when oxides of nitrogen (NO_x) and volatile organic compounds (VOCs) react in the presence of sunlight. On the other hand, PM can be directly emitted, or it can be formed when emissions of NO_x, sulfur oxides (SO_x), ammonia (NH_3), organic compounds, and other gases react in the atmosphere [1]. Therefore, there exists an interest in the detection of these components in the environment.

Metal oxide gas sensors represent a good option for air pollution control because of their portability and cheap production. The major problem is that they have poor selectivity, Although, this disadvantage can be partially solved by specific surface additives [2], the use of filters [3], catalysts and promoters [4], or temperature controls [5]. The performance of the sensing materials still strongly depends on their structural and morphological properties. It is well known that grain size reduction in metal oxide films has a substantial impact on the sensor performance [6, 7]. In our previous work [8-10], we have established that metal oxide thin films with small grain size can be created using a special regime of thin film deposition by rf sputtering of pure metal. This regime implies the deposition of thin films with one or several interruptions during the deposition process. Using this technology resulted in a grain size reduction from 24 nm to 14 nm in the WO_3 thin films deposited with interruptions.

WO_3 films have been used as one of the most attractive and promising materials for semiconductor gas sensors. The main advantage of this wide band gap n-type semiconductor

Accepted Manuscript

ISBN:978-84-691-9748-6 /DL:T-1249
ACCEPTED MANUSCRIPT

is related to its sensitivity to various air pollutants; for instance, NO_x [11-13], O_3 [14, 15], NH_3 [16] and SO_2 [17]. Basically, the probability of gas adsorption in the WO_3 film depends on the nature of gaseous species, its concentration (C_{gas}) and operating temperature (T_{op}).

In this work, we studied the response and selectivity of silicon micro-machined sensors based on WO_3 sensing films deposited with interruptions to some important oxidizing and reducing air pollutant gases. The results obtained were compared with those published earlier.

2. Experimental

The experiments included fabrication of gas micro-sensors and characterization of their gas sensing properties. The micro-sensor fabrication consisted in two steps: (1) preparation of micro-machined substrate arrays and (2) deposition of WO_3 thin films by rf sputtering.

2.1. Micro-machined substrate arrays

The sensor substrate consisted of four-element integrated micro-hotplate arrays constructed using microsystem technology. The devices were fabricated on double-side polished p-type <100> Si substrates with a 300 µm thickness. Each chip had four membranes of 1 mm × 1 mm. The membranes (Fig. 1a) consisted of a 0.3 µm thick Si_3N_4 layer grown by LPCVD, a $POCl_3$-doped polysilicon heating meander and sputtered interdigitated Pt electrodes. The electrodes had different spacing between fingers: two of the four micro-sensors had a 100 µm gap (wide electrode gap) and the other two had a 50 µm gap (narrow electrode gap). The electrode area in all cases was 400 µm × 400 µm. The layout of the sensor

Accepted Manuscript

ISBN:978-84-691-9748-6 /DL:T-1249
ACCEPTED MANUSCRIPT

array is presented in Fig. 1b. More detailed information about substrate fabrication is described in Ref. [2].

2.2. WO_3 thin film deposition

An ESM100 Edwards sputtering system was used for deposition of tungsten trioxide sensing layers. The sputtering atmosphere consisted of Ar-O_2 mixed gas with an Ar : O_2 flow ratio of 1 : 1. The pressure in the deposition chamber during sputtering was 5×10^{-3} mbar. A tungsten target of 99.95% purity was used. The radio frequency sputtering power was 100 W and the distance between the target and the substrate holder was up to 7 cm. The sensing films were deposited onto silicon micro-machined substrates by reactive rf magnetron sputtering using the interruptions regime. Three interruptions, each of 1.5 min, were performed during deposition. The actual deposition time was 2 h. Then, the active layer area was defined using a lift-off process. These deposition conditions allowed obtaining WO_3 films with a thickness up to 0.25 - 0.27 μm [9]. After that, the silicon micro-machined substrates with the sensing films were annealed at 400º C during 2 h in ambient atmosphere. The XRD characterization showed that after annealing one WO_3 monoclinic phase exists in the film, which is described with the space group *Pc* (ICDD card no. 87- 2386, cell parameters: a= 5.277 Ǻ, b= 5.156 Ǻ, c=7.666 Ǻ, β=91.742º) [9]. Finally, the 4 - element micro-sensors were packaged in standard TO – 8 packages.

2.3. Gas sensing characterization

The response of the WO_3 micro-sensors to various gases was analyzed at three operating temperatures (250 ºC, 350 ºC, 450 ºC). Target gases and their concentrations used in the experiments are presented in Table 1. In order to obtain the desired target gas concentration, mixtures of pure air and pollutant gases were performed using a mass flow

Accepted Manuscript

ISBN:978-84-691-9748-6 /DL:T-1249
ACCEPTED MANUSCRIPT

system consists of a PC and computer-controlled mass flow controllers (Bronkhorst hi-tech 7.03.241) having a scale resolution about 1%. For the experiments, commercially available calibrated gas bottles were employed. The mass flow controllers were calibrated with synthetic air. This did not lead to significant errors, since the experiments were performed with target gases that were highly diluted in air. Ozone (O_3) was produced by an ozone generator made by UVP, Inc. and its concentrations were adjusted in accordance with the calibration curves of the generator [18]. The generator consisted of a stable source of 185 nm radiation, a quartz reaction duct and radiation housing that produced ozone from oxygen. Two devices with four micro-sensors each were placed in a continuous flow test chamber. The volume of the test chamber was 36 cm^3. The total flow rate was adjusted to 100 cm^3/min.

The sensor characterization was achieved by dc resistance measurements. The measuring electronic system consisted of an electrometer from Keathley Instruments Inc. (model 6517A) with a data acquisition card (model 6522) that provided ten channels for measuring the resistance of active layers. Measurements of active layer resistance for each operating temperature and target gases at different concentrations were replicated 5 times in order to determine the repeatability of the sensor response. This resistance in air was varied from180-400 MOhm at 250°C to 30-70 MOhm at 450°C and depended on the interdigitated electrode configuration. The sensors were exposed to each gas concentration for 5 min after that air was purged for 30 min. The sensor response was defined as $S= R_{gas}/R_{air}$ in the case of oxidizing gases and $S= R_{air}/R_{gas}$ in the case of reducing gases, where R_{air} is the sensor resistance in air (stationary state) and R_{gas} represents the sensor resistance after 5 min of gas exposure.

3. Results and discussion

Accepted Manuscript

ISBN:978-84-691-9748-6 /DL:T-1249
ACCEPTED MANUSCRIPT

Figure 2 shows the baseline normalized responses of WO_3 micro-sensors with two different electrode geometries to various oxidizing (ozone O_3, nitrogen dioxide NO_2, nitrogen oxide NO_x) and reducing (ammonia NH_3, carbon monoxide CO, ethanol C_2H_6O) target gases. The responses of the sensors to reducing gases were not as high as those observed to oxidizing gases. Table 2 shows the maximum responses of the WO_3 sensors to O_3, NO_2, NO_x, NH_3, CO and C_2H_6O at various operating temperatures and gas concentrations. In accordance with the model of resistivity presented in Ref. [19], there is an optimal sensor operating temperature which provides the highest sensor response. Our results show that the optimal operating temperature changes as a function of the target gas and its concentration. It can be seen that the higher sensor responses to O_3, NO_x, and C_2H_6O were obtained at 250 ºC. In the case of high NO_2 concentrations, WO_3 sensors showed higher responses at 450ºC. The maximal values of the responses to NH_3 and CO were obtained at 350ºC. The results presented in Fig. 2 and Table 2 show that the response of the films deposited both with and without interruptions is higher in the sensors with a 100 μm electrode gap. The influence of electrode geometry on sensor response was discussed in Ref. [20].

The sensors show an enhanced sensitivity to oxidizing gases as compared to sensors deposited without interruptions (see Fig. 3) and low cross-sensitivity to reducing gases (see Fig. 2). The sensitivity of the WO_3 thin films deposited with interruptions to O_3 and NO_2 is higher than that obtained for the WO_3 thin films deposited with basic technology. This result is related to the decrease of grain size in tungsten oxide films deposited with interruptions [9, 10]. Decreasing the grain size from 24 nm to 15 nm promoted an increase in sensor response to O_3 by a factor of 2.43 to 0.8 ppm of ozone [20]. The response of the fabricated micro-sensors to 1 ppm of NO_2 was up to 4 times higher than that of those prepared using basic technology. Fig. 3 presents these results. For comparison, the experimental data obtained in Refs. [2] and [20] are presented in Fig. 3 as well. Earlier it was shown that decreasing the

ACCEPTED MANUSCRIPT
ISBN:978-84-691-9748-6 /DL:T-1249

grain size from 100 nm to 60 nm raised the sensor response to O_3 by a factor of 5 [15]. Similar results were presented in Ref. [21] where decreasing the grain size from 33 nm to 25 nm increased the sensor response to NO_2 by a factor of 3 approximately.

Figure 4 shows the response time of the micro-sensors for three oxidizing gases. The response time was defined as the time elapsed from 10% to 90% of the response measured from the baseline resistance. It can be seen that the response to O_3, NO_2 and NO_x is faster between 350 ºC and 450ºC.

Figure 5 shows the sensor response spaces obtained combining the responses of two micro-sensors with wide and narrow gap electrode configurations. X-axis and y-axis of the sensor response space represent the response of micro-sensors with wide and narrow electrode configurations, respectively. The sensor response spaces contain the sensor responses to various target gases of different concentrations (each measurement was replicated 5 times). The responses were obtained at operating temperatures of 250ºC (Fig. 5a), 350ºC (Fig. 5b) and 450ºC (Fig. 5c). It can be noted that the repeatability of the micro-sensors with a narrow electrode gap is higher (standard error up to 1.8 %) than that achieved by the micro-sensors with a wide electrode gap (standard error up to 14 %). Moreover, in the sensor space it can be seen that the measurements show a tendency to cluster together according to the species and their concentration. This behaviour is clear at the operating temperature of 350 ºC where a minimal dispersion of the responses to O_3 (0.2 ppm, 0.4 ppm, 0.8 ppm), NO_2 (0.5 ppm, 1 ppm, 2 ppm) and NO_x (1 ppm, 2 ppm, 3 ppm) is observed. On the contrary, the dispersions of the responses to the gases are worse at other temperatures. At 450 ºC the dispersions are higher, especially for NO_x and O_3. In order to improve the selectivity of our sensors to oxidizing gases the pattern recognitions techniques could be applied as well [22].

So, the results obtained show that a decrease in grain size of the WO_3-based sensing layer results in an increased sensitivity and selectivity to oxidizing gases. In a previous work

ISBN:978-84-691-9748-6 /DL:T-1249
ACCEPTED MANUSCRIPT

the dependence of specific adsorptivity on the degree of dispersion of the crystalline adsorbent has been investigated in detail [23]. It is shown that the effect happens when the separate crystals, in our case the WO_3 grain size, are small, i.e., B/S ≤ 1000-10 nm, where S is the surface area, B the volume of the crystal. In this case the position of the Fermi level at the crystal surface, and hence the adsorptivity, depend on B/S. The surface defects of the crystal take part in the adsorption process as adsorption centres as well. They are also localization centres for free surface valences. The charge of the crystal surface influences on the position of the Fermi level at the crystal surface and on the adsorption properties with respect to an oxidizing gas or to a reducing gas [23]. It was noted that WO_3 thin films are excellent NO_x sensing layers because the W ions have different oxidation states (W^{6+}, W^{5+}) enhancing the oxidizing power of NO_x molecules on the surface of WO_3 thin films [24]. Actually the study of the reconstruction of the WO_3 crystal surface, which dealt with a WO_2 surface layer with half a monolayer of oxygen ions, showed that electrical neutrality was maintained by the tungsten ions reduced from $W^{6+}$to W^{5+} with a localized $5d^1$ electron configuration [25, 26]. In our case (B/S ~ 15 nm) a decrease in grain size in the WO_3-based sensing layer of the micro-sensor increases the surface area of the grain, and hence the number of reduced ions (adsorption centres) on the grain surface. It could be suggested that sensitivity and selectivity to the oxidizing gases will increase in this case. Certainly, this suggestion demands a more detail analysis (e.g. an investigation of the change of the Fermi level position on the surface of WO_3 grain by the action of oxidizing or reducing gases). This analysis will be performed in the near future.

4. Conclusions

The WO_3 micro-sensors prepared using the deposition of metal oxide sensing layers with interruptions are sensitive and selective to oxidizing gases. This effect is related to a

Accepted Manuscript

ISBN:978-84-691-9748-6 /DL:T-1249
ACCEPTED MANUSCRIPT

decrease in grain size of the metal oxide films. The decreased grain size is a result of the features of thin film formation. The introduction of "extra" interfaces into the thin film body during interruptions influences the process of WO_3 crystallisation and film surface morphology. Decreasing the grain size in the WO_3-based sensing layer of the micro-sensor increases the surface area of the grain, and hence the number of adsorption centres to oxidizing gases.

Acknowledgements

This work was funded in part by the Spanish Commission for Science and Technology (CICYT) under grant no. TIC2006-03671/MIC. V. K. acknowledges the Ramon y Cajal Fellowship from the Spanish Ministerio de Educación y Ciencia.

Accepted Manuscript

ACCEPTED MANUSCRIPT
ISBN:978-84-691-9748-6 /DL:T-1249

References

[1] www.epa.gov/air/criteria.html

[2] M. Stankova, X. Vilanova, J. Calderer, E. Llobet, J. Brezmes, I. Gràcia, C. Cané, X. Correig, Sensitivity and selectivity improvement of rf sputtered WO_3 microhotplate gas sensors, Sens. Actuators B, Chem., 113 (2006) 241-248.

[3] J. P. Viricelle, A. Pauly, L. Mazet, J. Brunet, M. Bouvet, C. Varenne, C. Pijolat, Selectivity improvement of semi-conducting gas sensors by selective filter for atmospheric pollutants detection, Mater. Sci. Eng. C, 26 (2006) 186-195

[4] S.R. Morrison, Selectivity in semiconductor gas sensors, Sens. Actuators B, Chem., 12 (1987) 425-440

[5] R. Ionescu, E. Llobet, Wavelet transform-base fast feature extraction from temperature modulated semiconductor gas sensors, Sens. Actuators B, Chem., 81 (2002) 289–295.

[6] N. Yamazoe, G. Sakai, K. Shimanoe, Oxide semiconductor gas sensor, Catal. Surv. Asia, 7 (2003) 63-75.

[7] M. E. Franke, T. J. Koplin, U. Simon, Metal and metal oxide nanoparticles in chemiresistors: Does the nanoscale matter?, Small, 2 (2006) 36-50

[8] V. Khatko, J. Calderer, E. Llobet, X. Correig, New technology of metal oxide thin film preparation for chemical sensor application, Sens. Actuators 109 (2005) 128-134.

[9] V. Khatko, S. Vallejos, J. Calderer, E. Llobet, X. Vilanova, X. Correig, Gas sensing properties of WO_3 thin films deposited by RF sputtering, Sens. Actuators B, Chem., 126 (2007) 400-405.

[10] V. Khatko, J. Calderer, S. Vallejos, E. Llobet, X. Correig, Technology of metal oxide thin film deposition with interruptions, Surf. Coat. Tech., 202 (2007) 453-459.

Accepted Manuscript

ACCEPTED MANUSCRIPT

[11] Y.G. Choi, G. Sakai, K. Shimanoe, N. Yamazoe, Wet process-based fabrication of WO_3 thin film for NO_2 detection, Sens. Actuators B, Chem., 101 (2004) 107-111.

[12] S.H. Wang, T.C. Chou, C.C. Liu, Nano-crystalline tungsten oxide NO_2 sensor, Sens. Actuators B, Chem., 94 (2003) 343-351.

[13] J. Tamaki, A. Hayashi, Y. Yamamoto, M. Matsuoka, Detection of dilute nitrogen dioxide and thickness effect of tungsten oxide thin film sensors, Sens. Actuators B, Chem., 95 (2003) 111-115.

[14] S.R. Utembe, G.M. Hansford, M.G. Sanderson, R.A. Freshwater, K.F.E. Pratt, D.E. Williams, R.A. Cox, R. L. Jones, An ozone monitoring instrument based on the tungsten trioxide (WO_3) semiconductors, Sens. Actuators B, Chem., 114 (2006) 507-512.

[15] M. Gillet, K. Aguir, M. Bendahan, P. Mennini, Grain size effect in sputtered tungsten trioxide thin films on the sensitivity to ozone, Thin Solid Films, 484 (2005) 358-363.

[16] B. T. Marquis, J. Vetelino, A semiconductor metal oxide sensor array for the detection of NO_x and NH_3, Sens. Actuators B, Chem., 77 (2001) 100-110.

[17] M. Stankova, X. Vilanova, J. Calderer, E. Llobet, P. Ivanov, I. Gràcia, C. Cané, X. Correig, Detection of SO_2 and H_2S in CO_2 stream by means of WO_3-based micro-hotplate sensors, Sens. Actuators B, Chem., 102 (2004) 219-225.

[18] http://uvp.com

[19] M. Bendahan, J. Guerin, R. Boulmani, K. Aguir, WO_3 sensor response according to operating temperature: Experimental and modeling, Sens. Actuators B, Chem., (2006) inpress.

[20] S. Vallejos, V. Khatko, K. Aguir, K. A. Ngo, J. Calderer, I. Gràcia, C. Cané, E. Llobet, X. Correig, Ozone monitoring by micro-machined sensors with WO_3 sensing films, Sens. Actuators B, Chem., 126 (2007) 573-578.

Accepted Manuscript

ACCEPTED MANUSCRIPT

[21] J. Tamaki, Z. Zhang, K. Fujimori, M. Akiyama, T. Harada, N, Miura, N. Yamazoe, Grain size effects in tungsten oxide-based sensor for nitrogen oxides, J. Electrochem. Soc., 141 (1994) 2207-2210.

[22] E. Llobet, R. Ionescu, S. Al-Khalifa, J. Brezmes, X. Vilanova, X. Correig, N.Bârsan, J.W. Gardner, Multicomponent gas mixture analysis using a single tin oxide sensor and dynamic pattern recognition, IEEE Sensors J., 1 (2001) 207–213.

[23] T. Wolkenstein, Electronic process on semiconductor surface during chemisorption: Consultants Bureau, New York, 1991, p. 444.

[24] M. Penza, M.A. Tagliente, L. Mirenghi, C. Gerardo, C. Martucci, G. Cassano, Tungsten trioxide (WO_3) sputtered thin films for a NO_x gas sensor, Sens. Actuators B, Chem., 50 (1998) 9-18.

[25] F.H. Jones, K. Rawlings, J.S. Foord, P.A. Cox, R.G. Egdell, J.B. Pethica, B.M.R. Wanklyn, Superstructures and defect structures revealed by atomic-scale STM imaging of WO_3 (001), Phys. Rev. B, 50 (1995) R14392-R14395.

[26] A. Kuzmin, J. Purans, E. Cazzanelli, C. Vinegoni, G. Mariotto, X-ray diffraction, extended x-ray absorption fine structure and Raman spectroscopy studies of WO_3 and (1-x)$WO_{3-y}\cdot xReO_2$ mixtures, J. Appl. Phys., 84 (1998) 5515-5524.

Accepted Manuscript

ISBN:978-84-691-9748-6 /DL:T-1249
ACCEPTED MANUSCRIPT

Table 1. Concentration of target gases and sensor operating temperatures used in this study

<table>
<tr><th>Gases</th><th>C (ppm)</th><th>T_{op} (ºC)</th></tr>
<tr><td>Nitrogen dioxide</td><td>0.5, 1, 2</td><td rowspan="6">250
350
450</td></tr>
<tr><td>Nitrogen oxide</td><td>1, 2, 3</td></tr>
<tr><td>Ozone</td><td>0.2, 0.4, 0.8</td></tr>
<tr><td>Carbon monoxide</td><td>10, 20, 30</td></tr>
<tr><td>Ammonia</td><td>1, 2, 3</td></tr>
<tr><td>Ethanol</td><td>10, 25, 50, 100</td></tr>
</table>

Accepted Manuscript

ISBN:978-84-691-9748-6 /DL:T-1249
ACCEPTED MANUSCRIPT

Table 2. Maximum responses of the WO_3 micro-sensors to ozone (O_3), nitrogen dioxide (NO_2), nitrogen oxide (NO_x), ammonia (NH_3), carbon monoxide (CO) and ethanol (C_2H_6O). EG: interdigitated electrode gap

Gas	C (ppm)	EG: 100 µm			EG: 50 µm		
		Operating temperature ºC					
		250	350	450	250	350	450
O_3	0.2	2.8	2.3	1.9	1.7	1.4	1.3
	0.4	4.5	3.1	2.6	2.3	1.8	1.5
	0.8	6.8	4.2	3.5	2.8	2.1	1.8
NO_2	0.5	2.9	3.8	3.5	2.3	3.5	3.3
	1	4.0	5.7	4.8	3.1	4.8	5.6
	2	6.4	10.7	20.6	4.1	6.9	18.4
NO_x	1	6.7	5.9	2.7	3.0	3.2	2.0
	2	9.0	7.7	4.5	4.2	3.8	2.3
	3	11.5	10.7	6.8	5.6	4.9	2.9
NH_3	1	1.0	1.3	1.0	1.0	1.6	1.0
	2	1.0	1.3	1.0	1.0	1.6	1.0
	3	1.0	1.4	1.0	1.0	1.8	1.0
CO	10	1.0	1.0	1.0	1.0	1.1	1.0
	20	1.0	1.0	1.0	1.0	1.1	1.0
	30	1.0	1.0	1.0	1.0	1.2	1.0
C_2H_6O	10	1.5	1.4	1.2	1.6	1.3	1.2
	25	2.5	2.5	2.0	2.9	2.5	2.0
	50	8.3	4.3	3.4	9.4	4.3	3.4
	100	15.2	9.6	6.2	16.7	9.5	6.1

Accepted Manuscript

ISBN:978-84-691-9748-6 /DL:T-1249
ACCEPTED MANUSCRIPT

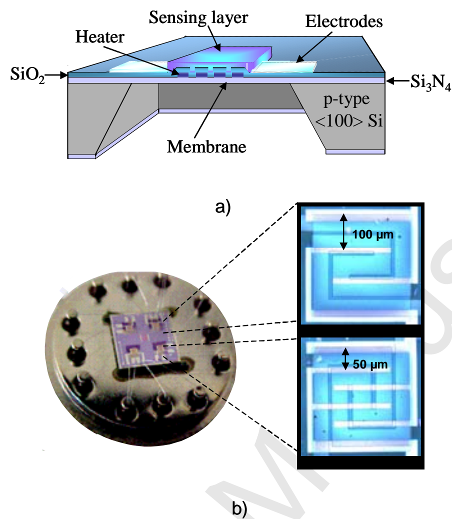

Figure 1.

Accepted Manuscript

ACCEPTED MANUSCRIPT

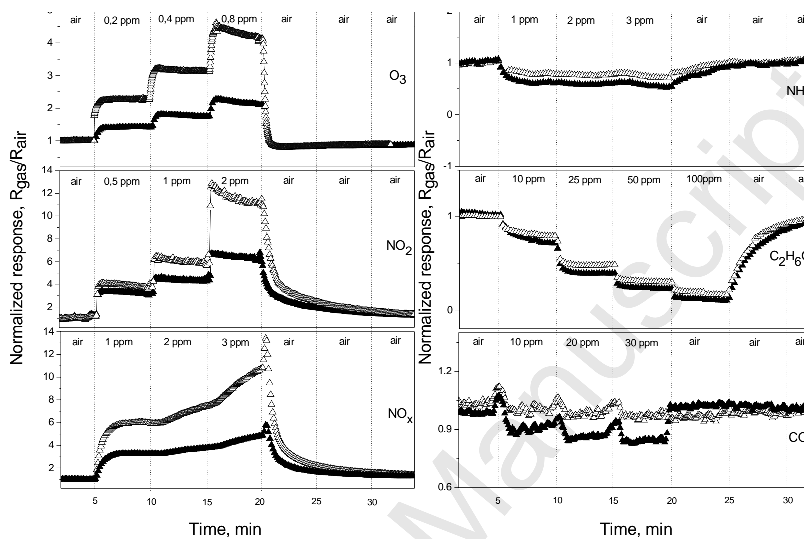

Figure 2.

Accepted Manuscript

ISBN:978-84-691-9748-6 /DL:T-1249
ACCEPTED MANUSCRIPT

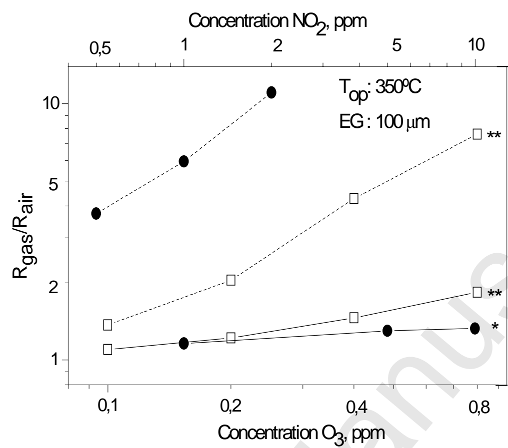

Accepted Manuscript

Figure 3.

ISBN:978-84-691-9748-6 /DL:T-1249
ACCEPTED MANUSCRIPT

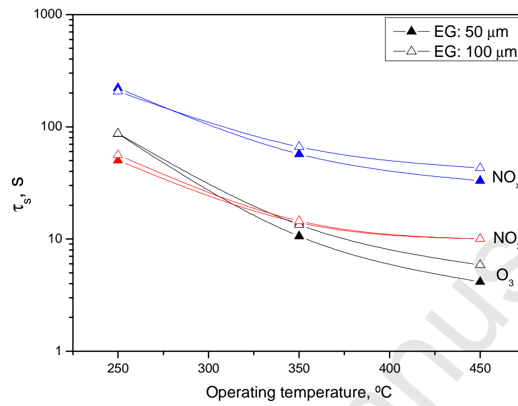

Accepted Manuscript

Figure 4

ISBN:978-84-691-9748-6 /DL:T-1249
ACCEPTED MANUSCRIPT

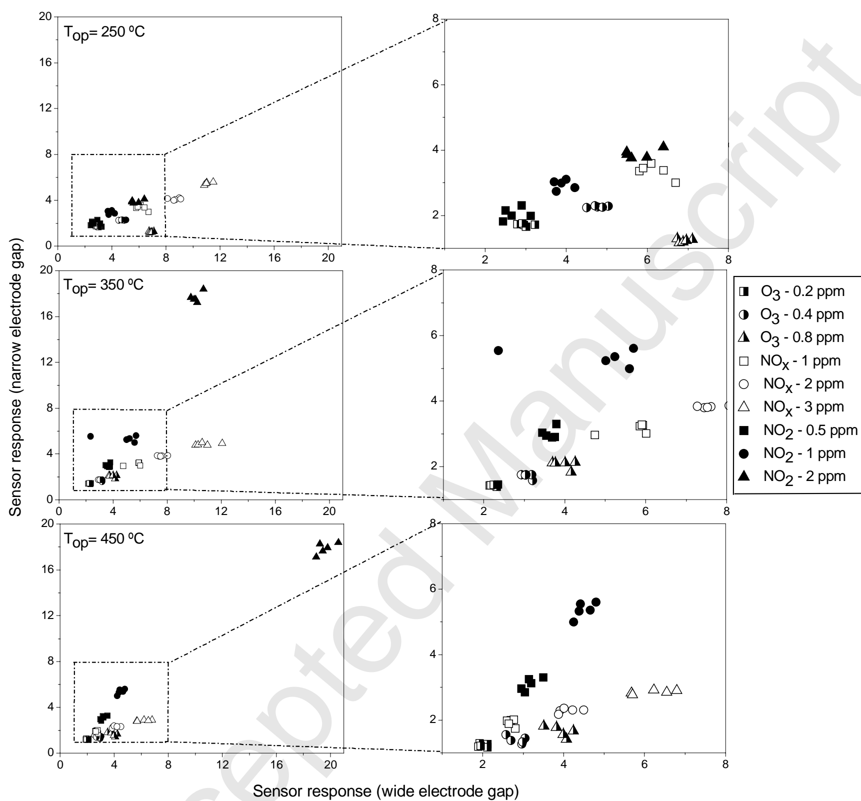

Figure 5

Accepted Manuscript

ISBN:978-84-691-9748-6 /DL:T-1249
ACCEPTED MANUSCRIPT

Figure captions

Fig. 1. (a) Schematic view of the micro-sensor cross section, and (b) on the left: view of the micro-array mounted on standard TO-8 and on the right: detailed views of the micro-machined sensor membranes with interdigitated electrodes of 100 µm gap and 50 µm gap.

Fig. 2. Baseline normalized WO_3-sensor responses to various oxidizing (O_3, NO_2, NO_x) and reducing (NH_3, C_2H_6O, CO) gases. The sensors operated at 350 ºC. Responses were acquired with electrodes of 100 µm (Δ) and 50 µm (▲) gap.

Fig. 3. Sensor responses to various O_3 (☐) and NO_2 (●) concentrations of WO_3 deposited without interruptions (——) and with interruptions (---). T_{op} is operation temperature. EG is electrode gap. The results (*) and (**) *were* adapted from Refs. [2] and [20], respectively.

Fig. 4. Response times to various target gases: O_3 (0.2 ppm), NO_2 (0.5 ppm) and NO_x (1 ppm). Responses were obtained with wide (Δ) and narrow (▲) interdigitated gap electrodes.

Fig. 5. Sensor response space obtained with wide and narrow electrode gap electrodes at various operating temperatures of (a) 250 ºC, (b) 350 ºC, and (c) 450ºC. X-axis represents the response obtained with wide electrode gap configuration and y-axis represents the response obtained with narrow electrode gap configuration. Half full scatters belong to ozone, empty scatters to nitrogen oxide and full scatters to nitrogen dioxide. Corresponding concentrations to each gas are presented in the graphic label.

Accepted Manuscript

ACCEPTED MANUSCRIPT

Biographies

Stella Vallejos was graduated in electrical engineering (2002) and electronic engineering (2003) from the Universidad Técnica de Oruro, Bolivia. She is currently a PhD student in the Electronic Engineering Department at the Universitat Rovira i Virgili, Spain. Her main areas of interest are fabrication and characterization of solid state gas sensors.

Viacheslav Khatko graduated in nuclear physics from the Belarusian State University (Minsk, Belarus) in 1971. He received his PhD in materials science in 1986 and Dr.Sc. in solid state electronics in 2001. In 1975-2003 he worked at the Physical Technical Institute of National Academy of Sciences of Belarus, Minsk, as a researcher, head of the Laboratory of Electronic Engineering Materials, head of the Thin Film Materials Department and then as Principal Investigator of the same institute. He was Ford SABIT Intern and Ford Visiting Scientist in 1998 and 1999, respectively. From April 2003 he is Ramón y Cajal professor in the Electronic Engineering Department of the Universitat Rovira i Virgili (Tarragona, Spain). His current research interests include the development and application of semiconductor thin and thick film gas sensors.

Josep Calderer received his degree in Physics in 1973 and the PhD in 1981 in the University of Barcelona. He has been working in technology and characterization of photovoltaic solar cells, heterojunction bipolar transistors and silicon-based integrated optical sensors. At present he is a staff member of the Department of Electronic Engineering (DEE) of the Polytechnic University of Catalonia (UPC, Barcelona). His main research activity focuses on resistive gas sensors using metal oxide compounds.

Isabel Gràcia received the PhD degree in physics in 1993 from the Autonomous University of Barcelona, Spain, working on chemical sensors. Currently she is a full time senior researcher in the micro-nano systems department of the National Microelectronics Center (Barcelona, Spain). Her work is focused on gas sensing technologies and MEMS reliability.

Carles Cané received the PhD in 1989. Since 1990 he is a full time senior researcher at the National Microelectronics Center (Barcelona, Spain). He works on the development of CMOS technologies, mechanical and chemical sensors microsystems. He is a member of the technical committee of EURIMUS-EUREKA programme since 1999. Over the last years he has been a co-ordinator of several R&D projects, both at national and international level in the MST field. He has performed management activities as well, as head of the Microsystems and Silicon Technologies Department of CNM and as vice-director of CNM Barcelona site. He is the co-ordinator of the GoodFood Integrated Project from the 6th Framework Programme (FP6-IST-508774-IP).

Eduard Llobet was graduated in telecommunication engineering from the Universitat Politècnica de Catalunya (UPC), (Barcelona, Spain) in 1991, and received his PhD in 1997 from the same university. During 1998, he was a visiting fellow at the School of Engineering, University of Warwick (UK). He is currently an associate professor in the Electronic Engineering Department at the Universitat Rovira i Virgili (Tarragona, Spain). His main areas of interest are in the fabrication, and modelling, of semiconductor chemical sensors and in the application of intelligent systems to complex odour analysis.

Xavier Correig was graduated in telecommunication engineering from the Universitat Politècnica de Catalunya (UPC), (Barcelona, Spain) in 1984, and received his PhD in 1988 from the same university. He is a full professor of Electronic Technology in the Electronic

Accepted Manuscript

ISBN:978-84-691-9748-6 /DL:T-1249
ACCEPTED MANUSCRIPT

Engineering Department at the Universitat Rovira i Virgili (Tarragona, Spain). His research interests include heterojunction semiconductor devices and solid-state gas sensors.

Accepted Manuscript